UNIVERSITÀ DEGLI STUDI DI MILANO

PhD Course in Veterinary and Animal Science

(Class XXXIV)

Department of Agricultural and Environmental Sciences - Production, Landscape, Agroenergy

Doctoral thesis

Morphological And Functional Characterization of the Rainbow Trout *(Oncorhynchus mykiss)* Gut To Develop A Predictive *In Vitro* Intestinal Model

VET-01

<div align="right">

Dr. **NICOLE VERDILE**
Academic ID: **R12211-R35**

</div>

Tutor: Prof. **FULVIO GANDOLFI**

PhD Course Coordinator: Prof**. FABRIZIO CECILIANI**

Academic year 2020-2021

Table of Contents

Chapter 1

State of the Art

Farming carnivorous fish: an environmental concern

In the last fifty years the human population has more than doubled, passing from 3.7 billion people to more than 7.8 billion [1] and leading to a substantial boost in global food demand.

Fish is an essential source of animal proteins and an important ingredient for a healthy and balanced diet [2] therefore fish production has been particularly affected by the above mentioned demand raise. In order to meet the customer's needs, and at the same time reduce pressure on wild-caught species and the ecological impact on oceanic wild-life, the industry has remarkably increased intensive farming of all commonly consumed species [3] (Figure 1). However, carnivorous fish such as rainbow trout, salmon, sea bass and shrimp constitute a serious limit to the environmental sustainability of aquaculture: the nutritional habits of these species require feeds based on fish oil and fishmeal, in order to provide the necessary amount of energy and animal proteins [3,4]. These ingredients are obtained by processing small oily fish species caught for non-food
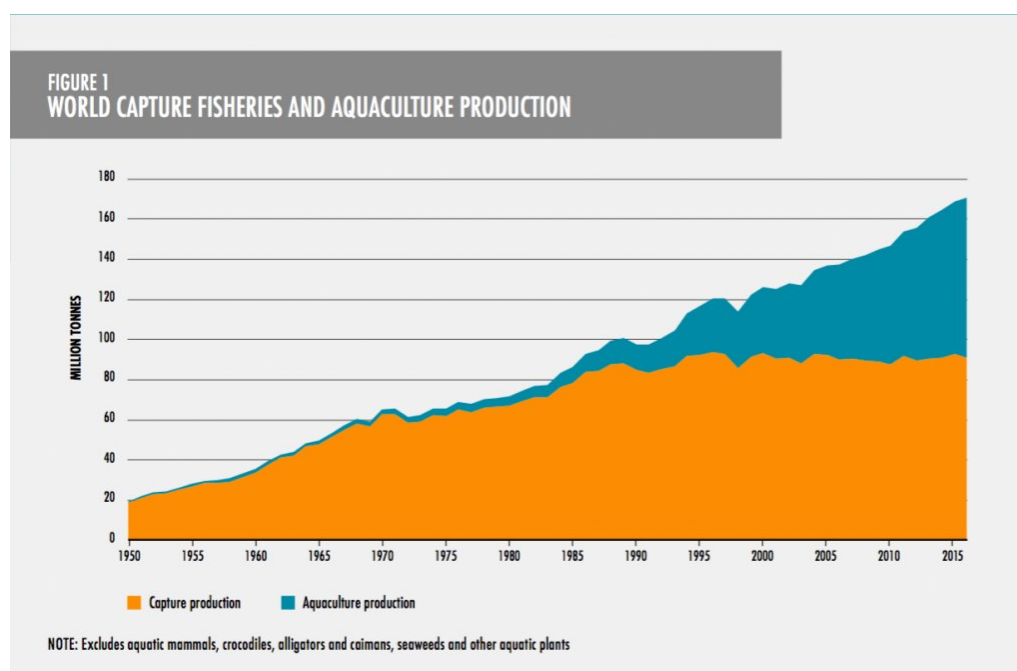
Figure 1: Comparison between wild-caught fisheries and aquaculture production from 1950 to date, from the 2016 State of World Fisheries and Aquaculture report released by the United Nations Food and Agriculture Organization (FAO).

purposes, and therefore heavily impacting on oceanic wild-life at lower levels of the natural food chain [5].

The main response to this environmental issue has been the gradual substitution of these essential feedstuff with alternative ingredients. However, substitution of marine ingredients with ingredients derived from a more sustainable sources such as maize gluten, soybean meal or wheat gluten is known to negative affect survival rate in early stages of development, to reduce growth rate in adult individuals [5,6] and to severely compromise animal welfare causing inflammation and gastrointestinal disorders. Consequently, continuous, and extensive raw material evaluation programs together with detailed comprehension of the intestinal morphology and physiology are essential to predict and assess their final effect on the gastrointestinal tract.

I*n vivo* test are expensive, subject to restricted rules, and require many animals. The concerns for animal welfare and the high costs drive academia and feed industries in reducing *in vivo* trials, by using *in vitro* models, at least in the preliminary phases.
However, the gastrointestinal tract (GI) is a very complex and dynamic system. It is the major site of nutrient absorption, acting as a selective filter between the lumen and the circulatory system: it simultaneously promotes the absorption of nutrients and it prevents the passage of harmful intraluminal entities including foreign antigens, microorganisms and toxins [7]. All these functions are realized through a complex morphological architecture [8]. This makes it difficult to develop *in vitro* models able to accurately mimic the gut mucosa.

Currently, the most common models used to evaluate the intestinal absorption mechanism are based on the use of immortalized Caco2 cells derived from human colorectal adenocarcinoma [9,10]. They, show the advantage of spontaneously differentiate *in vitro* into a monolayer of cells displaying typical properties of absorptive enterocytes. Moreover, being of tumors origins they easily grow in culture, but lack a fully mature phenotype and therefore are not able to

mimic faithfully the physiological environment [11,12]. Furthermore, they also lack the classical cell heterogeneity which distinguishes the intestinal mucosa. Similarly, RTgutGC, a stable intestinal cell line, was derived from the more distal portion of the rainbow trout intestine [13].

Recently, the improvement in stem cell culture techniques has allowed to use primary, non-transformed cells to create specialized tissues *in vitro* as an alternative to the immortalized cell lines [14]. These complex structures, known as enteroids, are made up by several differentiated cells types and by their progenitors making them more similar to the intestinal epithelium [15]. However, the cystic, spherical architecture of enteroids severely limits their use in functional studies. Their enclosed lumen is buried within a thick mass a hydrogel [16] therefore the compounds that must be tested cannot easily access the luminal compartment. In this regard, the development of sophisticated *in vitro* models able to reproduce accurately the fish intestinal mucosa would be a helpful tool to screen rapidly and efficiently innovative feedstuff.

Among the different livestock species, in this thesis rainbow trout (*Oncorhynchus mykiss*) has been selected as experimental model due to its widespread occurrence in the local and European aquaculture industry.

The intestinal tract structure and physiology

The intestine is a complex and multifunctional organ. It works as a selective biological barrier whose purpose is to digest and absorb nutrients, keeping at the same time pathogens and harmful elements out. Fish species are heterogenous and numerous and the morphology of theirs digestive tract is extremely dynamic, easily adaptable to environmental changes and strongly conditioned by several external factors (e.g. feeding habitats, food and frequency of food intake, as well as taxonomy, body size and shape) [17,18]. In particular, their gastrointestinal tract differs for the presence or the absence of digestive organs such as the stomach, the pyloric caeca, and the gall bladder, for their stomach shape (U-shaped, Y-shaped or straight), and for the length and the coiling of the intestine [19] (Figure 2).
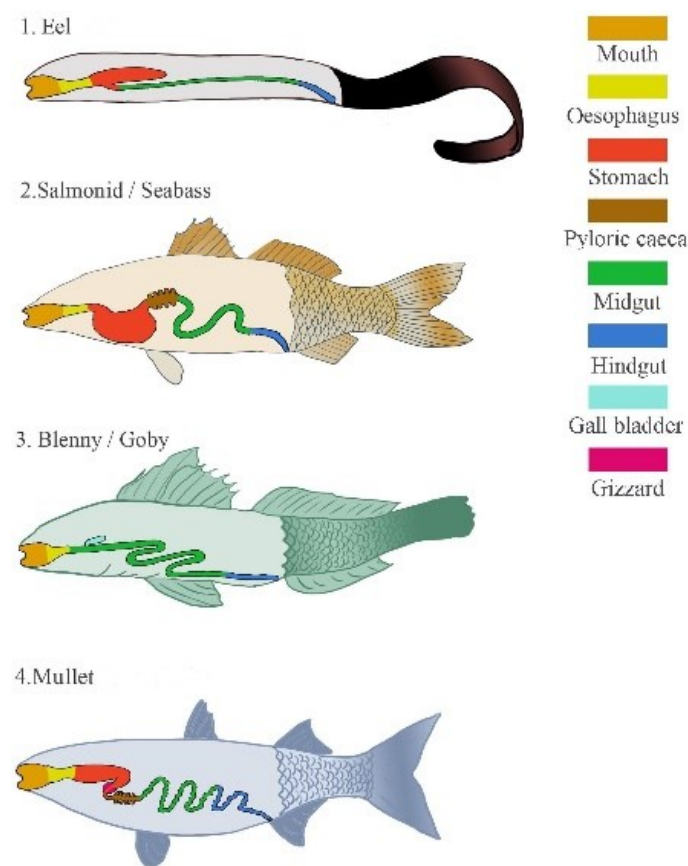
Figure 2: Schematic representation of the digestive system organization in different fish species [20].

Feed is assumed through the mouth, where teeth, extensively present on jaws, tongue (as in rainbow trout) and pharynx (in Cyprinidae), are organized depending on the diet. Then, oesophagus originates and produces mucus to facilitate food transit, its length varies between marine and freshwater fish.

Rainbow trout presents a Y-shaped stomach which is typical of carnivorous and omnivorous species. It consists of a larger cranial district rich in gastric glands and of a smaller caudal which instead do not present them. This latter is also characterized by the presence of a thicker muscular layer directly connected to the pylorus. Similarly to mammals, gastric glands are constituted of epithelial cells secreting hydrochloric acid and pepsin [21]. Consequently, the acid environment allows the digestion occurrence and simultaneously it enables the conversion of pepsinogen into pepsin.

From the posterior portion of the pyloric sphincter, rainbow trout develops pyloric caeca, hollow tubes whose role it is not yet fully clear. Recent data suggest that these protrusions are involved in the secretion of digestive substances as well as in the increased absorption surface area. They branch off the proximal part of the anterior intestine aimed to increase the absorptive surface. The number and the length of these typical structures differ among species; rainbow trout develops about 56±2 pyloric caeca that measures about 1.9±0.1 cm [22].

Structurally, the rainbow trout intestine comprises of two main regions: the proximal intestine and the distal intestine. Specifically, the first is thin, nearly transparent and is defined by the presence of pyloric caeca. The latter is thicker compared to the proximal counterpart and it is characterised by a darker pigmentation due to the presence of circularly-arranged blood vessels.

Intestine is the major site of absorption of nutrients of carbohydrates and lipids. Initially, salivary and pancreatic amylases break-down polymeric carbohydrate. Then, mucosal enzymes of the intestine further digest carbohydrates to glucose [23]. Similarly, lipids digestion begins with lingual lipase in mouth, and continues with gastric lipase in stomach. In the intestine, the pancreatic lipase and

colipase activity contribute to lipid digestion and consequently to their absorption. As in mammals, nutrients absorption and internalization trough the brush border of the enterocytes is mediated by transporter proteins. In particular, sodium-dependent glucose transporters (SGLTs) and Glucose transporter 2 (GLUT2) allow the transport of glucose from the lumen into the cytosol and from the cytosol to the blood respectively [24,25].

Similarly, CD36 and LFABP enable the internalization of long-chain fatty acids and monoglycerides into the enterocytes. Subsequently, they are re-esterified emulsified by the bile, and transferred to the bloodstream [23]. Therefore, pancreas and liver play a key role in intestinal digestion releasing substances that allow nutrients break-down. While the exocrine pancreas produces amylase, maltase, lactase and lipase, whose purpose is to digest carbohydrates and lipids [26], liver actively contributes to lipids emulsion through its bile production, released in the proximal portion of the intestine.

Intestinal microscopic anatomy

Histologically, the general structure of the intestine in teleosts is fairly similar to mammals. It is composed of four main layers: mucosa, submucosa, muscularis and serosa [27–29]. The tunica mucosa consists of the epithelium and the lamina propria, whereas *muscularis mucosae* has not been identified in teleosts. It is organised in folds, finger-like protrusions which significantly increase the contact surface and, consequently, the absorptive capacity of the organ. The epithelium is composed of a single columnar layer which comprises absorptive enterocytes, apically coated by a microvilli-covered brush border membrane to promote absorption, scattered goblet cells and few enteroendocrine cells; all these cells are sideways jointed each other by tight junctions constituting a real barrier [18,30].

The mucosal organization in teleosts shows some peculiarities: folds are present in both proximal and distal intestine, unlike in mammals where they are

absent in the large intestine, and intestinal crypts are absent in both regions of the tract (Figure 3). The term "crypts" describes invaginated glands present in the connective tissue at the base of the villi where progenitors' cells house and differentiation of epithelial cells originates in mammals [31]. The fate of undifferentiated cell types depends on the direction of their migration. After their division, most of cells migrate up towards the villus tip differentiating into enterocytes, goblet cells, or enteroendocrine cells, only a few of them remain at crypt base and differentiate into Paneth cells [8]. Analogous invaginations are not present in fish intestine [32]. However, previous studies performed in teleost fish, identified the folds base as their functional equivalent [28,32].

The submucosa consists of a thick layer of dense connective tissue, the *stratum compactum*, interposed between two loosed layer of submucosa hosting numerous eosinophilic granular cells called stratum granulosum

The tunica muscularis is formed by a circular and longitudinal layer of smooth muscle fibres. Finally, all these structure are enveloped in a thin membrane of connective tissue covered by squamous epithelium: the tunica serosa. As mentioned above, the fish intestinal epithelium presents three main types of differentiated cells: enterocytes, goblet and enteroendocrine cells.
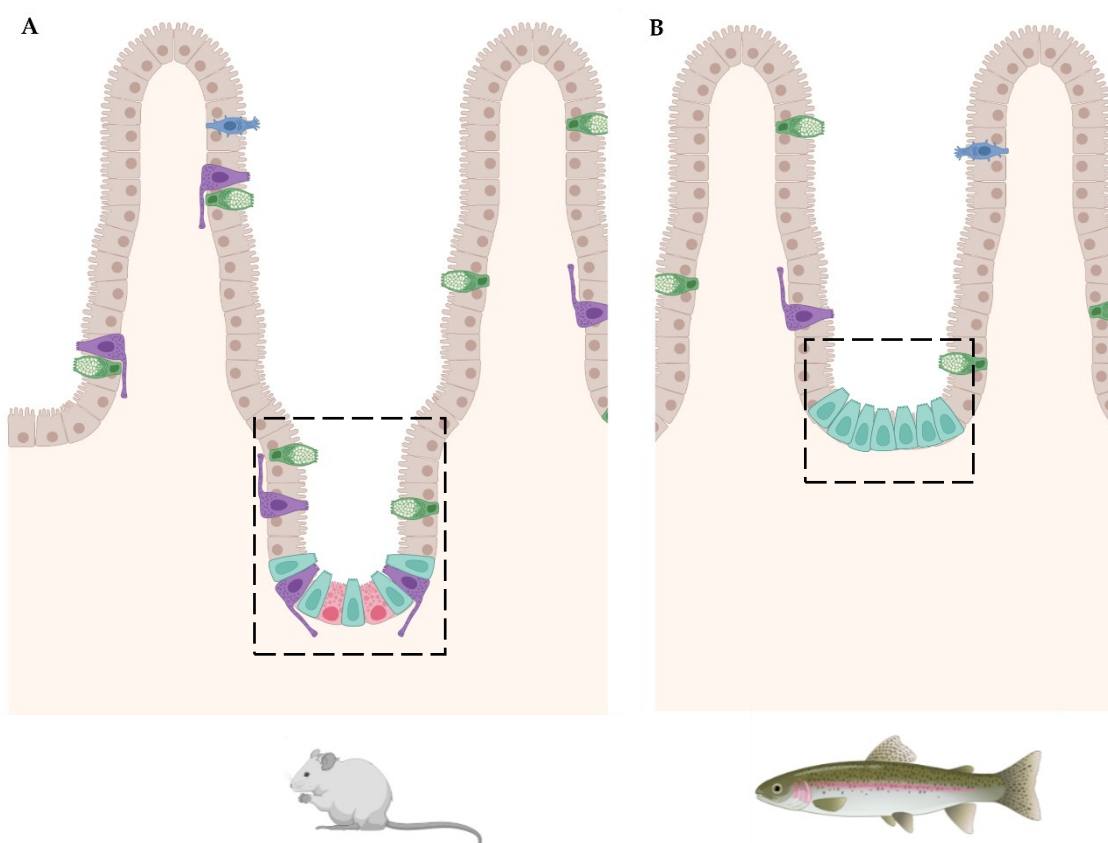
Figure 3: Schematic illustration showing the anatomical site in which intestinal epithelial proliferating cells are located. In mouse the proliferative and stem cell zone is localized within the intestinal crypts (A), whereas in rainbow trout, these structures are absent and substituted with the folds' base (B). Image created using BioRender.com

Enterocytes

Enterocytes (Figure 4A) are typical intestinal cells which carry out the main purpose of the intestinal tract: to select and absorb nutrients. These cells are disposed in a single, tightly adhered columnar layer; the basal part of the cell hosts many mitochondria, and well-developed Golgi apparatus and endoplasmic reticulum, while apically protrusive structures called microvilli increase absorptive capacity and expose specific receptors for nutrients transport [33].

Enterocytes originate from the base of the villi (or from crypts, in mammals) and migrate towards the upper portion while differentiating. Fully mature

enterocytes secrete into the lumen, the intestinal alkaline phosphatase enzyme, an essential and crucial factor to maintain intestinal homeostasis, to modulate intestinal long-chain fatty acids (LCFA) absorption, and to preserve the gut health inactivating endotoxins' lipopolysaccharide (LPS) [34,35].

Goblet cells

Goblet cells (Figure 4B) are mucus-producing cells that can be found along the intestinal tract. These cells are, as the name recalls, goblet-shaped and highly polarised: cell components are basally located or aligned along the lateral margins, compressed by the presence of abundant mucus-secreting granules.

Mucus is released in the intestinal lumen through simple or compound exocytosis and it has a multifunctional role: it provides lubrification for food passage, transports digestive enzymes and fluids, and protects the organ acting as a barrier for pathogens and digestive secretions. Many studies suggest a role in osmoregulation as well. The viscous, gel-like properties of mucus derive from its major glycoprotein components called mucins. These molecules have a protein core with several glycosylated domains linked to oligosaccharides chains, which may or may not be terminated with acidic groups [36,37]. This possibility accounts for the chemical distinction between two types of mucus, acidic and neutral, and for the heterogeneity of goblet cells- secreted granules [29,38–40].

Enteroendocrine cells

Enteroendocrine cells (Figure 4C) are scarcely diffused, comprising only 1% of the intestinal epithelium, however they play a key role in regulating physiological responses to luminal stimuli by secreting several hormone peptides. These cells are also involved in the arousal of sensations such as hunger, appetite and satiety [41].
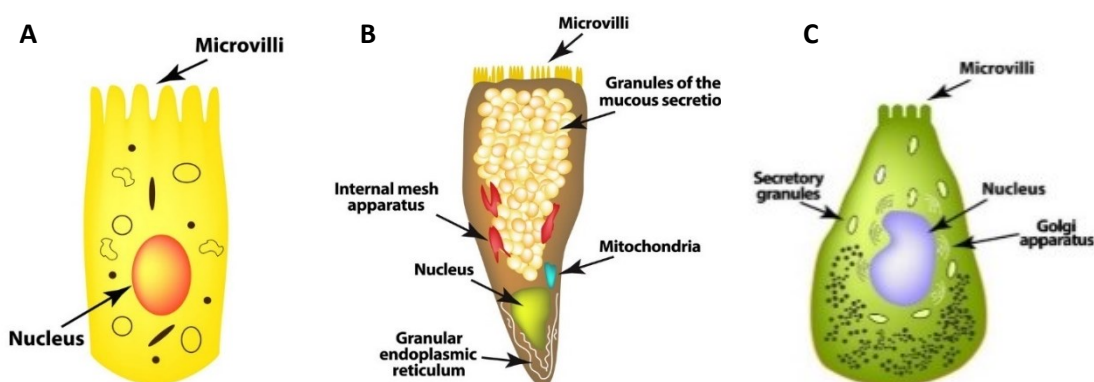
Figure 4: Schematic representation of an enterocyte (A), of a goblet cell (B) and of an enteroendocrine cell (C).

Paneth cells- eosinophilic granules cells

Paneth cells and their distinct granules are located only in the crypts of some mammals' small intestine. Their primary role is to inhibit and discourage bacterial invasion by secreting antimicrobial peptides such as α-defensins and lysozyme. These substances play a central role in the host defense against foreign entities such as enteric pathogens [42]. Increasingly amount of data suggest that loss of Paneth cell expose the host organism to both microbial and helminth infections. Moreover, this cell type, is also known to play a pivotal role in intestinal stem cells guidance through the production of specific factors promoting migration [43–45]. Nevertheless their essential role, the presence of Paneth cells is still controversial in many domestic and fish species [32,46]. However, in fish, eosinophilic granular cells

(EGCs) share common features with mammals' Paneth cell [47]. As mentioned above, in the intestine, EGCs constitute, the two *stratum granulosum* which enveloped the dense compactum layer of the submucosa. These cells are packed with ovoid eosinophilic granules and it has been demonstrated that in Atlantic salmon produced lysozyme, suggesting a possible role of EGCs in host defense mechanisms [47].

Intestinal homeostasis

For a tissue, to properly exert its function, it is necessary that each cell that has been damaged by wear or direct insult is promptly repaired or substituted through a general process called tissue *homeostasis*. Moreover, it is commonly known that a proliferating cell cannot exert a specialized function and, conversely, a fully mature functional cell has lost its ability to proliferate. It follows that proliferation is limited to specific cell populations in each organ. Two main cell types constitute this specialized population, stem cells and transient amplifying cells.

Stem cells have no particular morphological features and therefore are scarcely identifiable; they are rare, and their divisions are limited in order to reduce the risk of genetic mistakes that often occur during DNA duplication. They are the only cells that can undergo through an asymmetric division, from which originates a daughter cell identical to its mother (self-renewal) and a daughter cell that will undergoes to the differentiation process leading to the substitution of the mature cell types that needs to be replaced. The latter will originate the transient amplifying cells that will generate a pool of differentiated cell proportional to those that have been lost. Once cells have reached their terminally differentiate state, they stop dividing and assume their definitive shape and function.

Therefore, the tissue *homeostasis*, is ensured by a thin regulated and modulated balance among proliferation differentiation and cell death. The equilibrium is maintained by the appropriate combination between continuous

physiological cell death and proliferation of intestinal epithelial cells (IECs) [15,48]. Several factors conditionate this equilibrium, including luminal contents, bacteria and growth factors. In physiological conditions, the dominant mechanism which drive IEC death is the *anoikis*. It is a peculiar form of programmed cell death in which dying cells detach from the supportive extracellular matrix and then from adjacent cells to shed into the intestinal lumen [49]. An early event that take place few minutes prior to cell shedding, is the translocation of the tight junction protein zonula occludens 1 (ZO1) from the apical to the basolateral portion of the cells. This redistribution is essential in the preservation of barrier function and integrity while cells are being shed.

Intestinal Stem cell and the role of the niche

Stem cells reside in specific niches, local microenvironments capable to ensure a well-defined balance between self-renewal and differentiation through both intrinsic and extrinsic stimuli. These comprise cell-to-cell and cell-matrix interactions, as well as signals that activate and/or repress genes and transcription pathways [50]. As described above, intestinal epithelium is subjected to intense wear and tear and, consequently, to intense cell renewal. However, the renewal rate varies among different species. While in mammals' the complete renewal of the intestinal epithelium occurs in 3-4 days [46], in fish species this phenomenon is slower, as recently demonstrated in zebrafish intestine where the whole turnover requires about 10-15 days. It is driven by intestinal epithelial stem cells (IESCs) that reside in the crypt base in mammals and which are continuously stimulated to produce a pool of highly proliferating cells called transit amplifying (TA) population, committed to produce the intestine mature cell lineages: columnar enterocytes, mucin-producing goblet cells, Paneth cells, and enteroendocrine cells. To date, IESCs knowledge are growing exponentially in mice and humans, however such understanding and mechanisms are still extremely limited in other

domestic species especially in fish. Moreover, a full characterization of IESCs is still elusive due to the lack of specific markers and suitable methodologies for the evaluation of intestinal function. Almost 4 decades ago, Cheng and Leblond [51], discovered the presence of slender, cycling epithelial cells, the so-called crypt base columnar (CBC) cells in the mouse small intestine. CBC were described as being actively cycling and phagocytic, helping to clear dead cells from the crypt base and interposed between the Paneth cells. They divide once every day thereby demonstrating that the crypt base is not populated only by post-mitotic Paneth cells. Leblond and Cheng have proposed that the CBC cells may represent the true stem cells. They proposed the existence of a stem cell zone from which has been derived the model called "the stem cell zone model". In this model, mix cells are proposed to represent the direct offspring of the CBC cells [52,53]. Mix cells would occupy the positions directly in contact with the Paneth cells, the "common origin of differentiation". At the "common origin", the cells commit to one of the various fates. Maturing Paneth cells precursors will migrate downward, with the oldest Paneth cells residing at very base of the crypt. All other cell types migrate upward.

An alternative model, in mouse, has been proposed by Potten et al., the so called "+4 model", based on the identification of 16 cells organized within a ring immediately above the Paneth cells which occupy the fourth position from the crypt base [54]. These cells present several typical features of stem cells since they are relatively quiescent and are resistant to acute injury. The increasingly amount of data and the increasingly knowledge of intestinal stem cells, enable the identification of specific and selective markers for these two cell populations. The G protein-coupled receptor Lgr5 and the homeobox only protein, are two described molecular markers of self-renewing and multipotent adult stem cell populations residing in the crypt of the small intestine, capable of supporting regeneration of the intestinal epithelium [55]. Lgr5 (Leu-rich repeat- containing G protein-coupled receptor 5) was the first marker exclusively expressed by CBCs at the base of adult intestinal crypts. Hopx+ IESCs are mostly restricted to the "+4" cell position

abutting the uppermost Paneth cell in proximal small intestine crypts [56–58]. Lgr5+ IESCs are actively cycling and contribute to intestinal homeostasis by neutral drift competition, whereas hopx+ IESCs are less well characterized, and because of the lack of direct evidence, their cell cycle status is variably ascribed to be rapidly vs. slowly cycling. Further, a systematic comparison of hopx+ and Lgr5+ IESC function during homeostasis and injury repair has shown that they are two functionally distinct IESCs populations. Hopx+ marks quiescent IESCs located at the 4+ position, that are insensitive to Wnt perturbations and contribute weakly to homeostatic regeneration [59]. Lgr5 marks mitotically active IESCs that exhibit exquisite sensitivity to canonical Wnt modulation and contribute robustly to homeostatic regeneration. The intestinal stem cell niche is formed by three major components. The first one is the extracellular matrix (ECM), made of a network of fibrous structural proteins (such as fibronectin, laminin, collagens) arranged as a scaffold to provide sustain, support and to maintain the three-dimensional architecture of the intestine. The second is the stromal microenvironment that comprises the mesenchymal cell types embedded within the ECM. Among these cell type, peri-cryptal cells and telocytes arouses ever-increasing interest. Peri-cryptal cells are mesenchymal cells with no morphological particular features, but responsible of the secretion of specific soluble factors which induce stem cells proliferation. Instead, telocytes are slender cells characterized by a thin cell body of around 15μm and displaying long and thin protrusions, known as telopods (Figure 4). Overall, these structures allow the realization of a 3D supportive scaffold which enable the adequate mucosa organization as well as cell-signaling exchange [60]. To date in mice and humans intestine, PDGFRα, FOXL1, and CD34 are well-accepted telocytes and telocytes' subset markers [61]. Finally, Paneth cells as mentioned above, play a fundamental role in IESCs niche maintenance and homeostasis through the secretion of factors and essential signals. During cell lineages differentiation, several complex molecular pathways act to allow the acquisition of structural features such as polarization, formation of important junctional complexes and structure

involved in intestinal epithelium integrity and absorption. Wnt signaling represents the principal force behind intestinal epithelium homeostasis, it is tightly controlled to prevent (over)proliferation of ISCs. This pathway is highly conserved throughout the animal kingdom. Numerous studies conducted both *in vivo* and *in vitro* have firmly established the role of Wnt signaling in the preservation of stem cell proliferation and pluripotency. The expression of the Wnt cues displays a diminishing slope along the crypt-villus axis. In addition, the Wnt proteins are locally attenuated at the+4 position by production of the Wnt antagonists secreted Frizzled-related proteins (sFRPs). Furthermore, the Wnt pathway output is modulated by co-operative activity of the Hedgehog and bone morphogenic protein (BMP) cascades. In more detail, as the progenitor cells further decline from the crypt base, the Hedgehog-induced, mesenchyme-to- epithelium BMP signaling promotes differentiation while restraining proliferation. Wnt signaling plays multiple roles during intestinal homeostasis and includes a canonical and a non-canonical pathway. β-catenin is the cytoplasmatic protein that plays a key role In the first one. When this pathway is activated, β-catenin is phosphorylated and is transferred from the cytoplasm to the nucleus. It is essential for crypt maintenance and promotes the proliferation of stem/TA cells. Furthermore, Wnt canonical pathway is involved in Paneth cell maturation. The non-canonical pathway is responsible for crypt rearrangement and new crypts formation. Notch in another signaling pathway active in intestinal crypt compartments. When activated, it contributes to epithelium regeneration, assists Wnt pathway in promoting stem cell proliferation and negatively regulates differentiation into the secretory lineage (Figure 5) [62–64].
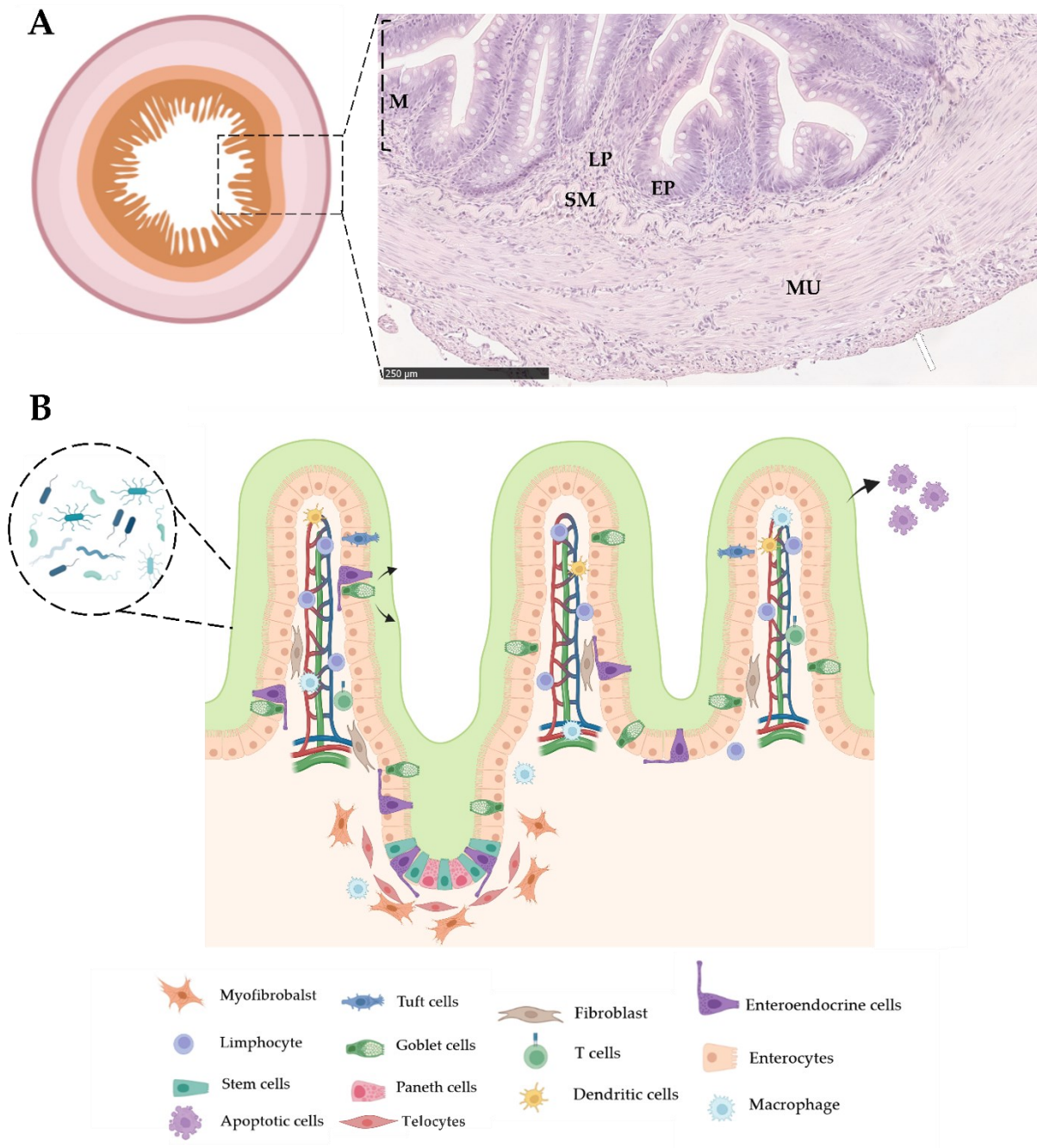
Figure 5: Schematic representation of a transversal section of intestine (A); representative image showing the organization of the fish intestinal wall (MU: tunica mucosa, SM: tunica submucosa, EP: epithelium, LP: lamina propria, MU: tunica muscolaris, arrow: serosa. Schematic representation of the organization of the mouse small intestine (B), the scheme shows the general architecture of the intestinal mucosa as well as the distribution of the different cell types. Image created using BioRender.com

Aim of the thesis

This thesis had several purposes:

1. To gain a more detailed knowledge of the rainbow trout intestinal morphology and physiology, including the mechanisms that regulate homeostasis and repair of the mucosa.

2. To assemble the first reference data set describing the different cell types that constitute the stem cell niche. This includes the molecular markers that identify them as well as their reciprocal interactions.

3. To use this data set for characterizing the novel primary intestinal cell lines established in our laboratory from the proximal and the distal intestine of the rainbow trout and to compare them with the only stable RT intestinal cell lines previously available (RTgutGC).

4. To provide the starting material for developing a sophisticated and complex *in vitro* model to be used as a predictive tool for evaluating the biological value of different feed formulations.

Chapter 2

Digestive And Absorptive Capacity Are Mingled Along The Rainbow Trout (Oncorhynchus Mykiss) Gut

Overview

To obtain an adequate comprehension of the intestinal morphology and function, I performed a detailed morphological evaluation of the intestinal epithelial cells lining the rainbow trout gut. This was obtained through histological, histochemical and immunohistochemical observation, accurate stereological analysis, morphometric measurements, and fine qualitative and quantitative characterization of goblet cells secreting activity at typical time points of *in vivo* feeding trials (50, 150 and 500 g).

The gross anatomy of the rainbow trout gut corresponds to the general description of the organ in teleost fish. It consists of a proximal intestine with annexed pyloric caeca, easily distinguishable from the distal intestine, which presents a larger diameter, dark pigmentation, and circularly arranged blood vessels. Microscopically, the proximal intestine was characterized by simple folds whereas the distal intestine displayed a more complicated mucosa arrangement. In fact, this latter, was defined by the presence of peculiar complex folds from which other simpler originated. While only minor changes took place along the classical time points of *in vivo* feeding trials, two morphological and functional compartments not linearly distributed were observed along the trout gut. The first included the proximal intestine and the apical part of the complex folds of the distal portion. This was characterized by abundant and actively secreting goblet cells, no pinocytotic vacuoles, high expression of three defined functional enterocytes markers (PepT1, Sglt1 and Fabp2), low proliferation rate, few round apoptotic cells and an extended area of fully differentiated cells. The other, comprised the basal part of the complex folds and the pyloric caeca and was defined by few goblet cells with deflated mucus vacuoles, pinocytotic vacuolization, weak expression of the classical functional enterocytes markers, high proliferation and apoptotic rate and by a smaller extension of fully differentiated epithelial cells. The presence of these

distinct morphological and functional compartments suggest that digestive and absorptive function are mingled along the trout gut and that possibly in this species, the proximal intestine extend itself in the distal portion of the intestine to maximize its absorptive capacity [65] (Figure 6).
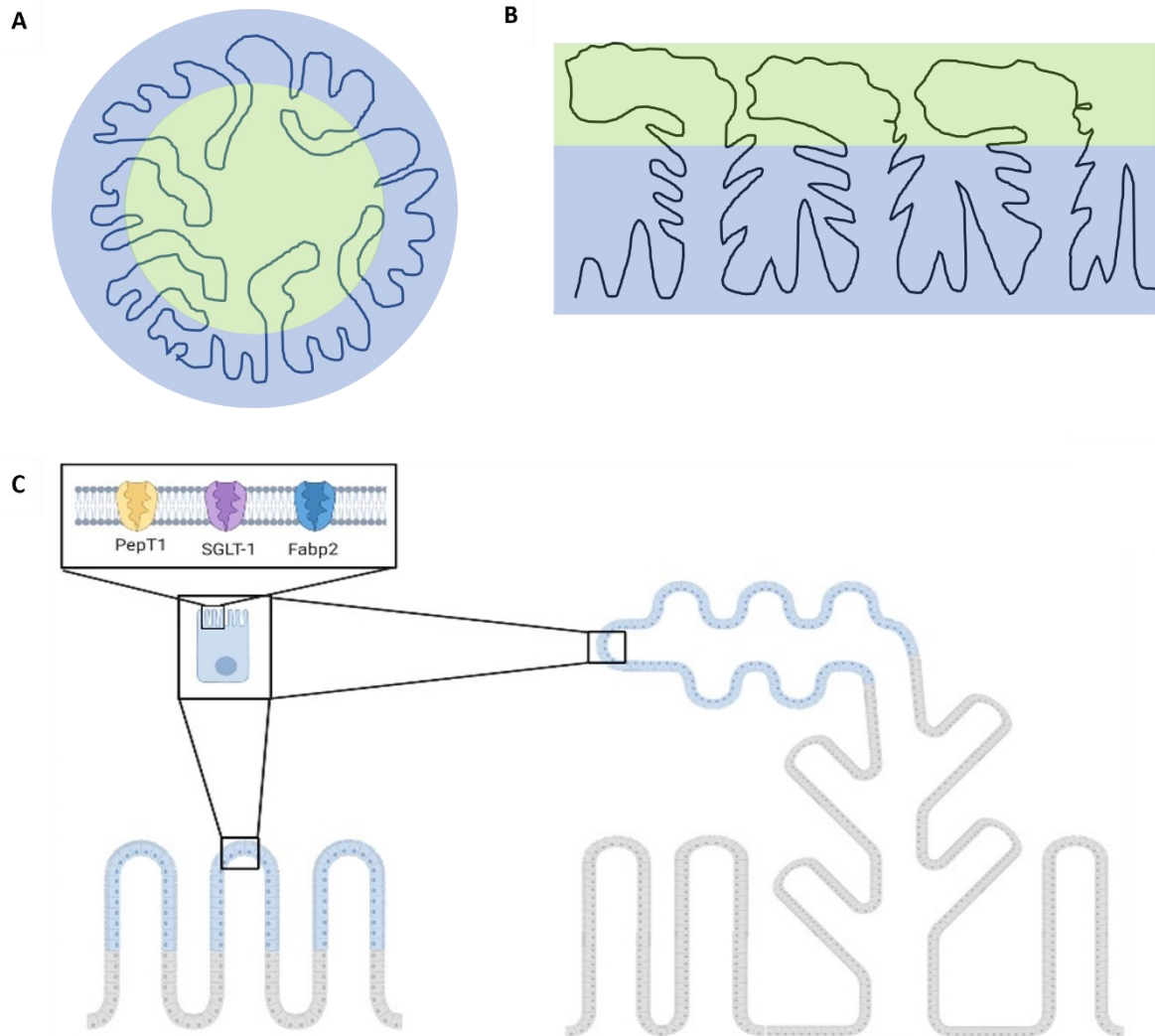
Figure 6: Graphical abstract summarizing the main results observed in this chapter. Transversal and longitudinal representative schemes of the proximal (A) and distal intestine (B), and cartoons showing the distribution of three functional enterocytes' markers in proximal and distal intestine. The typical morphological and functional bivalence that we observed is highlighted in scheme A and B with the use of different colors. (Green: area morphologically and functionally similar to the proximal tract; Blue: area morphologically and functionally different from the proximal tract. Image created using biorender.com.

Introduction

While extensive and accurate intestinal morphological and functional studies have been performed in several livestock species such as pig and poultry [46,66], similar detailed characterization are still limited in fish species, including rainbow trout (RT). This because, fish is an extremely various and heterogeneous group of vertebrates [17]. Teleost constitute the largest category among vertebrate animals accounting of around 32,500 species belonging of 515 different families [67]. Their gastrointestinal tract is able to quickly and reversibly adapt to environmental changes based on their physiological requirements. Moreover, their alimentary canal morphology is strongly conditioned by different feeding habitats, food and frequency of food intake, as well as taxonomy, body size and shape [18], making its extensive study and characterization challenging.

Furthermore, classical histological parameters and evident changes in mucosal architecture (e.g folds shortening and branching, nuclear positioning disparity, widening of the lamina propria, presence of supranuclear vacuolization within the proximal intestine and their absence within the distal tract and presence of intraepithelial lymphocytes), are currently used to evaluate the RT gut health.

Moreover, most of these studies are focused on the proximal portion of the gut while the more distal one is less considered. This is presumably because while the mucosa of the proximal intestine is simple in terms of organization, the one lining the more distal tract presents typical complex mucosal folds which have been only poorly described [28]. In addition, only a few studies report extensive quantitative data, do not often consider animal growth and rarely animals are reared in standardized and optimal conditions. Therefore, this chapter described a detailed characterization of the intestinal epithelial cells in rainbow trout along the

first year of development to establish accurate reference values and parameters to develop a predictive *in vitro* model.

Methodologies

Sample collection

A total of 15 female rainbow trout *(Oncorhynchus mykiss)* (weighing n=5: 50g, n=5: 150 g, n=5: 500 g) were raised at Skretting Italia Spa (Verona, Italy) and were maintained in 600 L volume tanks with a water flow of 700 L/h and were reared under a photoperiod regimen of 24 h light. The water temperature was maintained constant at 15 ∘C. RT were fed a with commercial diet formulation (Optiline, Skretting) characterized by stepwise increase of digestible energy : 18 MJ/kg up to 50 g, 18.5 MJ/kg from 50 to 150g and 19 MJ/kg up to 500g (table 1).

Table 1: Nutritional values of the administered diet (Optiline, Skretting)

Composition %	1st period (up to 50 g)	2nd period (up to 150 g)	3rd period (up to 500g)
Crude Protein	43.0	42.0	40.0
Crude Fat and Oils	20.0	22.0	24.0
Crude Fiber	3.0	3.0	3.0
Crude Ash	6.5	6.0	6.0
Phosphorus	0.9	0.9	0.9
Digestible Energy (MJ/kg)	18.0	18.5	19.0

Animals included in this study were healthy and raised in optimal conditions. Rainbow trout were euthanized according to current Italian regulation.

Immediately after sacrifice, a longitudinal incision along the ventral line was performed and the whole gastrointestinal (GI) tract was removed. Several unopened pieces were taken from both proximal and distal intestine. The anterior

intestine was defined as the region comprised between the pyloric sphincter and the ileum-rectal valve. For consistency, only the segments with annexed pyloric caeca were sampled. The tract downstream of the ileum-rectal valve characterized by larger diameter, darker pigmentation and circularly arranged blood vessels was considered as the posterior intestine [65].

Samples processing

Samples for histology were promptly fixed in 10% neutral buffer formalin for 24 h in agitation at room temperature. They were then dehydrated in graded alcohols, cleared with xylene and embedded in paraffin. Paraffin blocks were stores at -20°C until sectioning. Sections of 5 μm were cut using a rotary microtome (Microm HM335E) placed on glass slides and stored on a heating plate at 37°C overnight.

Histology

After dewaxing and re-hydration, thin sections of 5 μm were stained with hematoxylin/eosin (HE) to evaluate the morphological features of the intestine. Other sections were stained with Periodic acid–Schiff (PAS)-Alcian Blue (AB) for the qualitative characterization of goblet cells mucous substances. Slides were treated with Alcian blue pH 2,5 staining solution to identify acid mucins and then exposed to periodic acid solution and Shiff's reagent to recognize neutral mucins. Lendrum's staining was used to identify acidophilic granules containing cells in the rainbow trout intestine. Sections were exposed to Phloxine B to highlight acidophilic compounds and then to Tartrazine to remove the background.

Morphometric evaluation

Stained slides were examined under a Nikon Eclipse E600 microscope equipped of a Ds-fi2 camera and the NIS-Elements software package. Slides were

then scanned at the Interdepartmental Centre Of Advanced Microscopy (NoLimits) using the NanoZoomer S60 Digital slide scanner (C-13210-01, Hamamatsu) that rapidly scans glass slides converting the images into digital data. Images were then observed at continuous magnifications between 20 and 400 through NDP.view software. In the proximal tract, 20 folds from each individual were randomly chosen and measured using a dedicated feature on NDP.view software.

In order to reduce the wide standard deviation and facilitate a meaningful statistical analysis, these were divided into two arbitrary groups: shorter and longer than 400 μm. Using the same procedure, 20 folds and 10 complex folds from the distal intestine of each individual were measured.

Goblet cells characterization

All goblet cells distributed along 1 mm of epithelium as either neutral (magenta, PAS- positive), acidic (light blue, AB- positive) or mixed (dark blue, AB/PAS positive) were counted for each intestinal compartment.

Goblet cells quantification

In order to quantify goblet cells, two parameters were considered: the density relative to the epithelium and the volume of the secreting granule.

The goblet cell density was evaluated by counting the number of active goblet cells for 1mm of epithelium on each sample. In distal tracts 1mm of epithelium was considered for each intestinal compartment. Instead, the volume of granules was observed through an accurate measurement of the mucus-secreting granule circumferences (using a measuring feature of NDP.view software). For the measurement, 50 goblet cells in the proximal intestine and 100 goblet cells from the distal intestine (50 from the parietal epithelium and 25 for both basal ad apical part of the complex *plicae*) were chosen, randomly but with caution to pick only round-

shaped granules. From the circumference (C), the radius (r) was deducted using the simple equation $r = \frac{C}{2\pi}$.

Once the radius is known, $V = \frac{4\pi r^3}{3}$ makes it possible to estimate the volume (V) of mucus about to be secreted from each granule.

Quantitative stereological analysis

Systematic sampling and quantitative measurements were performed in agreement with the principles of design-based stereology [68], as described in detail previously (sections of5 µm thick, were cut perpendicular to the longitudinal axis of each organ (vertical sections) and collected at systematic random positions. HE-stained vertical sections were used to estimate the volume densities (Vv) of the separate intestinal layers following the general principle of Delesse [68]. The volume of each layer was estimated from the fractional area of the structure of interest (e.g., the mucosa) and the total area of the reference compartment (i.e., the intestinal wall). Area-measurements were performed by point-counting, as specified below. For estimation of the volume densities of the different layers, the regions of interest containing the respective reference compartments were defined in the histological sections. Within these regions of interest, randomly sampled areas (70% of the total sectional area of the region of interest) were systematically photographed and superimposed with an adequately sized grid of equally distant points. The number of points hitting the interested structure and the respective reference compartment were counted and the fractional area of the structure of interest and the total area of the reference compartment were then calculated from the respective quotient of points hitting these structures [65]. The magnification was chosen to allow the relevant portion of the intestinal wall to be contained in each field of vision.

V_v were expressed as percentages and were calculated as follows:

V_v (analyzed compartment, reference compartment)= [$\sum$ P (analyzed compartment)/ $\sum$ P(reference compartment)] x 100

where $\sum$P(analyzed compartment) is the number of points hitting the compartment under study and $\sum$P (reference compartment) is the number of points hitting the relevant structure.

Histochemistry

The alkaline phosphatase expression was used as a marker of intestinal epithelial cell differentiation. Briefly, slides were rehydrated and brought to distilled water, then sections were immersed in freshly Tris HCL (pH 9.5) solution for 5 minutes to create the alkaline environment. Slides were then exposed to BCIP/NBT (Vector Laboratories, SK-4500 USA) (5-bromo-4-chloro-3-indolyl phosphate/ nitroblue tetrazolium) substrate which produces an indigo reaction product in the presence of alkaline phosphatase (AP) enzyme. Sections were then rinsed in tap water, counterstained using Mayer's hematoxylin, dehydrated and permanently mounted.

Immunohistochemistry

We tested several antibodies, specific for the following antigens to characterize different cell population in the intestinal mucosa:

- *Homeodomain-only protein homeobox* (HOPX): a typical marker of quiescent stem cells which occupies the fourth position from the crypt base in mammals' intestine

- *Sex-determining region Y-box 9+* (SOX9 and SOX9a): a transcription factor expressed by active stem cells and by the transient amplifying population

- *Cleaved Caspase-3* (CASP3): a molecule that marks cells undergoing apoptosis

- *Leucine rich repeat containing G protein-coupled receptor 5* (LGR5): specific marker of highly cycling intestinal stem cells

- *Lysozyme* (LZY): as an indirect marker to evaluate the presence of Paneth cells

- *Proliferating cell nuclear antigen* (PCNA) as marker of cells in mitosis

However, only PCNA antibodies gives a specific and repeatable signal. Main antibodies features are summarized in Table 2.

Table 2: main antibodies features

	SOURCE	CAT.N	HOST	CONCENTRATION
HOP (FL-73)	Santa Cruz	Sc-30126	Rabbit	1:500-1:120-1:50
SOX9	Millipore	Ab5535	Rabbit	1:250-1:125-1:50
SOX9A	GeneTex	128370	Rabbit	1:200-1:100-1:50
CASP3	Cell Signaling	9661s	Rabbit	1:250-1:125
PCNA	Millipore	MAB424R	Mouse	1:1600
LGR5	Novus Biologicals	NBP1-28904	Rabbit	1:100-1:30
LGR5	Custom	-	Rabbit	1:125-1:230-1:50
LZY	Diagnostic biosystem	RP028	Rabbit	1:125-1:150

Specific antigen localization was characterized by indirect immunohistochemistry using the Avidin Biotin Complex method (VECTASTAIN® Elite® ABC, Vector Laboratories, USA) following manufacturer instructions. Briefly, slides were brought to boiling in 10 mM sodium citrate buffer, 0.05% Tween20 (pH 6) in a pressure cooker for 1 minute for antigen retrieval. After cooling at room temperature for 20 min, sections were rinsed in PBS (phosphate-buffered saline, pH 7.4) and then were immersed in a freshly prepared 3% H_2O_2 solution in methanol for 15 minutes to block the endogenous peroxidase. Aspecific binding was prevented incubating sections in Normal Blocking Serum Vectastain (ABC Elite KIT) at room temperature for 30 minutes. Sections were incubated with primary antibody, diluted in 4% BSA in PBS with 0.05% Tween20, for 60 minutes at room

temperature in a humid chamber. Sections were then incubated with appropriate biotinylated secondary antibody for 30 minutes at room temperature in a humidified chamber followed by the avidin-biotinylated horseradish peroxidase (HRP) complex (Vectastain ABC Elite KIT) for another 30 minutes. Finally, sections were incubated with ImmPACT NovaRED substrate (Vector Laboratories, SK-4105, USA) which produces a red reaction product in the presence of peroxidase (HRP) enzyme. Sections were then briefly counterstained with Mayer's hematoxylin, dehydrated and permanently mounted with an aqueous mounting media (Biomount®, Bio-Optica, Italy). Secondary antibodies controls were performed following the same staining protocol but omitting the primary antibody.

TUNEL test

Peroxidase *in situ* detection Apoptosis kit (Millipore Corporation, S7100, USA) was used to detect cell undergoing apoptosis following the manufacturer indications. In brief, sections were brought to boiling in 10 mM sodium citrate buffer, 0.05% Tween20 (pH 6) in a pressure cooker for 1 minute to improve the access of the terminal deoxynucleotidyl transferase (TdT) to the fragmented DNA. Slides were then cooled at room temperature for 20 minutes, washed in PBS, and incubated in a humidified chamber for 15 minutes in 3% H_2O_2 in methanol to quench endogenous peroxidase. Sections were rinsed in distilled water, exposed to equilibration buffer (Millipore Corporation, S7100, USA) for 20 seconds and incubated with TdT enzyme digoxigenin-conjugated in a humidified chamber at 37°C for one hour. TdT enzyme was previously diluted in reaction buffer (1:32) (Millipore Corporation, S7100, USA).

Reaction was stopped by immersing sections in fresh prepared stop/wash buffer in Coplin jar for 10 minutes. Anti-Digoxigenin peroxidase conjugated antibody was applied to slides for 30 minutes at room temperature. Samples were then washed in PBS and were incubated with diaminobenzidine solution (ImmPACT® DAB, SK-4105 Vector Laboratoris, USA), which in presence of

peroxidase (HRP) enzyme, produces a brown reaction product. Sections were then briefly counterstained with Mayer's hematoxylin, dehydrated and permanently mounted with an aqueous mounting media (Biomount®, Bio-Optica, Italy).

Statistical analysis

Quantitative data were expressed as mean ± SD. Results were analyzed by using One-way or Two-way analysis of variance (ANOVA) followed by all-pairwise multiple comparison test with the Holm–Sidak method. Differences were considered statistically significant if $p < 0.05$.

Results

Gross anatomy evaluation

Macroscopically, the intestine corresponded to the expectations according to previous descriptions of this organ in teleost fish species (Figure 7A). It comprised of a proximal intestine, with annexed hollow-tubes called pyloric caeca emerging from its cranial region, and a distal intestine. The latter is characterized by a larger diameter, dark pigmentation and circularly arranged blood vessels. Circular folds protruding from the distal intestinal wall towards the lumen were also evident (Figure7B).
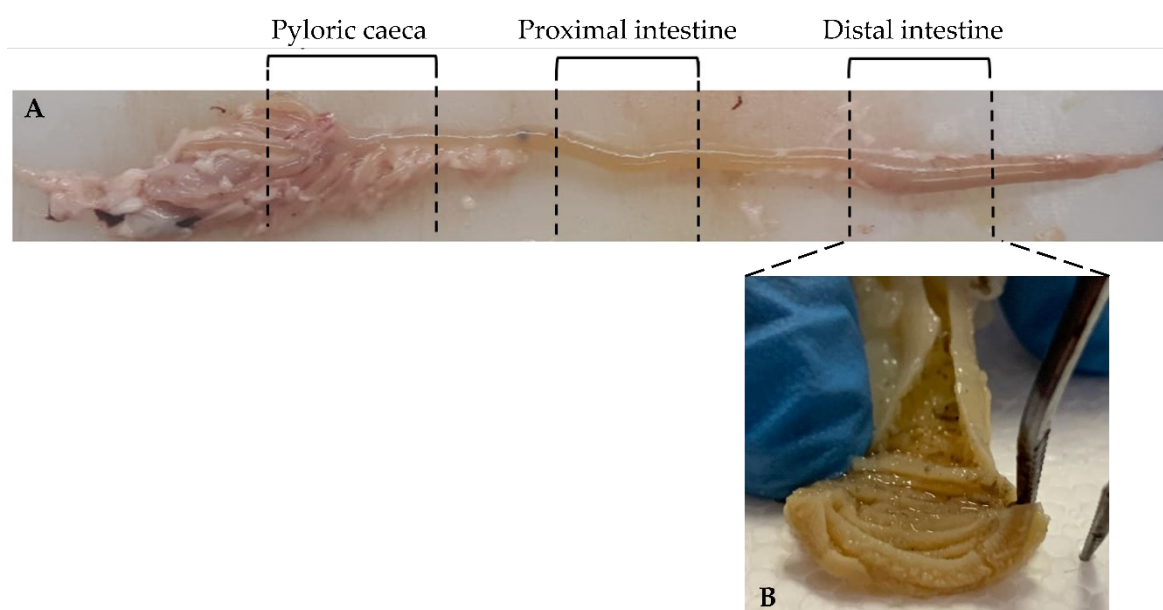

Figure 7: Complete view of rainbow trout intestine comprising of proximal intestine with annexed pyloric caeca and distal intestine with microscopical zoom on the internal folds (A); Up-close view of the folds in a sample of distal intestine length wisely opened (B)

Morphological and morphometrical evaluation

Hematoxylin and eosin staining confirmed a substantial morphological difference between proximal and distal intestine. In proximal intestine, the mucosa is regularly covered by numerous folds. These finger-like protrusions are disposed radially, with numerous swollen goblet cells and a wide variation of length between

one another. Short villi (below 400 µm) length remains constant during growth, whereas long villi (above 400 µm) increase significantly their length when animals reach 500g (Table 3) (P>0.05).

Table *3*: Histometric values of folds length and width and evaluation of folds branching along development (5 individuals/each weight)

Trout weight	Proximal intestine			
	Short folds length (µm)	Long folds length (µm)	folds width (µm)	folds branching
50g	251 ± 13.5	470.4[a] ± 64.6	96.0[a] ± 11.4	-
150g	310.3 ± 44.5	555.8[a] ± 28.7	122.9[b] ± 10.1	+
500g	250.3 ± 42.1	657.8[b] ± 49,1	116.9[b] ± 14,4	++

Values are expressed as mean ± SD
[a-b] different superscripts in same column indicate significant differences (P<0.05)

Moreover, short folds became rarer and a significant increase in folds branching was also observed along development (Figure 8).

In the distal intestine a more articulated structure was observed (Figure 9). Indeed, the distal intestinal wall showed complex folds regularly interspersed among numerous folds apically covered by supranuclear vacuolization, from which secondary folds arise (Figure 10). Folds emerging from the apex of the complex fold exhibited a different morphology: they were devoid of pinocytotic vacuoles, with goblet cells scattered around, resembling the ones in the proximal tract (Figure 11).

Morphometric measurements in the distal intestine did not highlight any difference (P>0.05) neither in folds length, nor in complex fold height , between 150g and 500g individuals, as shown in table 4. Folds as well as complex folds in the distal tract had to be measured on longitudinally embedded samples, since the complexity of the architecture did not allow an optimal view of the structure on transversal segments. Samples of 50g individuals were too small to be handled without undermining the mucosal organisation; therefore, these were omitted from the analysis.

Table 4: Histometric values of simple and complex folds length (5 individuals/ each age)

Trout weight	Distal intestine		
	Complex Fold height (μm)	Short folds length (μm)	Long folds length (μm)
50g	-	-	-
150g	1284.9± 51	211.1 ± 3.1	592.4± 19.3
500g	1410.1± 201.7	202.4± 60.1	556.5± 37

Values are expressed as mean ± SD

Stratum compactum and granulosum of the submucosa are not evident in the complex folds of the distal tract. Instead, the tunica muscularis is clearly present within the whole intestine, including the folds.
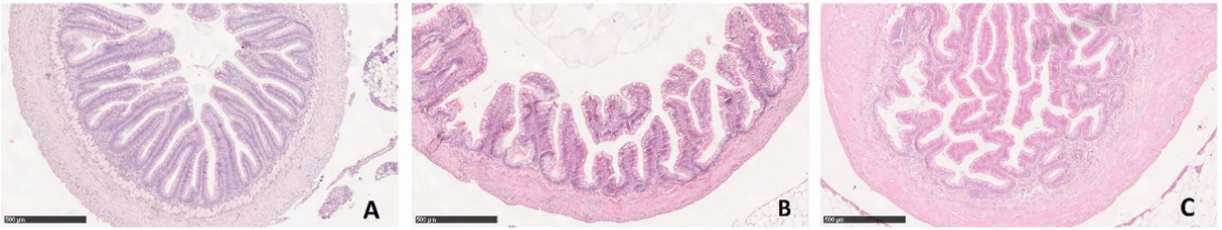
Figure 8: Folds branching in the proximal intestine during growth (A:50g; B:150g; C:500g); scale bar 500 µm
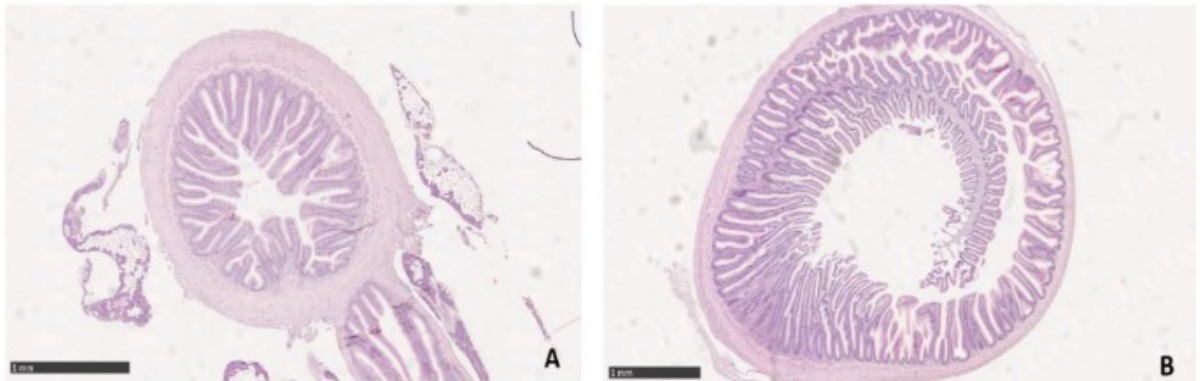

Figure 9: H&E staining of a section of proximal intestine. Pyloric caeca are slightly visible on the bottom right corner (A); Section of distal intestine with an optimal view of the internal fold, which seen transversally acquires a spiral-like form (B).
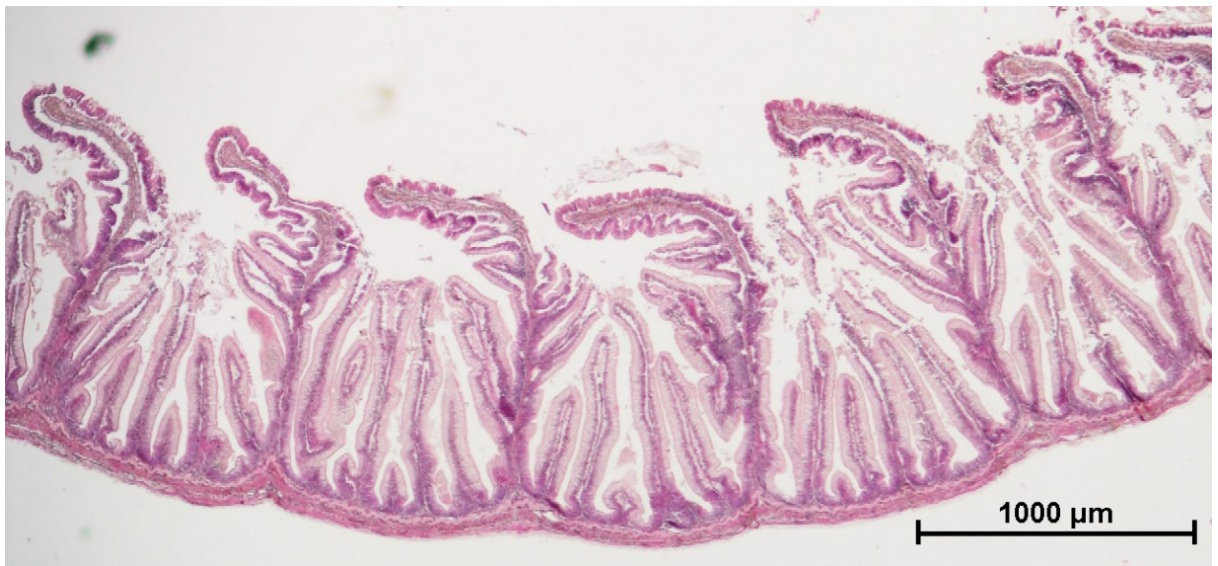
Figure 10: Longitudinal view of the distal tract: complex folds regularly interspersed between simple folds are evident. Ulterior folds can be seen branching-off from these structures.

Figure 11: Zoomed in view of a complex fold in the distal intestine: parietal folds are covered by pinocytotic vacuoles (A), as well as folds emerging from the basal side of the fold (B, C). At one point, the epithelium morphology along the fold drastically changes (D) and the apex of the fold presents goblet cells and non-vacuolated enterocytes (E).

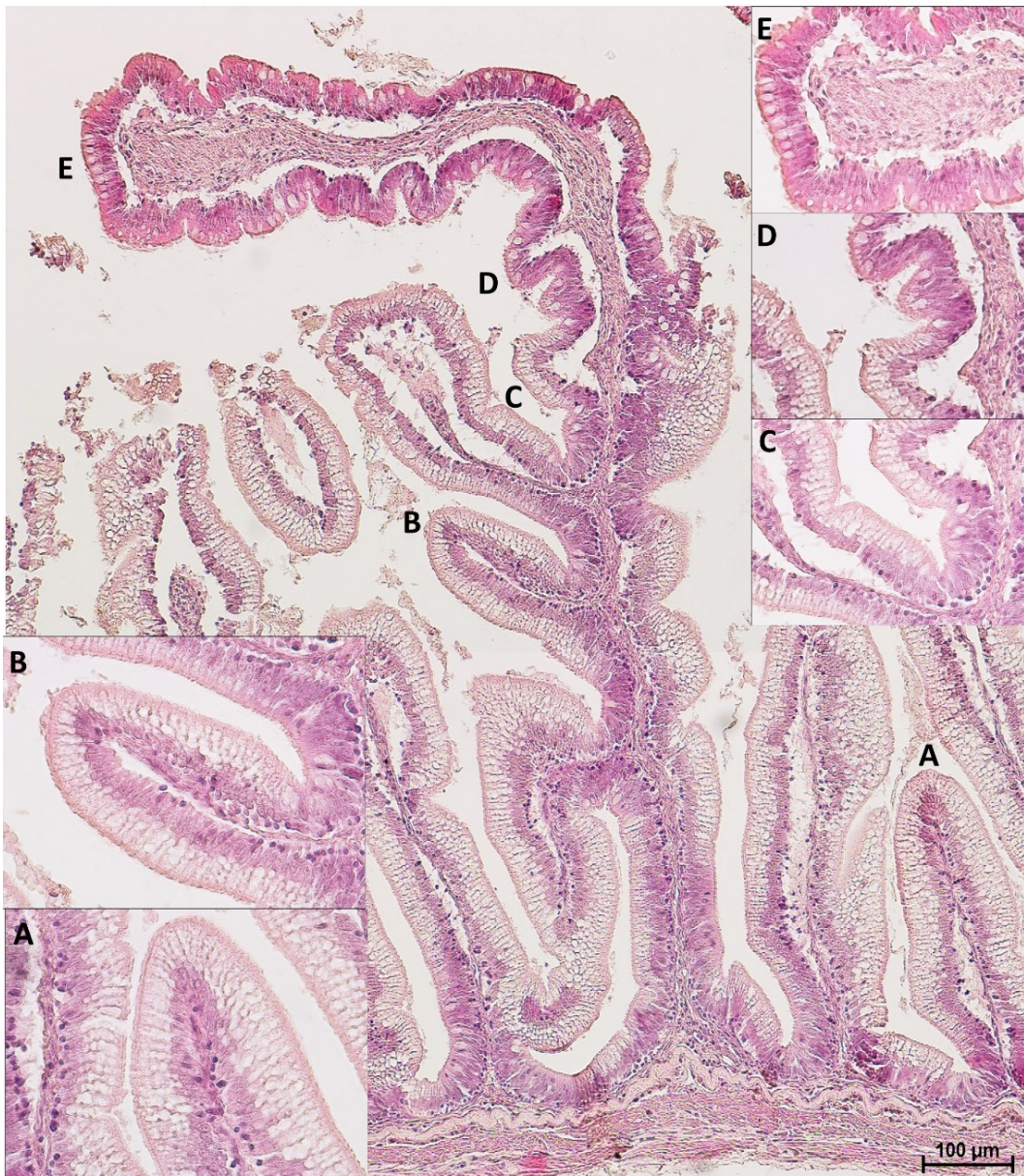Typical inflammation features such as villi shortening, nuclear positioning disparity, anterior intestine enterocytes vacuolization and lamina propria thickening were not observed. Few intraepithelial lymphocytes were found.

Quantitative Stereology

Volume estimation of each intestinal layer indicated that the mucosa was the predominant layer in both intestinal tracts. However, its volume was significantly higher in the distal than in the proximal part of the intestine at all ages (Figure 12-13). Furthermore, in the proximal intestine the volume of the mucosa gradually increased in individuals of 150 and 500 g. On the contrary no significant changes were observed in the volumes of the different layers of the distal intestine ($P>0.05$). The epithelium : lamina propria ratio within the same intestinal tract remained constant along the period considered.
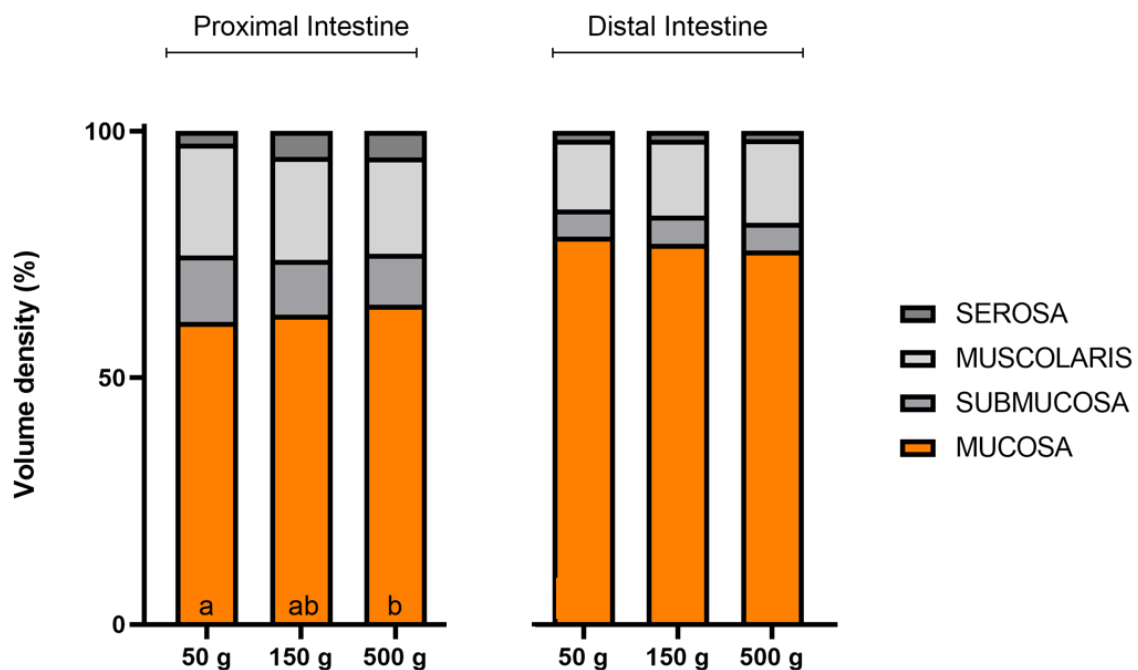

Figure 12. Volume density estimation of each intestinal layer of the proximal and distal intestine along the three stages of the development.
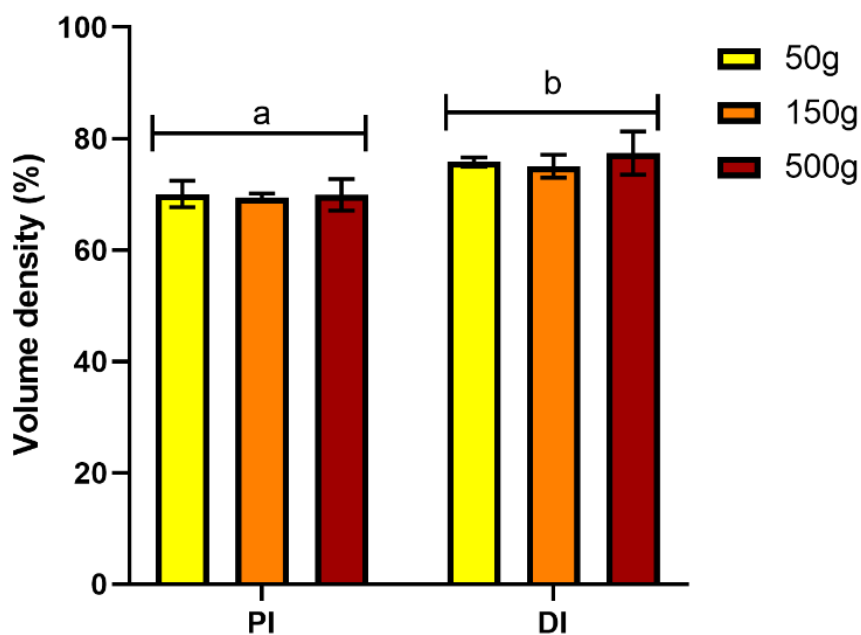
Figure 13: Volume density estimation of the intestinal mucosa in the proximal and distal intestine along the three main stages of the development

Goblet cells characterization

As expected, AB-PAS staining revealed that mucus in goblet cells is heterogenous. Most goblet cells in the proximal intestine were dark blue indicating the presence of a mixed population of acid and neutral granules of mucus. Instead, we observed only few light blue or magenta cells that contained exclusively acidic or neutral mucus, respectively (Figure 14). However, the percentage of cells producing solely acidic mucus significantly increased in individuals weighing 500g. Among goblet cells containing a mixed granule population, it was possible to detect a range of blue stain intensity, reflecting a mucus pH heterogeneity in the group. In the proximal tract, no differences in mucus pH were noticed between short and long folds (Figure 15).
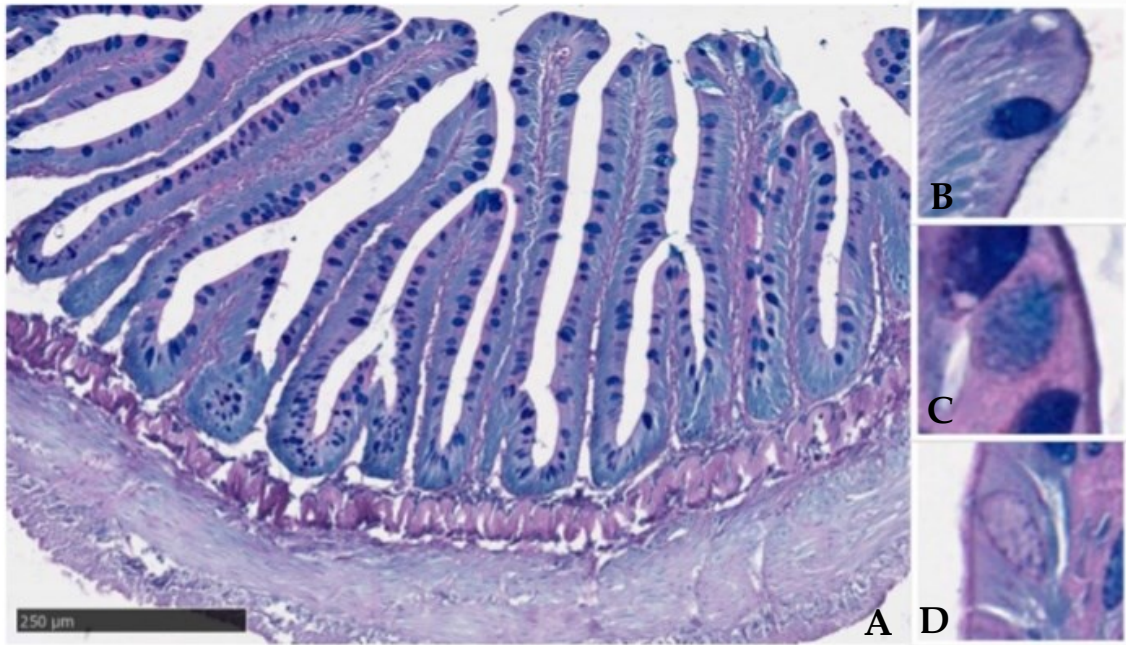
Figure 14: Representative image of AB-PAS staining (A). On the right side, an example of mixed granule (B, dark blue), acidic granule (C, light blue) and neutral granule (D, light magenta)

The same was true in the distal intestine, however the massive presence of PAS-positive pinocytotic vacuoles in the enterocytes of this tract has obstructed a more accurate quantitative analysis of goblet secretion by interfering with the mucus granules colour.
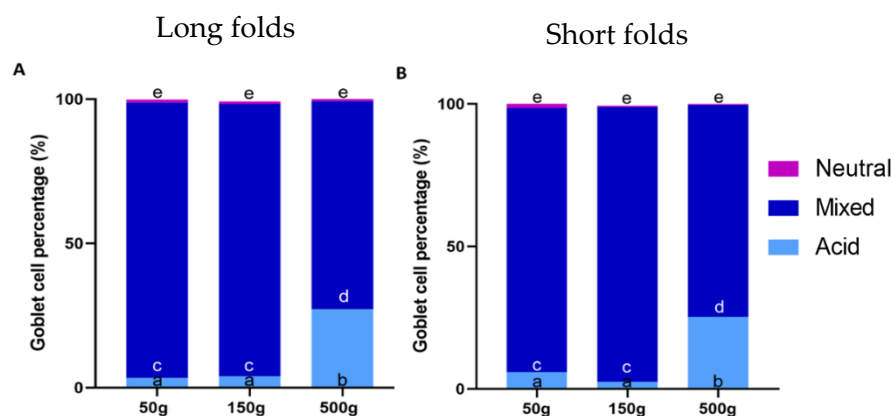
Figure 15: 100% stacked column chart describing mucus content in goblet cells of long (A) and short villi (B) in the proximal intestine. (c-d-e) different superscripts in same column indicate significant differences ($P<0.05$).

Goblet cells quantification

Goblet cells density was significantly higher in the proximal than in the distal tract. However, the number of goblet cells was not homogeneous along the length of the complex folds. At their base the number was the same as that of the shorter folds, whereas, at their apex the number of goblet cells was the same observed in the folds of the proximal intestine (Figure 16-A).

The same pattern was observed measuring the volume of goblet cells granules: these were significantly bigger and more swollen in the anterior than in the posterior intestine. However, goblet cells volume of the apical part of the complex fold has the same size of those measured in the proximal intestine (Figure 16-B).
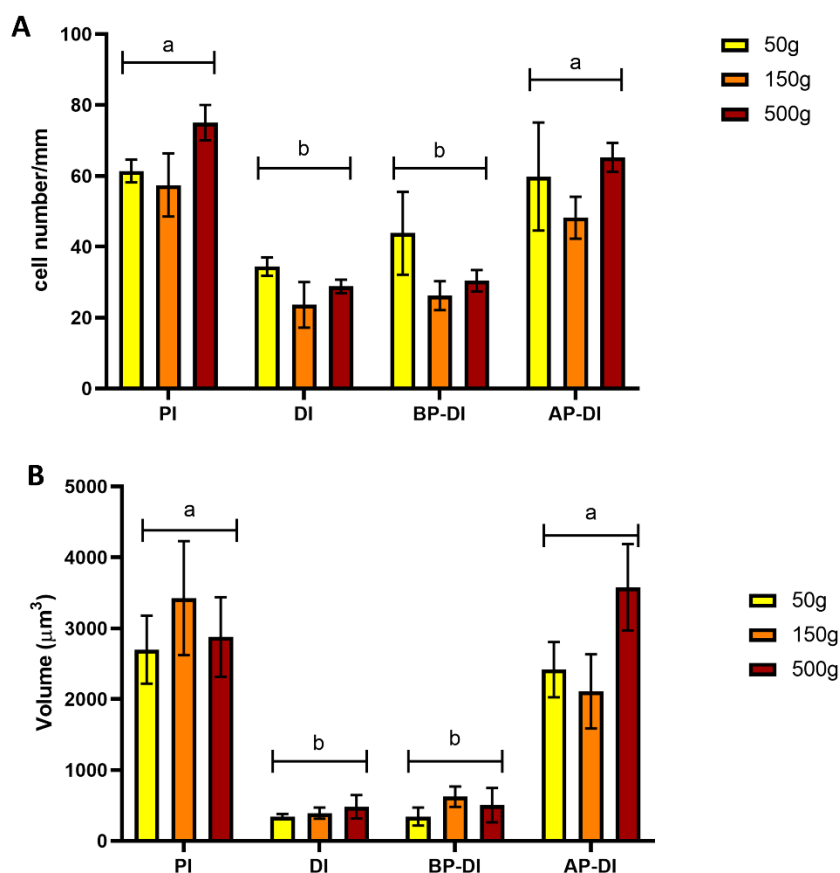

Figure 16: Column chart describing the number of goblet cells/ mm of epithelium (A) and the volume of the goblet cells granules (B) in different regions of trout intestine along development. (PI: proximal intestine folds; DI: distal intestine parietal folds; BP- DI: basal part of the distal intestine fold; AP-DI: apical part of the distal intestine fold).

Overall, our results indicate that the distal intestine is divided in two morphological compartments: one formed by the parietal villi and by the basal portion of the complex fold that is significantly different from the proximal tract, and another formed by the apical part of the complex folds that shows the same morphological characteristics of the proximal tract.

Intestinal eosinophilic granule cells

Cells positive to the Masson's trichrome and Phloxine tartrazine staining were observed in the upper and lower granulosum layers of the submucosa in both intestinal regions. At high magnification these cells showed the presence of cytoplasmatic granules enabling their classification as eosinophilic granule cells (EGC) (Figure 17). These cells, however, were negative for both alkaline phosphatase and peroxidase suggesting that EGC do not possess the morphological characteristics of Mast cells. Positive cells were also observed along the upper part of the folds within the epithelium, but no granular structures were observed in this case. This and their position indicated that these cells do not correspond to the typical Paneth cell.
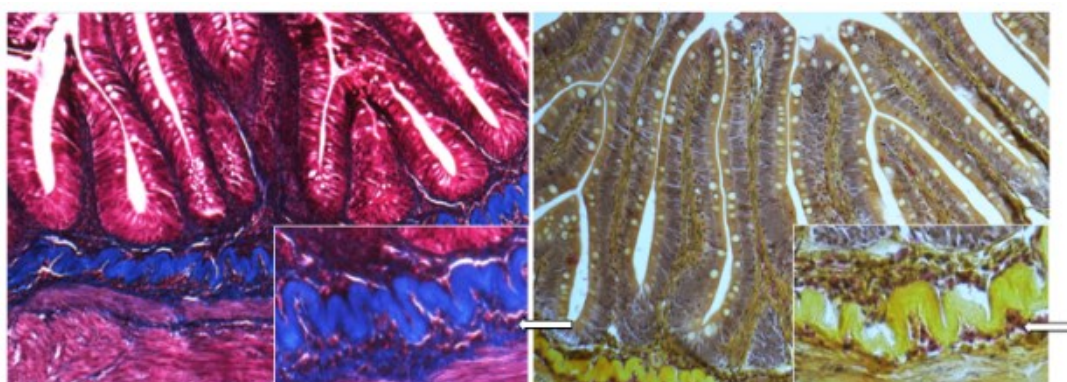

Figure 17: Representative figures of proximal intestine stained with Masson' trichrome (A) and Phloxine tartrazine (B), showing intestinal eosinophilic granule cells within the granulosum layers of submucosa (arrows*).*

Proliferation and differentiation compartments

A strong Pcna signal was detected within the intestinal folds at the basis of the folds, confirming that the stem/progenitor cell zone is located here at all ages all along the intestine. However, Pcna was not limited to the folds but was also expressed in correspondence of folds branching points in the proximal intestine. Furthermore, Pcna signal was more intense in the posterior than in the proximal intestine in all investigated stages.

Mature, fully differentiated enterocytes were identified by the histochemical detection of the alkaline phosphatase (AP) activity. As expected, the signal was detected along the folds length and at their apex. However alkaline phosphatase (AP) expression in the proximal intestine was stronger and spanned a longer portion of the folds than in the distal intestine at all ages. As expected, a more expanded AP signal corresponded to a more limited Pcna expression (Figure 18). However, it is was interesting to note that, the AP : Pcna staining pattern of the apical part of the folds to that of the proximal intestine and, different from that of pyloric caeca and to that of the basal part of complex folds (Figure 19).
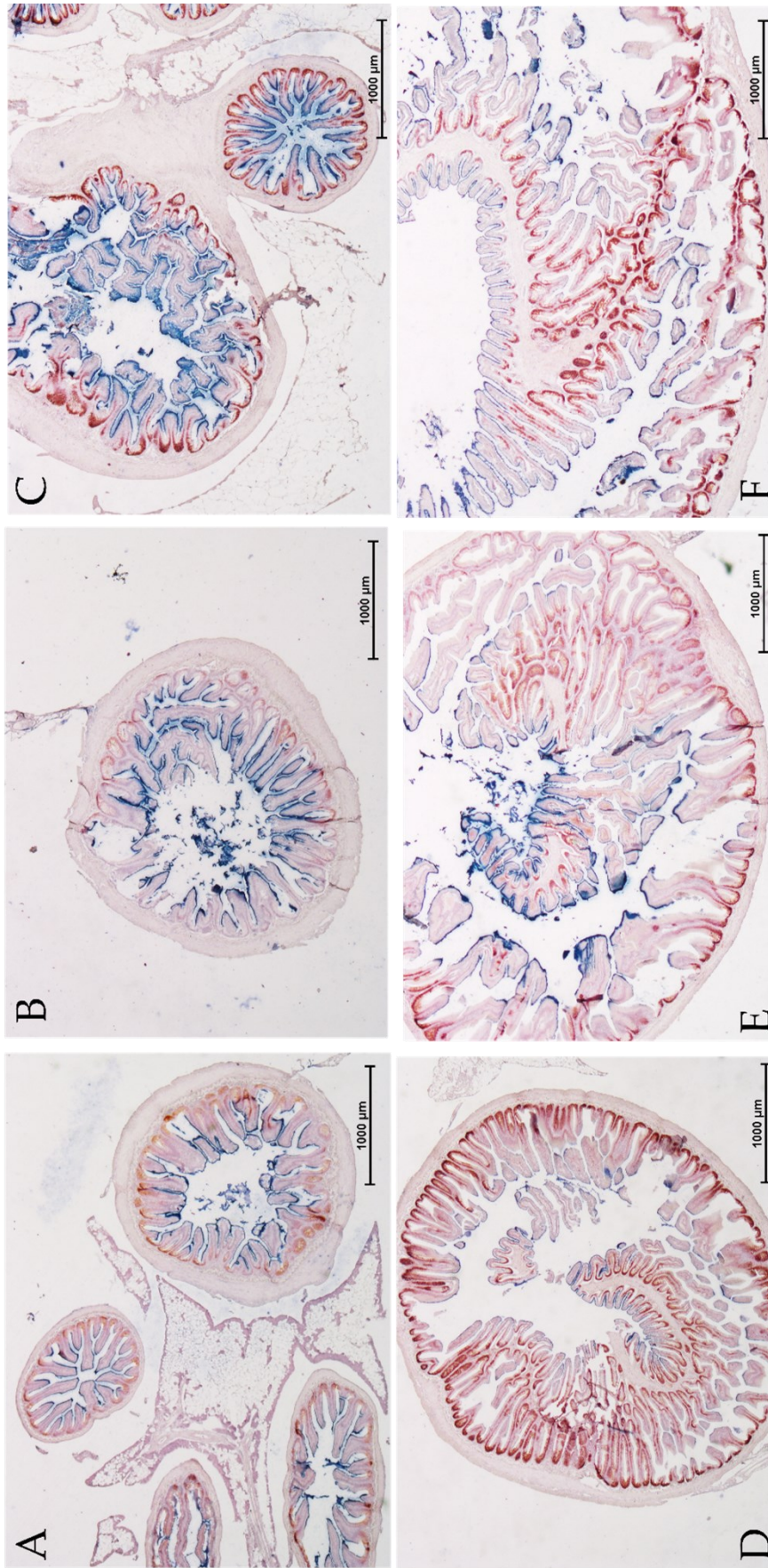
Figure 18: Figures show the distribution of the proliferation (red) and Differentiation (blue) compartments in the proximal (A-B- C) and in the distal intestine (D, E, F) along the three main stages of the development (A and D: 50 g trout, B and E: 150 g trout, C and F 500 g trout).
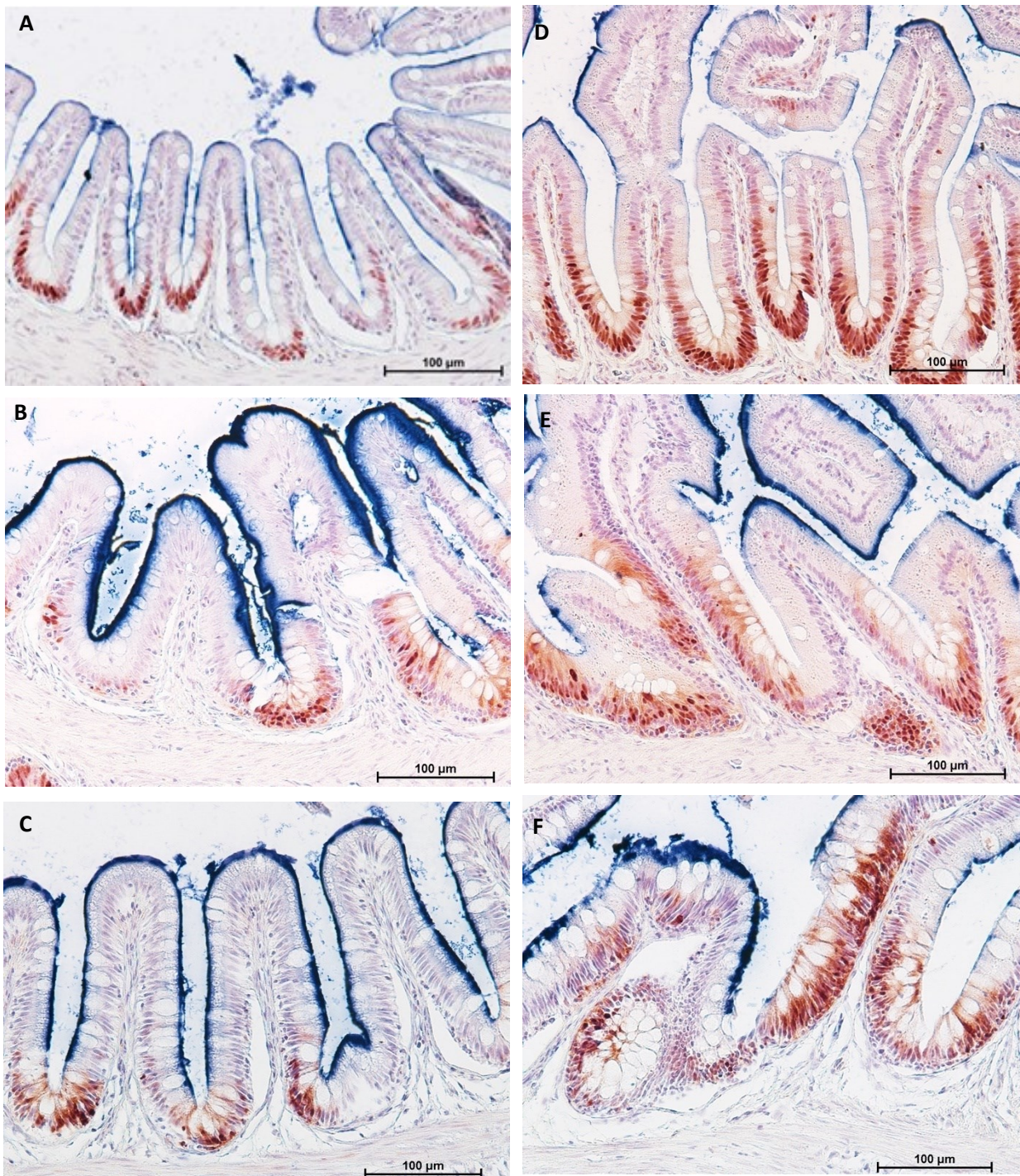
Figure 19: Distribution of the proliferation and differentiation compartment within the two regions of the complex folds of the distal intestine at 50g (A-D), 150g (B-E) and 500g (C-F), . In figures A, B and C (apical part of the complex folds) the signal of the alkaline phosphatase (blue) is extended along the folds length, while proliferation (red) is restricted to their bottom. On the contrary, in figures D, E and F (basal part of the complex folds) the proliferation (red) compartment is extended along the folds, whereas the alkaline phosphatase activity (blue) is limited at their apex.

Apoptotic cells

Cells undergoing apoptosis were detected via DNA fragmentation using the TUNEL assay all along the intestine. However only few cells undergoing apoptosis were visible in the proximal intestine and on the apical part of the complex folds of the distal, whereas, many more apoptotic cells were detected in their basal part, as well as, in the rest of the distal intestine.

Apoptotic cells presented two different morphology: round and slender (Figure 20). Round cells were present along the entire intestinal mucosa and could also be detected exfoliating into the intestinal lumen. Slender cells displayed a dark eosinophilic cytoplasm if stained with eosin, periodic acid-Shiff or phloxine and were found exclusively in the distal intestine and (Figure 21) in the basal part of the complex folds of the same tract, whereas they were absent in the proximal portion as well as at the complex folds apex.

Figure 20: Figure showing at high magnification the two different morphology of apoptotic cells obtained via TUNEL test. Arrow A indicates a slender apoptotic cell, whereas the arrow B indicates a round apoptotic cell. It is possible to observe the cells located on the villus apex preparing to undergo *anoikis*. The C arrow points a round apoptotic cell exfoliating into the intestinal lumen.

Overall it could be observed that proliferation, differentiation and apoptotic rate were not homogenously distributed along the intestinal epithelium. The distal intestine, pyloric caeca, as well as the apical portion of the complex folds were characterized by high proliferation and high apoptotic rate but low alkaline phosphatase expression, that also appeared to be fragmented. In contrast, proximal intestine and the basal part of the complex folds apex were characterized by a low Pcna expression, few round apoptotic cells and a strong alkaline phosphatase signal (Figure 22-23).
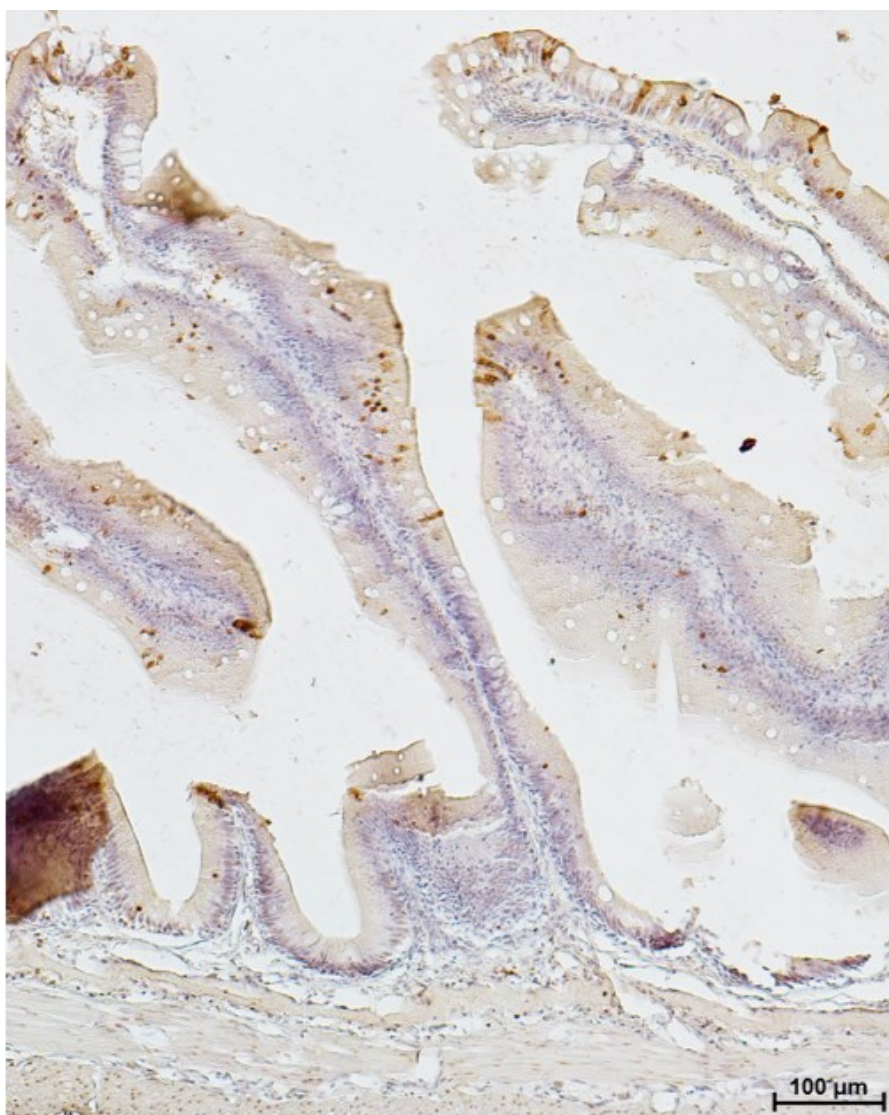
Figure 21: Representative figure showing apoptotic cells pattern in the wall of the distal intestine. The two characteristic morphologies of the apoptotic cells, funnel-like and rounded, can be observed along the folds length.
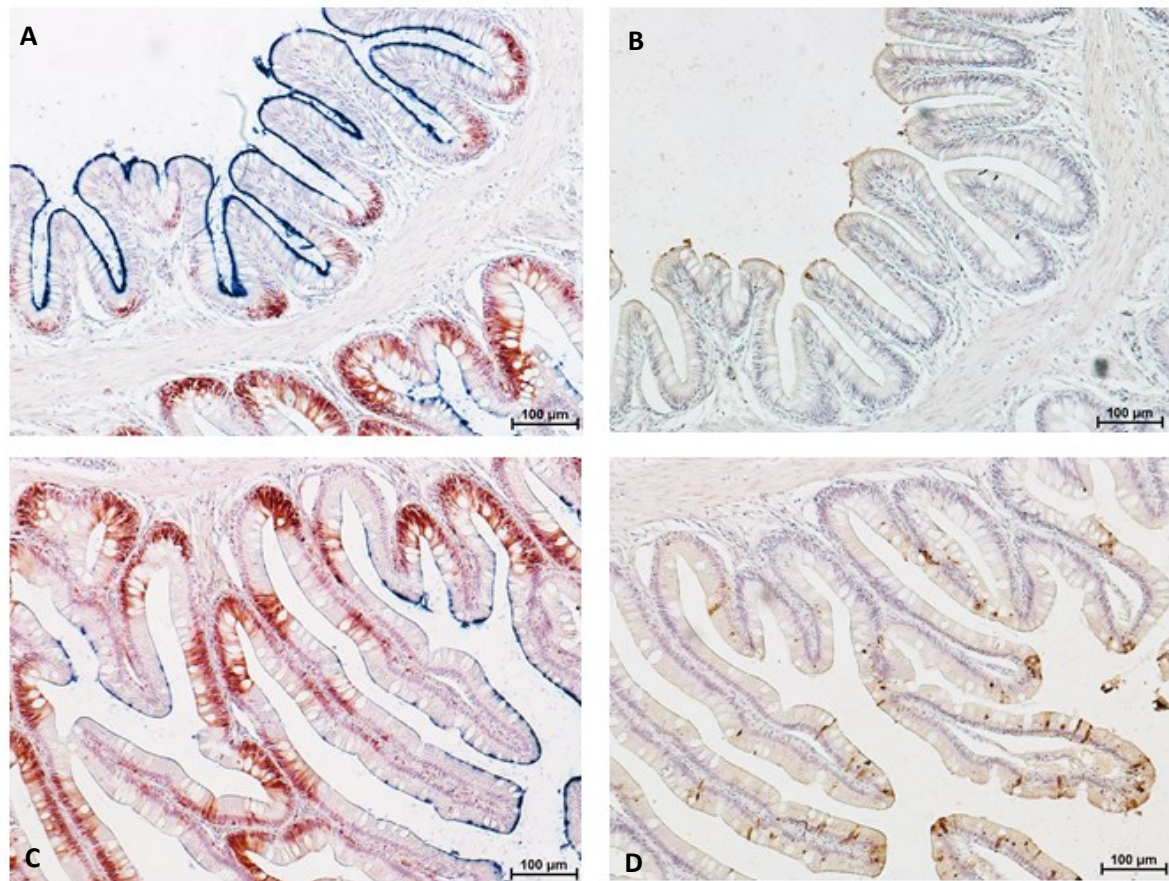
Figure 22: Representative figure of Pcna immunolocalization (red), histochemical detection of differentiated cells (blue) and in situ detection of apoptotic cells (brown). The apical part of the complex folds of the distal intestine was defined by a low Pcna expression, few round apoptotic cells and a strong alkaline phosphatase signal (A,B). On the contrary, high proliferation and high apoptotic rate associated with low alkaline phosphatase expression in the basal part of the complex folds were observed (C,D).
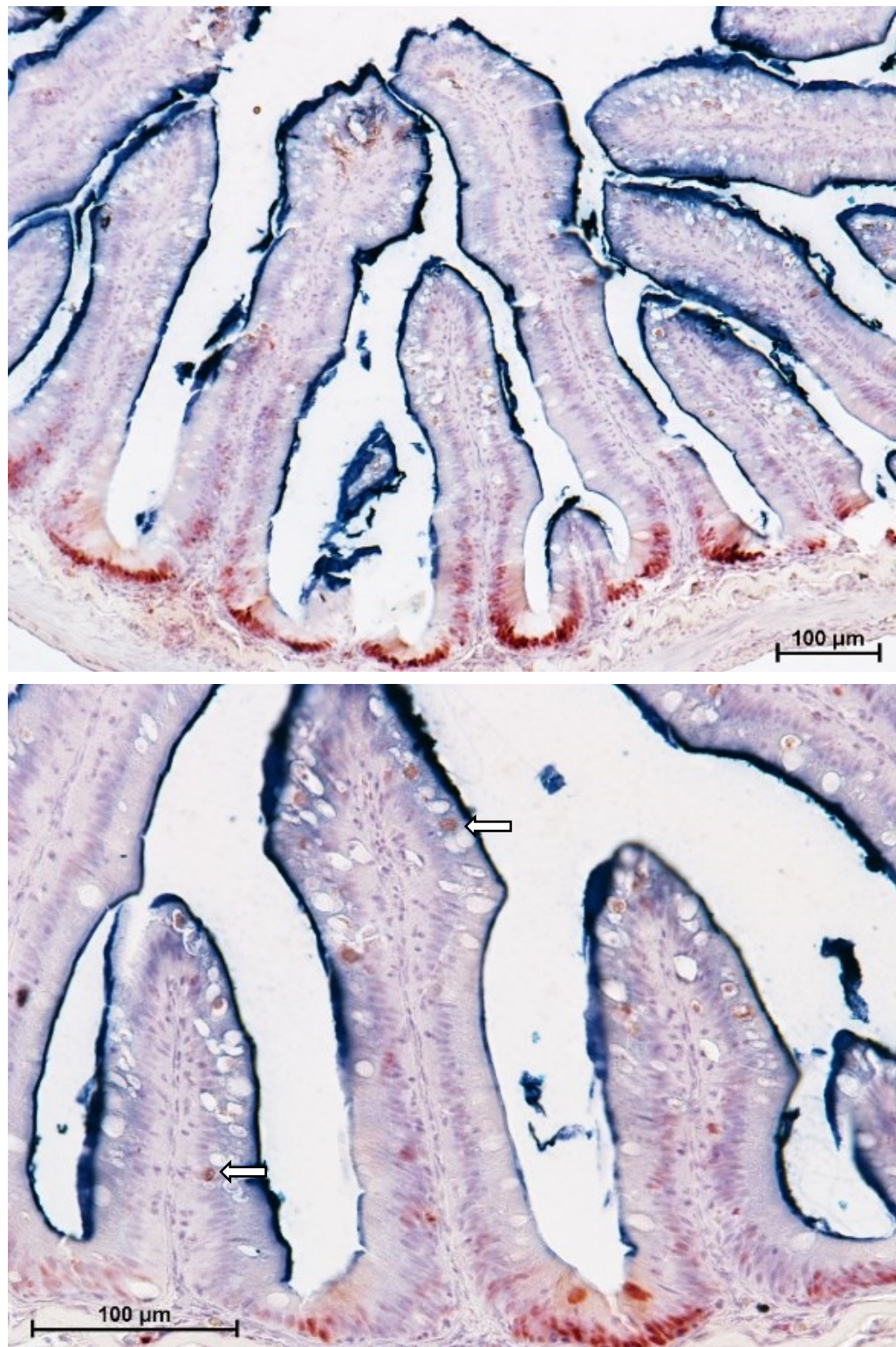
Figure 23: Representative figure of proximal intestine showing immunolocalization of proliferating cells (red), histochemical detection of differentiated cells (blue) and *in situ* detection of apoptotic cells (brown-arrows).

Functional enterocytes' marker

Peptide transporter 1 (PepT1), fatty-acid-binding protein 2 (Fabp2) and sodium–glucose/galactose transporter 1 (Sglt-1) were used as enterocytes' functional markers. A strong signal of PepT1, Fabp2 and SGLT-1 was detected in the proximal intestine, in the pyloric caeca and in the apical portion of the complex folds of the distal intestine. Instead, in their basal part, while Fabp2 and SGLT-1 were only weakly expressed, Pept1 was completely absent (Figure 24-25-26-27-28).
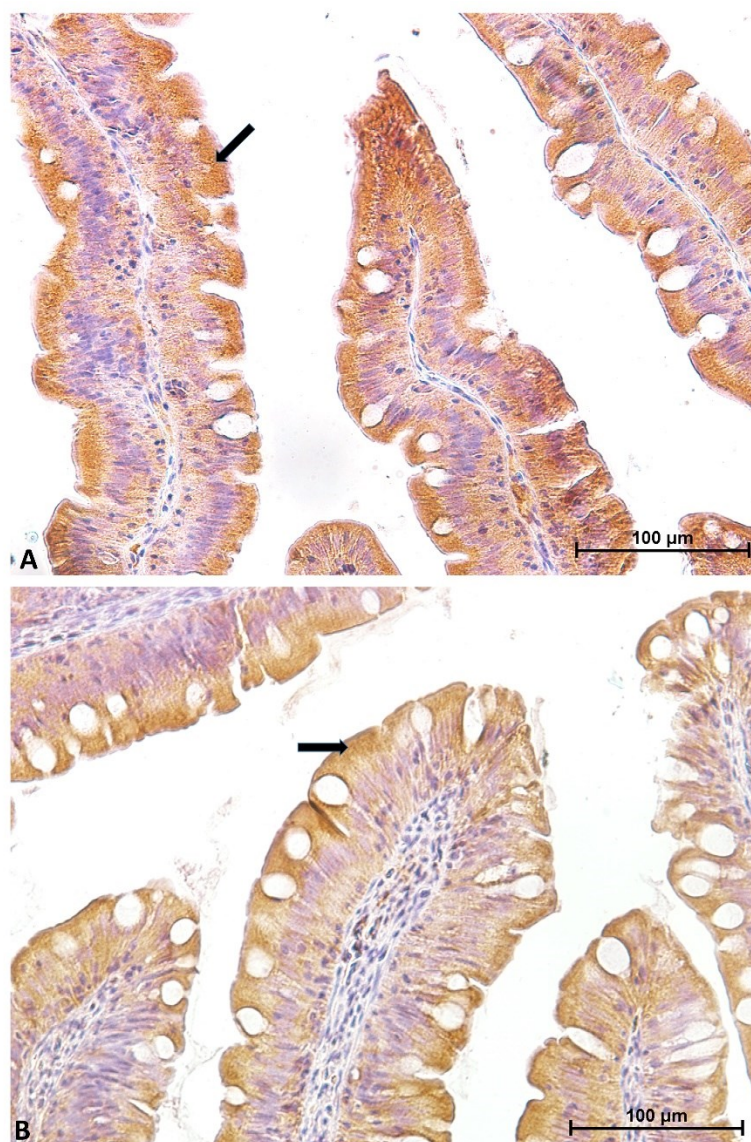
Figure 24: Representative images of pyloric caeca (A) and proximal intestine (B) showing the distribution of Pept1 (Brown-arrows). Its expression was detected along the enterocytes' brush border and in the apical part of the enterocyte's cytoplasm.
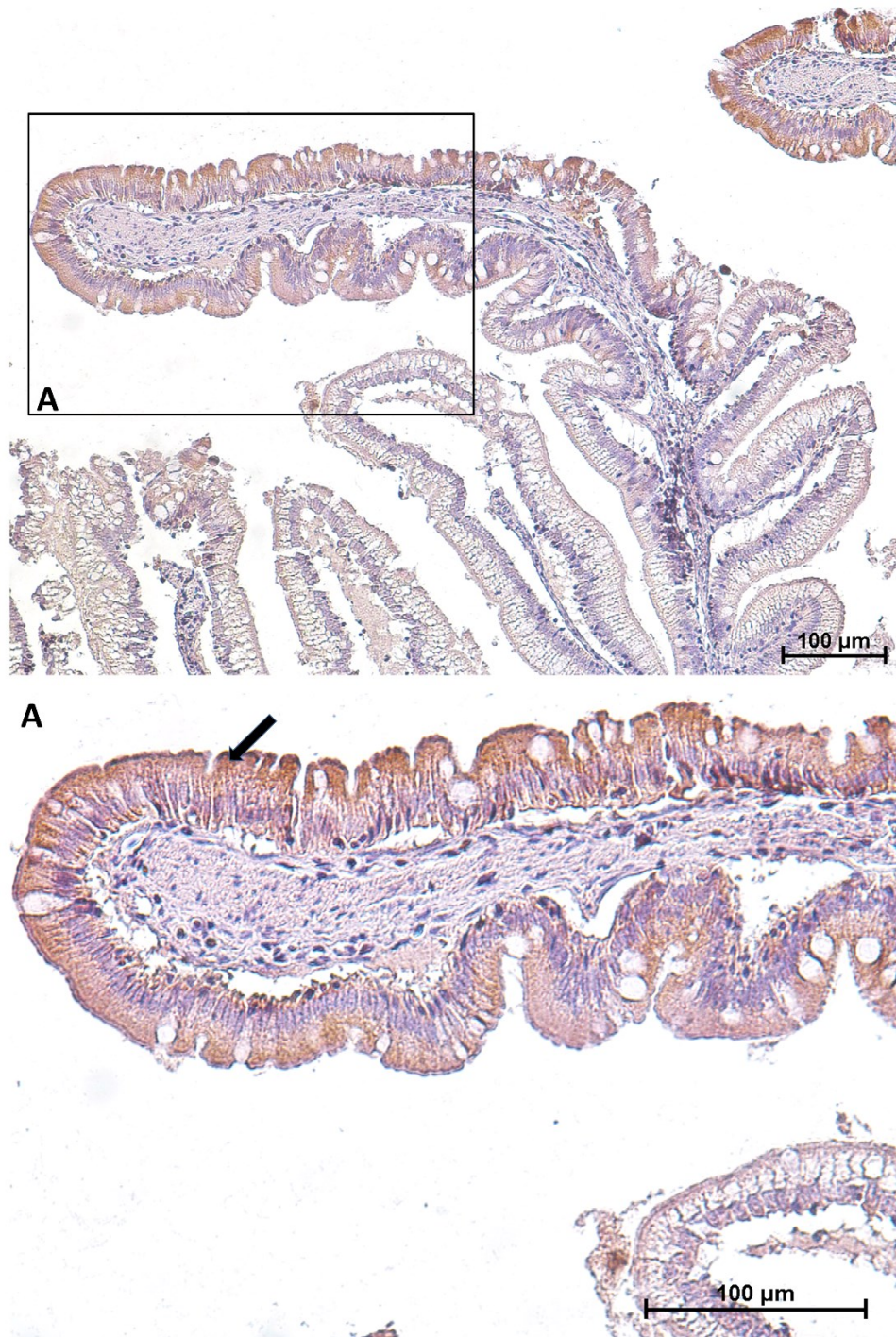
Figure 25: Representative image of the complex folds of the distal intestine showing high Pept1 expression in their apical part. Image A showed folds apex at higher magnification.
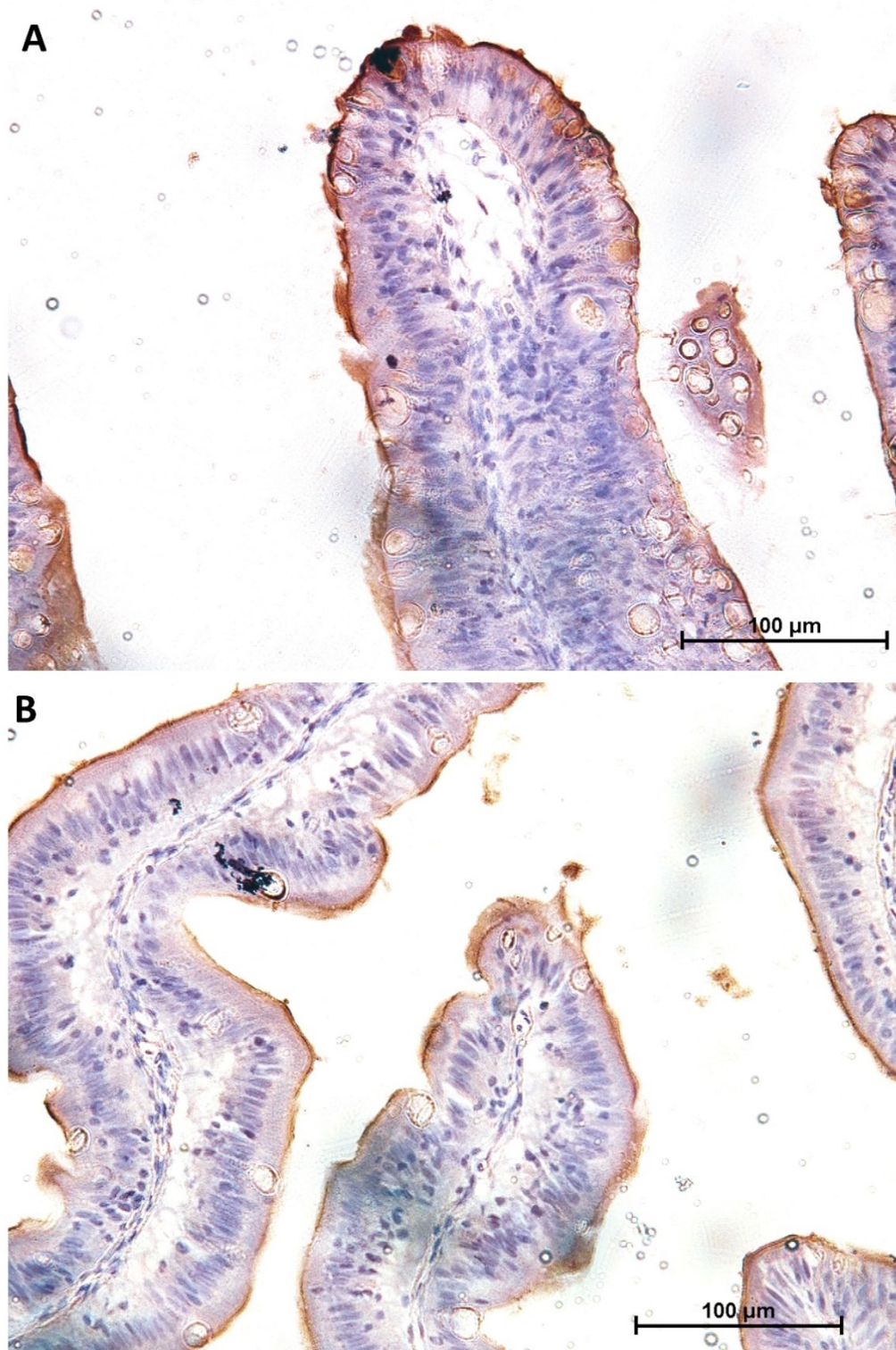
Figure 26: Representative figures showing Sglt1 distribution within proximal intestine (A) and pyloric caeca (B). The signal was limited to the enterocytes' brush border.
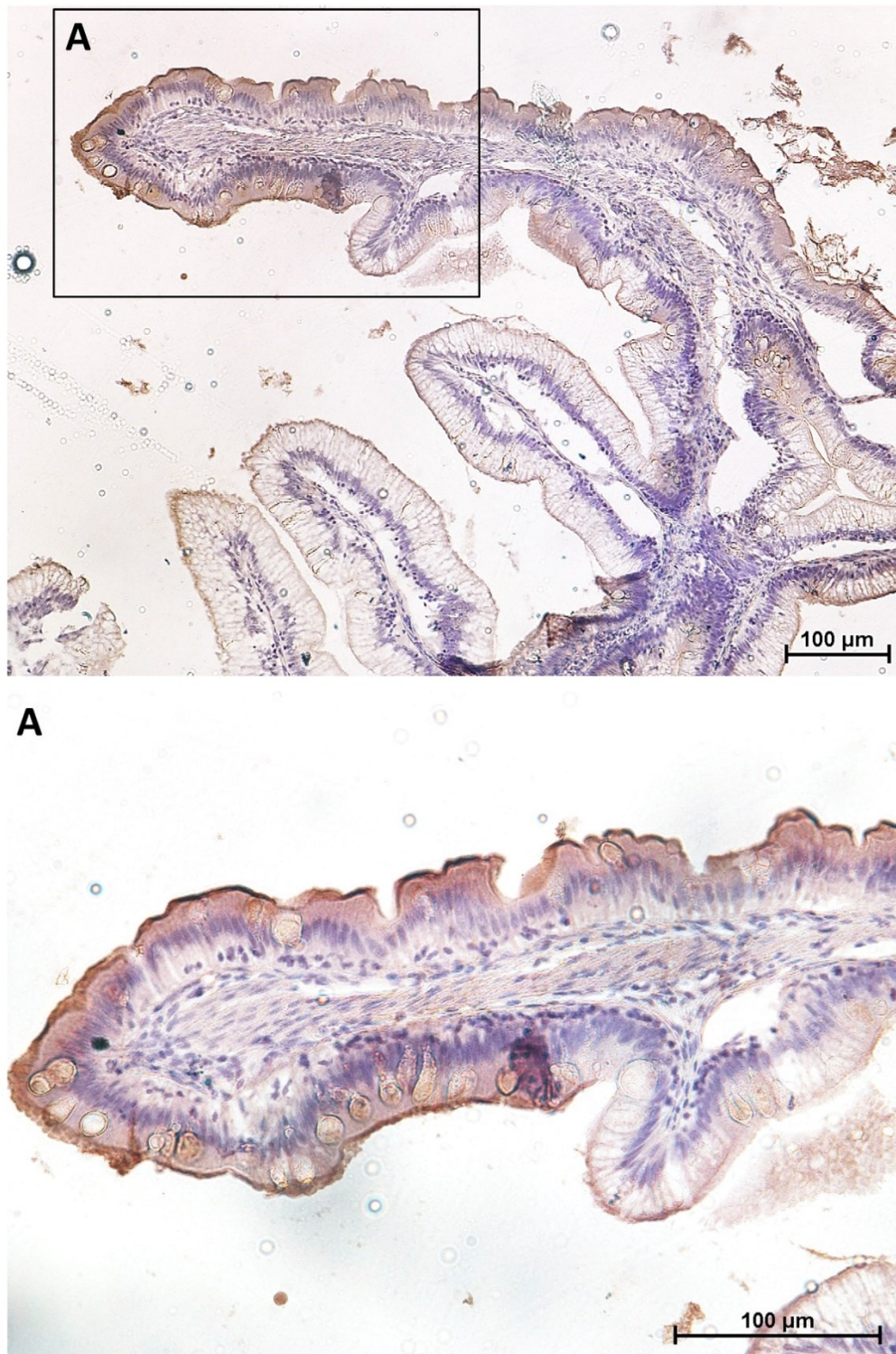
Figure 27: Representative image showing immunolocalization of Sglt1 within the complex folds of the distal intestine. A strong Sglt1 was detected in the apical part of the complex folds (A), whereas only a weak expression was found in their basal part.
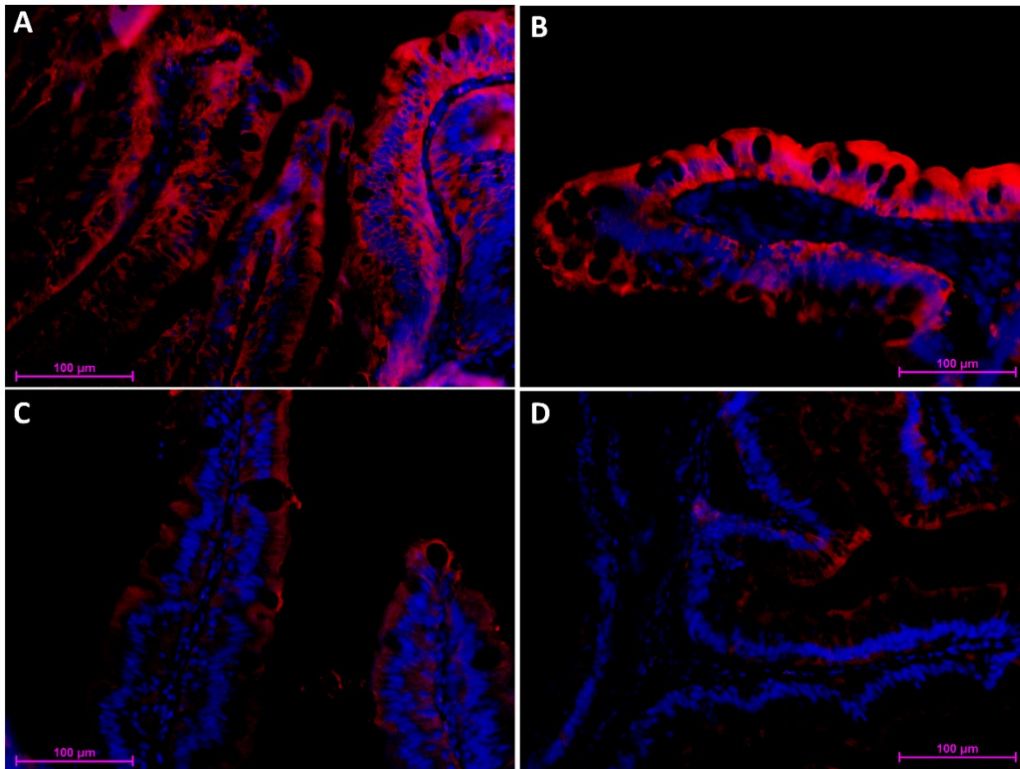
Figure 28: Immunofluorescence showing the distribution of Fabp2 along the different gut portions: A:proximal intestine, B: apical part of the complex folds of the distal intestine, C: pyloric caeca, D: basal part of the complex folds of the distal intestine. The proximal intestine and the apical part of the complex folds of the distal showed a similar expression pattern.

Discussion

In this chapter of the thesis, I performed a detailed characterization of the intestinal epithelial cells lining the intestinal tract in rainbow trout (RT) along the first year of development. I also provided for the first time, a detailed description of the presence of different mingled morphological and functional compartments along the whole gut.

Macroscopically, the rainbow trout intestine corresponds to the general description of the organ in teleost fish [69]. It comprised a proximal intestine with blind diverticula called pyloric caeca annexed to its upper part and a distal intestine. The latter is characterized by a larger diameter, dark pigmentation and circularly arranged blood vessels in agreement with a previous study performed in *Brown trout* [70]. Complex folds protruding from the distal intestinal wall toward the lumen were also evident. These structures have been previously described in analogous (*Salmo trutta* and *Salmo salar* [28,71]) and different species like sharks [72,73] but are not common to all teleost species. At present, their detailed morphology remains poorly known and their function is even less understood [28].

The tunica mucosa of the rainbow trout has the typical features described in *Salmonids* including a wide variation of folds length in the proximal intestine. However, we have been the firsts to group the folds into two populations based on their length. This enabled us to notice that, at 500 g, only the long folds increased their average length while the number of short folds diminished [65]. At the same time folds fusion and branching became evident. Some authors sustain that folds fusion represents a typical inflammation sign [28,74] whereas others support the hypothesis that mucosa folds get more complex in parallel with growth [28]. Based on our observations we hypothesize that branching may be accompanied or due to the short folds fusing into the long ones suggesting possible functional differences

between the two folds types [65]. We did not observe branching in pyloric caeca as previously described also in *Salmo salar* [28].

As mentioned above the presence of complex folds in the distal intestine has been described in *salmonids* but it not so common among other teleosts. It is interesting to note the predominance of circular muscle fibers within the tunica muscularis of the folds, while the tunica submucosa was reduced to a thin layer of connective tissue with neither compactum nor granulosum layers. This structure suggests that complex folds are able to contract independently from the rest of the distal intestinal wall [65].

In agreement with this hypothesis the two folds populations that we described in the distal intestine where not homogenously distributed. Indeed, pinocytotic vacuoles, sign of whole proteins absorption [75], were located on the wall of the distal intestine as well as along the epithelium lining the basal part of the complex folds. Instead, they were absent within the apical part of the complex folds of the distal intestine and in the proximal intestine. Goblet cells followed the same pattern: abundant, swollen, actively secreting were present in the proximal intestine, in the apical part of the complex folds of the distal intestine and in pyloric caeca. Whereas goblet cells along the wall of the distal intestine, and scattered along the epithelium covering the basal part of the complex folds, were less numerous and appeared deflated and inactive.

Taken together these observations indicate that the mucosa lining the apical part of the complex folds of the distal intestine is different from that of their basal part and of rest of the distal intestinal wall, but has the same features of the mucosa of the proximal intestine and share similarities with the one covering the pyloric caeca.

Although colleagues' observations are conflicting with the number of goblet cells, they were significantly more abundant in the proximal compared to the distal

intestine. A possible explanation is that goblet cells densities is strongly conditioned by several external factors including nutrition, physiology and immunology [37,76].

It was possible to distinguish goblet cells with a range of mucus composition in the proximal intestine and in the apical part of the complex folds of the distal intestine. On the contrary, the massive presence of PAS-positive pinocytotic vacuoles, made it difficult to characterize in detail the heterogeneity of mucus content in the rest of the distal intestine. Apart from their differential distribution in the distal intestine, the presence of goblet cells producing different mucousubstances is in agreement with previous results in teleosts and specifically in rainbow trout [77–79] . However, it is important to note that the significantly increase of the percentage of goblet cells secreting acidic mucous occurred together with the increase of villus branching, the appearance of vacuolized enterocytes in the pyloric caeca, and in correspondence with the increase of lipid concentration in diet. Consequently, since qualitative changes in mucins composition from neutral (glycosylated) to acidic (sulphated) are associated with gastrointestinal disorders our data support the hypothesis that the last diet change cause a mild stress [65,80].

We observed eosinophilic granule cells (EGCs) within the submucosa granular layers in agreement with previous observations in the *Salmon salar*. EGC are considered the functional equivalent of Paneth cells [47] and indeed, EGCs found in rainbow trout showed positivity to Phloxine-tartrazine staining, an histochemical staining that selectively identify Paneth cells. They play a central role in intestinal mucosa defense by secreting antimicrobic peptides and in intestinal stem cells guidance. However, their position outside the epithelium is not compatible with that of *bona fidae* Paneth cells [65]. Recent data report that these granular layers are house of numerous eosinophilic mast cells involved in inflammatory process [81]. Based on these observation, some authors consider simply eosinophilic granule cells to be mast cells [82]. Our data do not agree with

this conclusion since rainbow trout ECG did not express alkaline phosphatase nor peroxidase as instead take place in fish mast cells.

The identification of proliferating cells at the base of the folds along the whole gut, confirmed that the stem/progenitor cells zone is located within the intestinal folds, in agreement with previous observation in *Salmo Salar* [28] *and Salmo trutta* [83]. However, cell proliferation was not homogeneous in the different intestinal portions but followed the same pattern described above: in the proximal intestine and on the apical part of the complex folds of the distal intestine, proliferation was restricted to the folds bottom, conversely in pyloric caeca, in the distal intestinal wall and on the basal part of the complex of the distal intestine, the signal was more spread and extend along the folds length. Interestingly, proliferation cells' spot were observed also along the folds length but exclusively in the proximal intestine of individuals weighting 500g. This observation leads us to believe that proliferating cell spots correspond to newly generated branches.

Alkaline Phosphatase (AP) is generally considered a marker for mature enterocytes [35]. An evident AP signal was observed at the folds apex, where differentiated enterocytes house. This, was fully in agreement with previous observations in mouse small intestine [84]. As expected, cell proliferating zone was inversely proportional to the one of differentiated cells. However, it was interesting to note that proliferating and differentiating cells distribution followed the same patterns: the anterior intestine and the apical part of the complex folds of the distal intestines showed lower proliferation and more extensive differentiation while inversely, pyloric caeca, distal intestinal wall and the basal part of the complex folds of the distal intestine present higher proliferation and only restricted differentiation. In addition, the lower proliferation was associated to rare apoptotic cells, while higher proliferation corresponded to high frequency of cell death. Therefore, these novel insights suggest that the rainbow trout gut is subject to a lower renewal-rate in its proximal portion and in the apical part of complex folds of the distal intestine

compared to the pyloric caeca, distal intestine and the basal part of the complex folds.

Two different apoptotic cell morphologies were observed along the trout gut: round and slender cells. Round cells have been already described in mouse small intestine as apoptotic bodies [85], they were detected along the folds and at their apex as well as exfoliating into the intestinal lumen. They were distributed along the whole intestine. The other, instead displayed a peculiar strong eosinophilic cytoplasm, were selectively identified in the pyloric caeca, in the more distal region and along the epithelium lining the apical part of the complex folds. Their morphology fully correspond to the funnel-like structure that characterize the early apoptosis stages [48].

To evaluate whether the two diverse morphological compartments observed were also associated with different functional activities, we studied the expression and the localization of three well-defined and known enterocytes' functional markers. Peptide transporter 1 (PepT1) is a high capacity, low affinity symporter generally considered the main carrier for the dietary uptake of di- and tri-peptides [86], in both mammals and fish species. PepT1 was distributed along the enterocyte's brush border in agreement with other previous report in rainbow trout alevins [87]. Its expression was high in the pyloric caeca, proximal intestine, as well as, in the apical portion of the complex folds of the distal intestine. However, the signal was completely absent in their basal part and in the rest of the posterior intestine. These findings are fully in agreement with other previous studies conducted in salmon [88], rainbow trout [89], and sea bass [90] and explain the steady decrease in Pept1 messenger RNA expression detected by Colleagues. Our results are also in coherent with previous data showing a significant decrease in SGLT-1 in the distal intestine compared to the proximal and to the pyloric caeca, further supporting the thesis that rainbow trout presents three different kinetic glucose absorption systems corresponding to the diverse intestinal regions [25,91].

In addition, the heterogeneous expression and distribution of Fabp2 that we detected along the whole gut is fully consistent with a previous study conducted in salmon in which the authors investigated Fabp2 expression and localization along the different intestinal portions [92].

Overall, our results support the thesis that the two distinct morphological mingles compartments that we observed are also characterized by different functional activities.

Conclusion

Overall, our results strongly support the hypothesis that the rainbow trout intestine is composed by two well-defined different morphological and functional compartments. The first comprises of proximal intestine and apical part of the complex folds of the distal intestine and the other formed by the pyloric caeca, the basal part of the complex folds and the rest of the distal intestine. These novel insights strongly support the thesis that in RT the proximal intestine extend itself in its more distal portion and consequently that digestive and absorptive function are mingled along its entire length.

Chapter 3

The Specific Distribution Of Rainbow Trout (Oncorhynchus Mykiss) Intestinal Stem Cells

Overview

To achieve a better knowledge of the cellular and molecular mechanisms implied in the intestinal homeostasis preservation and to further investigate the two different renewal rate previously observed, I performed a detailed qualitative description of the organization of the intestinal epithelial stem cell (IESC) niche and their regulatory molecules. To this end, the typical mouse ISCs markers (LGR5, HOPX, SOX9, NOTCH1, DLL1, and WNT3A) have been selected as target genes, and subsequently their expression have been localized along the different portions of the trout gut trough *in situ* hybridization. All the target genes were expressed also in rainbow trout intestine. However, considering their typical position in mouse, we highlighted substantial differences. *Lgr5+* cells were rare but surprisingly in RT were located along the folds' stroma rather than restricted in the crypt epithelium. The folds' connective axis hosted also scattered *notch1+* as well as *wnt3a+* cells where they colocalized with *lgr5+* cells. Interestingly, also in mouse these markers colocalize, even if this occurs in the epithelium lining the crypt base. Moreover, close to *lgr5+* stromal cell population we observed elongated, epithelial cells expressing *dll1*. This marker in mouse is selectively expressed by Paneth cells at the crypt bottom. Despite the different spatial position of *dll1+* cells in mouse and rainbow trout, it is interesting to note that in both species *lgr5* and *dll1* are expressed by cells topographically close each other, suggesting a functional interaction. Moreover, the epithelium lining the intestinal folds base in rainbow trout showed exclusively positivity to *sox9*. Particularly, here, we observed slender cells expressing *sox9* at high level, strongly reminiscent of the crypt base columnar cells (CBCs) cells described in mouse intestinal crypts. *Sox9* expression tended to disappeared outside del fold base to give way to *hopx* which was abundantly detected along the folds rather than restricted to the +4 position as described in mouse. Based on these observation, it is reasonable to assume that in this species

the functional equivalent of *lgr5* is *sox9*, since sox9+ cells showed the typical location and shape of CBCs in mouse intestine. Whereas, *lgr5* expressed by a stromal population along the folds could represent a specific mesenchymal subsets involved in the maintenance of the folds tip epithelium (Figure 29) [93].
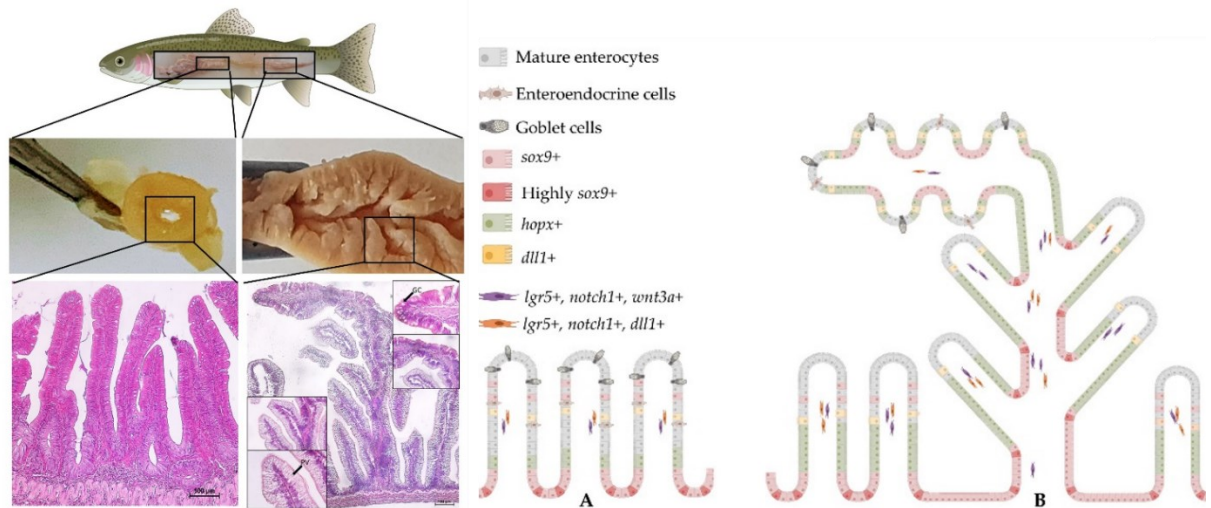

Figure 29: Schematic images showing the distribution and the organization of the stem cell niche and of their regulatory molecules in the proximal (A) and distal intestine (B). Image created using BioRender.com

Introduction

In recent years, detailed studies in mouse and humans have widely increased the knowledge and understanding of the intestinal epithelium stem cells (IESCs) and of their niche. To date, two different populations of intestinal stem cells coexist within the crypt base: the quiescent stem cells, which occupy the fourth position from the crypt base and characterized by a slow replication rate and the crypt base columnar (CBC) cells, slender, highly cycling and epithelial cells interposed between Paneth cells at the crypt bottom [8]. As described above, the gastrointestinal tract is a very dynamic system in which epithelial cells are physiologically rapidly and promptly renewed. However, the mechanisms and the specific cells types responsible of the intestinal homeostasis remain unclear in many domestic species, especially in fishes. To date, Intestinal stem cell knowledge are only available in small species as medaka (4-6 cm long) [32] and zebrafish [94] (3-4 cm long). The architecture of the intestinal stem cell (ISC) niche in medaka partially reflect the one observed in mouse. Indeed, it preserves the *lgr5* orthologs as well as their paralogs *lgr4* and *lgr6*. However, *sox9* is restricted to the folds base while in mouse is selectively expressed by the transient amplifying population [32].

Nowadays, there is no detailed study on the organization of the intestinal stem cell niche in zebrafish. However the possibility to generate, knock-out animals allowed a better understanding of the proliferative and stemness mechanisms. As in mammals, also in this species *notch* is essential to control and induce stem cells differentiation towards absorptive lineages and thus to preserve the epithelium integrity [95]. Moreover, organogenesis studies demonstrated also the evolutionary conservation of Wnt pathway which directly regulate stem and progenitor cell renewal, proliferation and differentiation [96].

Due to the key role of intestinal stem cells in homeostasis maintenance, their identification is essential to explore the mechanism that induce and guide their differentiation. Therefore, the second chapter of my thesis was dedicated to the identification and to the description of the cell populations and molecules that define the intestinal stem cell (ISC) niche in rainbow trout.

To this purpose, I selected the classical mouse intestinal stem cells markers as target genes (HOPX, SOX9, LGR5, NOTCH1, DLL1, and WNT3A) and I examined their expression and their topographical localization along the trout gut. These markers have been studied individually and with multiplex *in situ* hybridization to identify their eventual co-localization in order to understand to what extent the rainbow trout intestinal stem cell system compares with that of the mouse.

Methodologies

Sample collection

Five rainbow trout *(Oncorhynchus mykiss)* were collected at Laghi Verdi s.n.c. trout farm (Como, Italy). Animals were raised until they reached the weight of approximately 500 grams, corresponding to the commercial size. Individuals were euthanized with an overdose of anaesthetic according to current Italian regulations. Fish were immersed in a tank containing a concentration of 250 mg/l of tricaine methanesulfonate solution (MS-222, Sigma Aldrich, #E10521) in water. Individuals were weighed and immediately eviscerated. The evisceration was carried out with a longitudinal incision throughout the abdomen. Samples of pyloric caeca, proximal (anterior), and distal (posterior) intestine were collected.

Small pieces of 1 cm^2 of pyloric caeca and both intestinal tracts were collected for gene expression analysis. They were rinsed in phosphate buffered saline (PBS, Sigma-Aldrich, Germany, #D5773) and completely immersed in RNAlater (Thermo Fisher Scientific, USA, #AM7021). Samples were incubated overnight at +4°C and then stored at -80°C until RNA extraction. Samples intended for morphological analysis (around 2 cm in length) were immediately fixed in 10% neutral buffer formalin (Biooptica, Italy, #05-01020Q) for 24 h at room temperature (RT), dehydrated in graded alcohols, cleared with xylene and embedded in paraffin

Morphological evaluation

After dewaxing and rehydration, 5 μm thick sections were stained with Haematoxylin and Eosin (H&E) to assess tissue preservation and to evaluate the general morphological features of the intestine.

Characterization of intestinal stem cell niche through fluorescent in situ hybridization (FISH)

Since antibodies specific for rainbow trout antigens are not commercially available, I performed a detailed characterization of the intestinal stem cell niche using *in situ* hybridization. This technique allows gene expression localization through the hybridization of target mRNAs with labelled custom cDNA probes. Since mouse is the species in which the intestinal stem cell niche has been studied most extensively, I selected the following mouse intestinal stem cell markers as target genes:

- *Homeodomain-Only Protein* (*Hopx*) that is expressed by the "+4 stem cells" which occupies the fourth position from the crypt base, and identifies rare quiescent stem cell;

- *Leucine-rich repeat-containing G-protein coupled receptor 5* (*Lgr5*), the typical marker of crypt-base columnar cells (CBCs), actively cycling stem cells, located at the crypt base interposed among Paneth cells;

- *SRY-Box 9* (*Sox-9*), member of the SRY-family and a fundamental crypt transcription factor which is expressed by CBCs and by transient amplifying population;

- *Notch receptor 1* (*Notch1*), a receptor specifically expressed by CBCs involved in the differentiation of stem cells progenitors into absorptive lineages;

- *Delta-like protein 1* (*Dll1*), the transmembrane ligand-protein of Notch1;

- *Wnt family member 3A* (*Wnt3a*) secreted by Paneth cells, and essential for stem cell maintenance;

Target gene expression and FISH probe synthesis

RNA extraction was performed using TRIzol reagent (Thermo Fisher Scientific) combined to PureLink RNA Mini Kit (Thermo Fisher Scientific) according to the manufacturer's indications. To prevent DNA contamination, samples were treated with PureLink DNase. RNA samples were then transcribed into cDNA using iScript Advanced cDNA Synthesis Kit for RTqPCR (Bio-Rad). The synthesis was completed in accordance with the manufacturer's instructions and the resulting cDNA was stored at -20°C. Qualitative PCR was performed using GoTaq® G2 Flexi DNA Polymerase kit (Promega). The PCR products were extracted from the agarose gel and sequenced. Each band was processed using NucleoSpin® Gel and PCR Clean-up, Mini kit (Machery-Nagel GmbH & Co) to elute the cDNA. The eluted PCR products were sequenced using Custom DNA sequencing service of Eurofins Genomics (Milan, Italy). The obtained FASTA format sequences were sent to Advanced Cell Diagnostics (ACD) for the design of custom *in situ* hybridization probes (Table 4).

Specific mRNA transcripts within formalin-fixed paraffin-embedded (FFPE) samples were characterized through fluorescent in situ hybridization (FISH) using RNAscope Multiplex Fluorescent Reagent Kit V2 (Advanced Cell Diagnostics, USA, #323110). The assay allows to visualize simultaneously 2 targets when customized probes are conjugated with different channels. Briefly, of 5 μm thick sections were cut using a rotary manual microtome and were air-dried overnight at room temperature. The day after, slides were heated in a stove for 1 hour at 60°C and immersed in xylene to encourage the paraffin removal. Samples were later incubated with hydrogen peroxide (Advanced Cell Diagnostics, USA, #322281) for 10 minutes at room temperature and brought to boiling in a target retrieval solution (Advanced Cell Diagnostics, USA, #322000) for 25 minutes. Subsequently, slides were exposed to Protease Plus (Advanced Cell Diagnostics, USA, #322281) for 30 minutes at 40 °C to allow probes to reach their defined target. Afterwards, slices

were incubated with specific probes diluted 1:50 in diluent buffer for 2 hours at 40°C. Probes were conjugated with different channels (listed in table 5) in order to allow multiplex comparison.

Table 5: Probe targets and corresponding conjugated channels

Species	Gene	Channel		Target Region	Number Of Pairs	Cat. Number
Rainbow Trout	*Lgr5*	1	LOC110499401	738-1673	20	847731
Rainbow Trout	*Wnt3a*	2	LOC110530975	217-1287	20	847771-C2
Rainbow Trout	*Hopx*	2	LOC110505076	32-706	14	847761-C2
Rainbow Trout	*Notch1*	3	LOC100190917	2-1188	20	847741-C3
Rainbow Trout	*Dll1*	3	LOC110502965	1387-2256	20	853451-C3
Rainbow Trout	*Sox9*	3	LOC100135781	28-972	14	847751-C3
Rainbow Trout	*Ppib*	1	LOC110491579	178-1096	19	540651
Rainbow Trout	*DapB*	1	EF191515	414-862	10	312038

The exceeding probe volume was removed by washing twice for 2 minutes with wash buffer solution (Advanced Cell Diagnostics, USA, #310091). Signal amplification was performed incubating at 40°C, sequentially, in solution Amp1 for 30 minutes, in Amp 2 for 30 minutes and in Amp 3 for 15 minutes. After each step, slides were gently washed twice in wash buffer solution for 2 minutes each. HRP CH 1, 2 or 3 solution provided by Multiplex Fluorescent Reagent Kit V2 (Advanced Cell Diagnostics, USA, #323110) was applied according to the channel conjugated to the probe, and the slides were incubated at 40°C for 15 minutes. Then, OPAL 570 fluorescent (Akoya Biosciences, USA, #FP148800) was diluted 1:750 in TSA Buffer (Advanced Cell Diagnostics, USA, #322809), placed on sections and incubated for

30 minutes at 40°C. Afterwards, HRP blocker was applied for 15 minutes at 40°C. HRP blocker was discarded and slices were washed twice for 2 minutes each in Wash Buffer. Then, slides were covered by HRP CH 2 or 3 according to the conjugated channel and left to rest 15 minutes at 40°C. Washing steps were repeated and then, samples were exposed to OPAL 520 fluorophore (Akoya Biosciences, USA, #FP148700) diluted 1:750 in TSA Buffer (Advanced Cell Diagnostics, USA, #322809), and incubated for 30 minutes at 40°C. After washing step, HRP blocker was applied for 15 minutes at 40°C. Once again, it was discarded and the sections were counterstained with DAPI (Advanced Cell Diagnostics, USA, #323110) for 30 seconds at RT. Finally, slices were blotted and mounted with ProLong™ Gold Antifade Mountant (ThermoFisher Scientific, USA, #P10144).

mRNA quality and integrity within FFPE samples were checked using a constitutive control gene (*PPiB-Peptidylprolyl Isomerase B*), while negative controls were performed incubating slides with *Bacillus subtilis* dihydrodipicolinate reductase (*d*apB) gene.

Sections were evaluated using a Nikon Eclipse E600 microscope equipped of a Ds-fi2 camera and the NIS-Elements software package. Slides were then scanned at the interdepartmental centre of advanced microscopy (Unitech - University Technological Platforms Office) using the NanoZoomer S60 Digital slide scanner (C-13210-01, Hamamatsu). The images were then observed at continuous magnifications between 2x and 80x.

Results interpretation

According to the ACD RNAscope® indications, the signal from a single mRNA molecule is detected as a punctate dot, whereas larger dots (cluster) result from many mRNA molecules. Many clusters lead to the positiveness of the whole cytoplasm. Furthermore, high RNA expression can be easily seen at 10X

magnification whereas low RNA expression typically required a 40X magnification examination.

Results

Characterization of intestinal stem cell niche through fluorescent in situ hybridization (FISH)

Lgr5⁺ cells were rare. *Lgr5* was exclusively expressed in scattered cells located in the lamina propria of pyloric caeca, proximal and distal intestine (Figure 30 A-B-C) mostly at the middle of the villus height, the signal was higher in the basal part of the complex folds of the distal intestine.
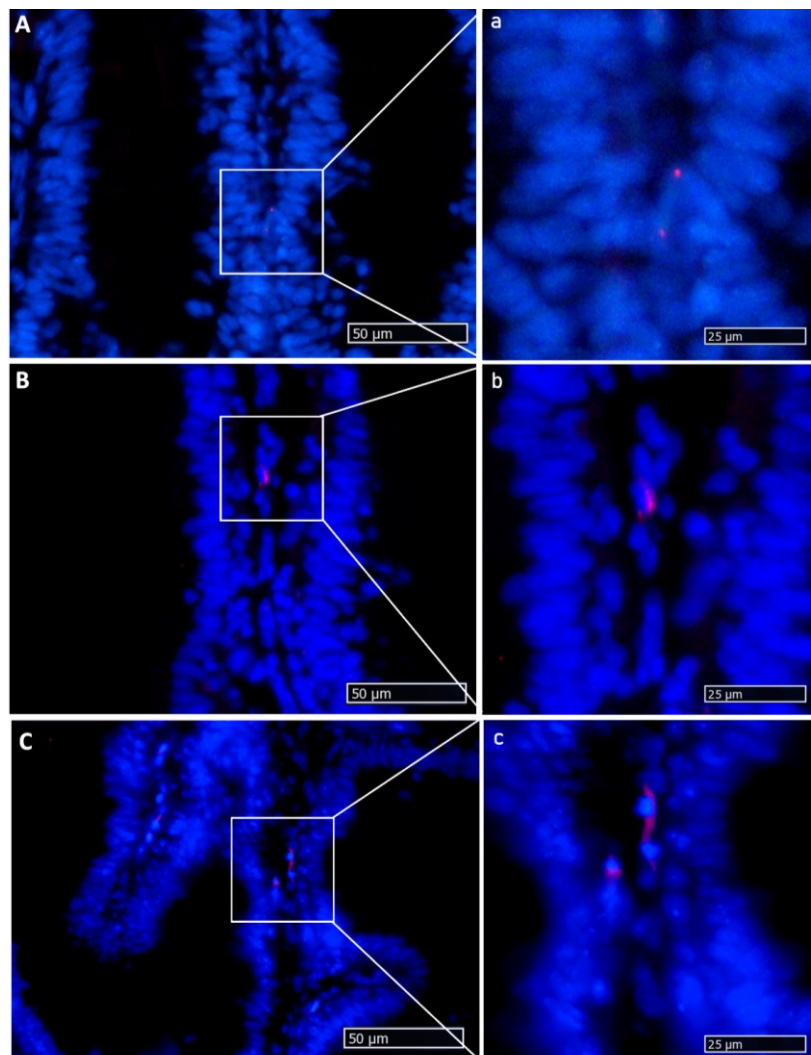

Figure 30: *In situ* hybridization showing *lgr5*⁺ cells (red). *Lgr5* was observed in the connective axis. The signal is lower in proximal intestine (A), intermediate in pyloric caeca (B) and higher distal intestine (C). DAPI (blue) shows nuclei.

Hopx⁺ cells were absent at the villus base, and were detected in the epithelial cells along the villus length. Moreover, its expression was low in the proximal intestine and in the apical part of the complex folds of the distal intestine, it increased in the pyloric caeca and in the distal intestine, and it was highest in the basal part of the complex folds. Furthermore, *hopx* expression was not limited to the epithelium but was also found along the gut stroma. In particular, the lamina propria of the distal intestine showed the highest level of *hopx* expression of the whole intestine (Figure 31 A-B-C-D).
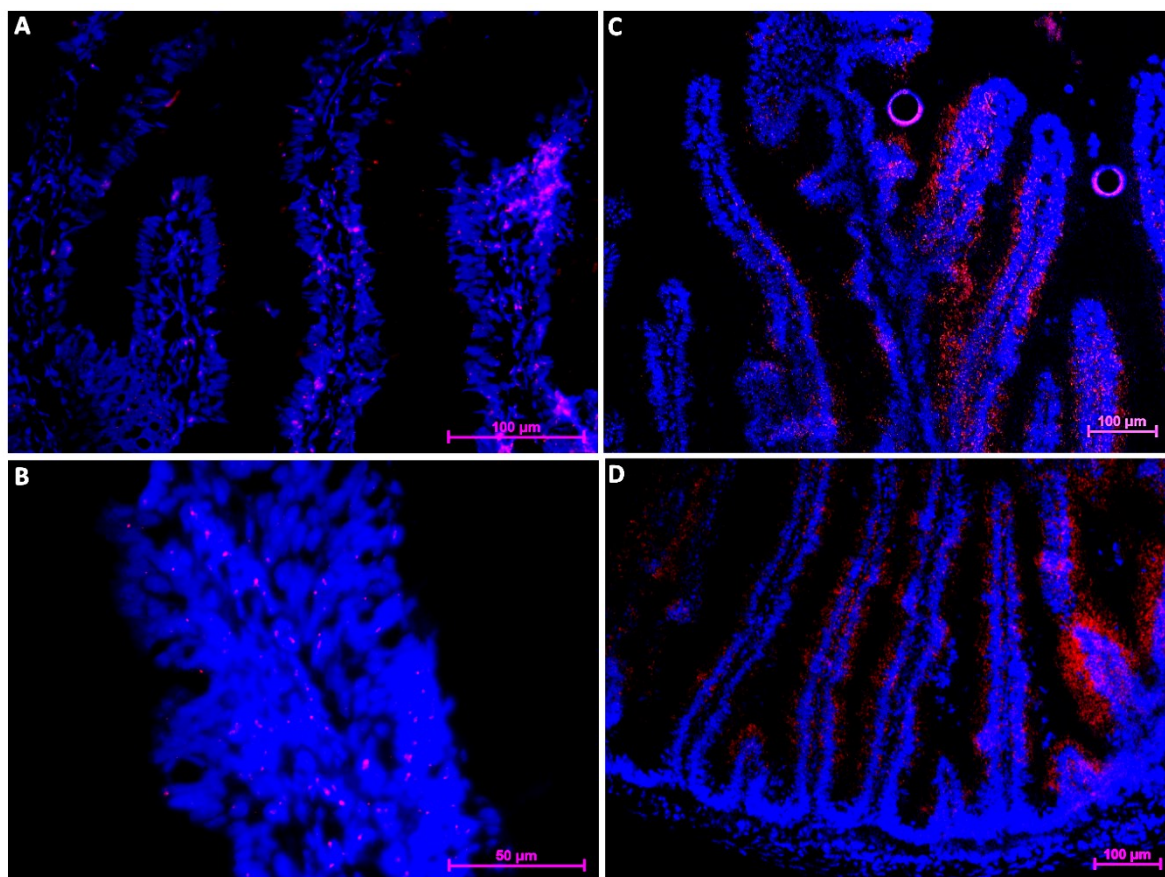

Figure 31: *In situ* hybridization showing *hopx⁺* cells (red). *Hopx* was observed in the epithelium lining the villus length and few *hopx⁺* cells were also found along the gut stroma. The signal is lower in proximal intestine (B), intermediate in pyloric caeca (A) and higher distal intestine (C-D). DAPI (blue) shows nuclei.

Sox9 was highly expressed exclusively by the epithelial cells lining the villus base in the pyloric caeca, in the proximal and distal intestine including the complex folds. The signal in the pyloric caeca, in the distal intestine and in the basal part of the complex folds, was stronger than in the proximal intestine and in the apical part of the complex folds (Figure 32 A-B-C). Along the whole intestine, we observed slender, epithelial cells expressing *sox9* at high level (Figure 33), located in the middles of the intestinal folds base. These peculiar cells were homogeneously distributed along the different portions of the intestine and were interposed among other cells expressing *sox9* at lower levels. *Sox9* expression gradually decreased outside the folds base, where *hopx* expression gradually increased and then faded at their apex (Figure 34).

In addition, we also found elongated epithelial, cells, strongly *sox9*⁺ along the folds all along the intestine .
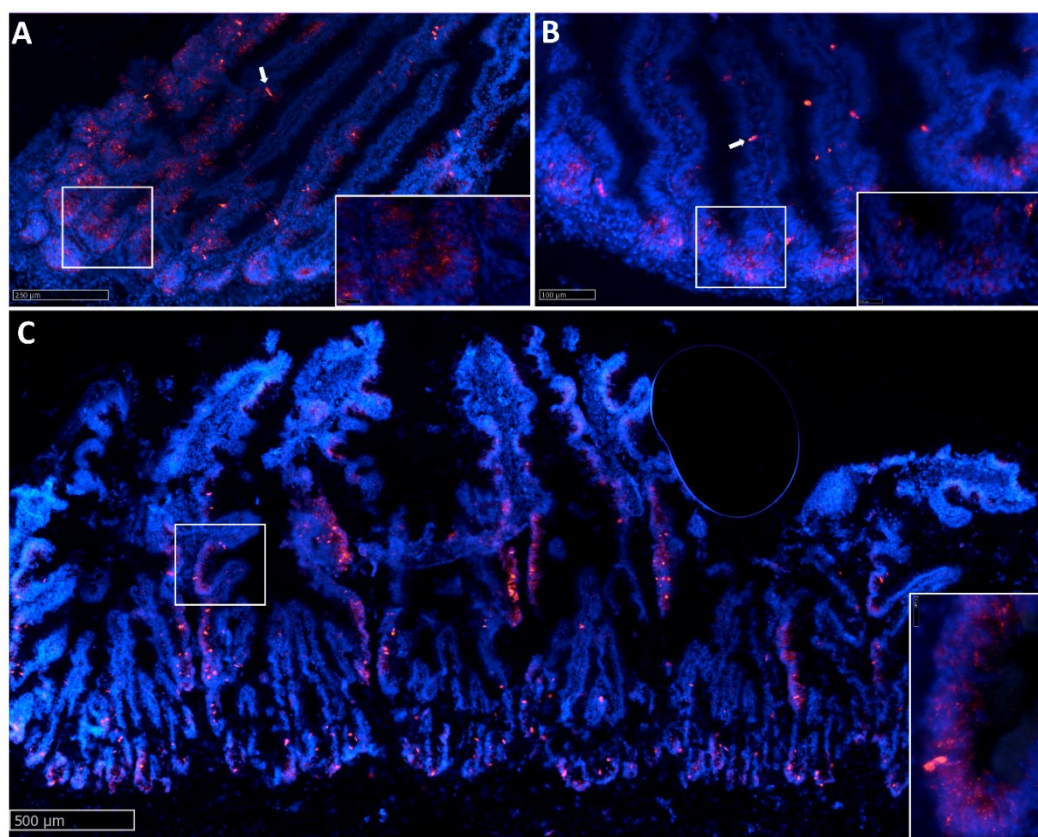
Figure 32: *In situ* hybridization showing *sox9*⁺ cells (red) in pyloric caeca (A), proximal intestine (B) and distal intestine (C).*Sox9* was observed in the epithelium lining the folds base. few *sox9*⁺ cells were also present along the folds length (arrows). DAPI (blue) shows nuclei
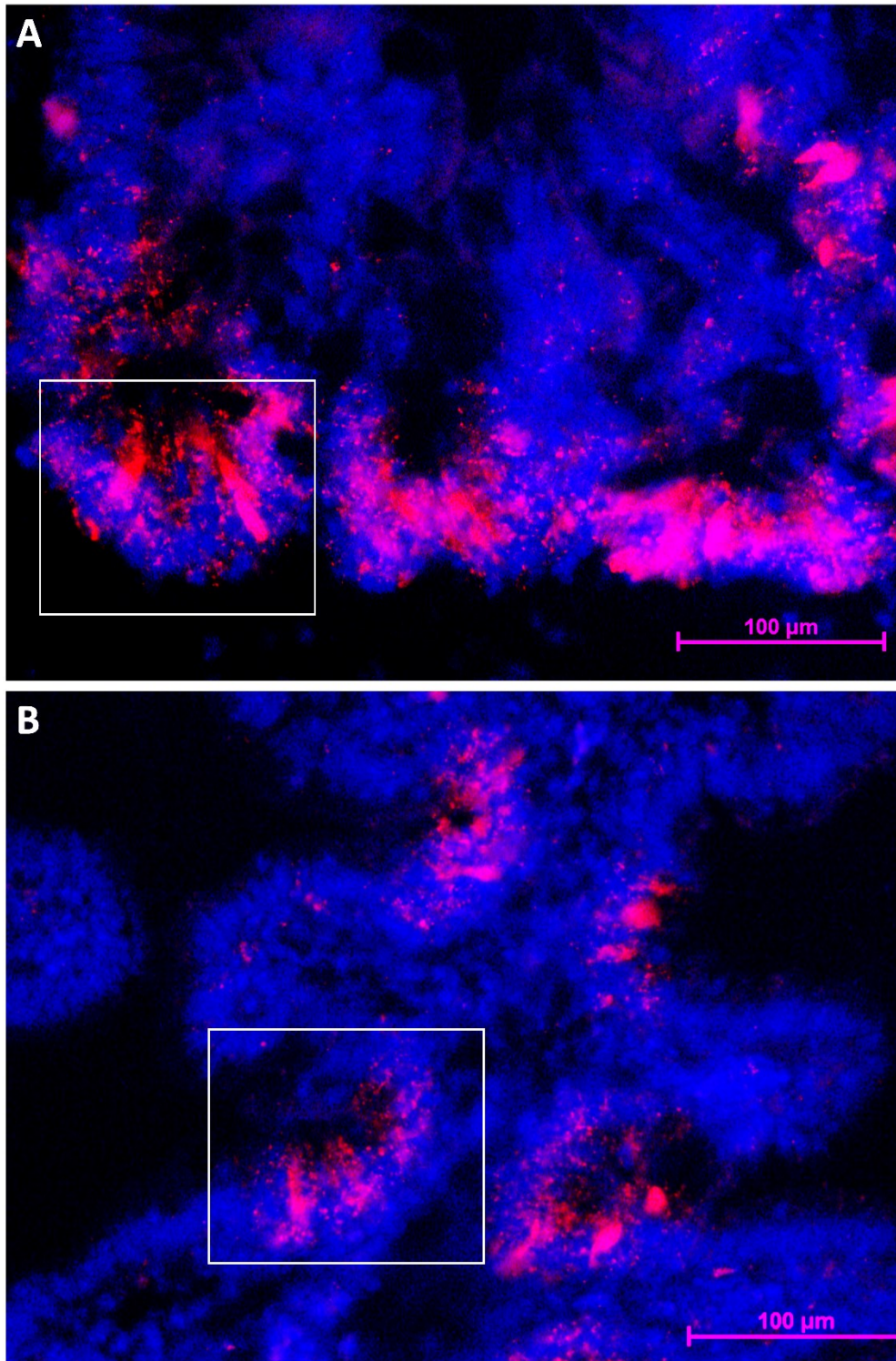
Figure 33: *In situ* hybridization showing columnar cells displaying *sox9* at high level (red) at the folds base in the typical position of CBCs. in both proximal (A) and distal (B) intestine DAPI (blue) shows nuclei.
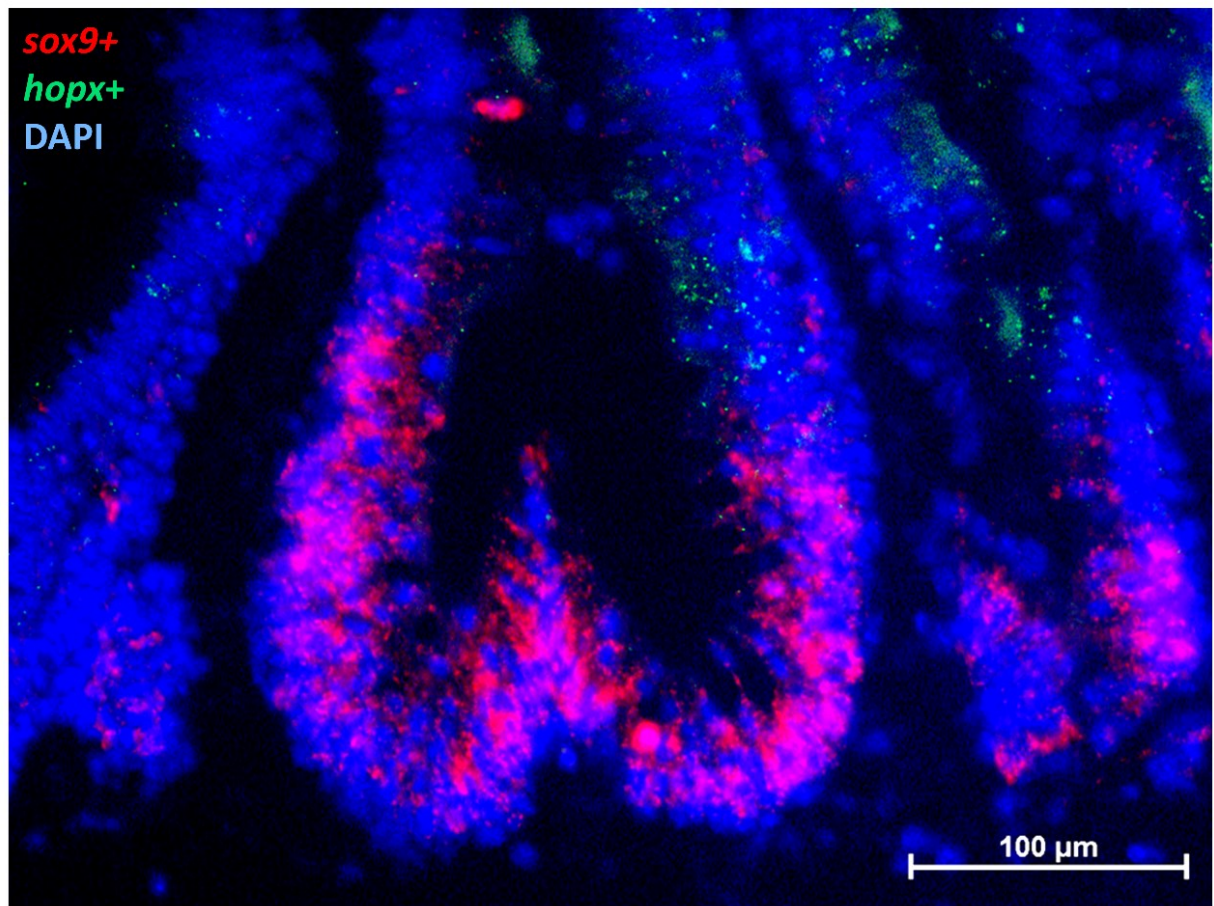
Figure 34: Multiplex *in situ* hybridization showing *sox9+* cells (red) and *hopx+* cells (green) in the complex folds of the distal intestine. *Sox9* was observed in the epithelium lining the folds base and *hopx* was present along the folds. DAPI (blue) shows nuclei

In rainbow trout we found *notch1* [+] cells scattered along the folds' connective axis (Figure 35), where it co-localizes with *lgr5* in the stromal cells (Figure 36).

Figure 35: *In situ* hybridization showing *notch*^{+} cells (red). Notch was observed in the connective axis. The signal is lower in proximal intestine (A), intermediate in pyloric caeca (B) and higher in the distal intestine (C). DAPI (blue) shows nuclei
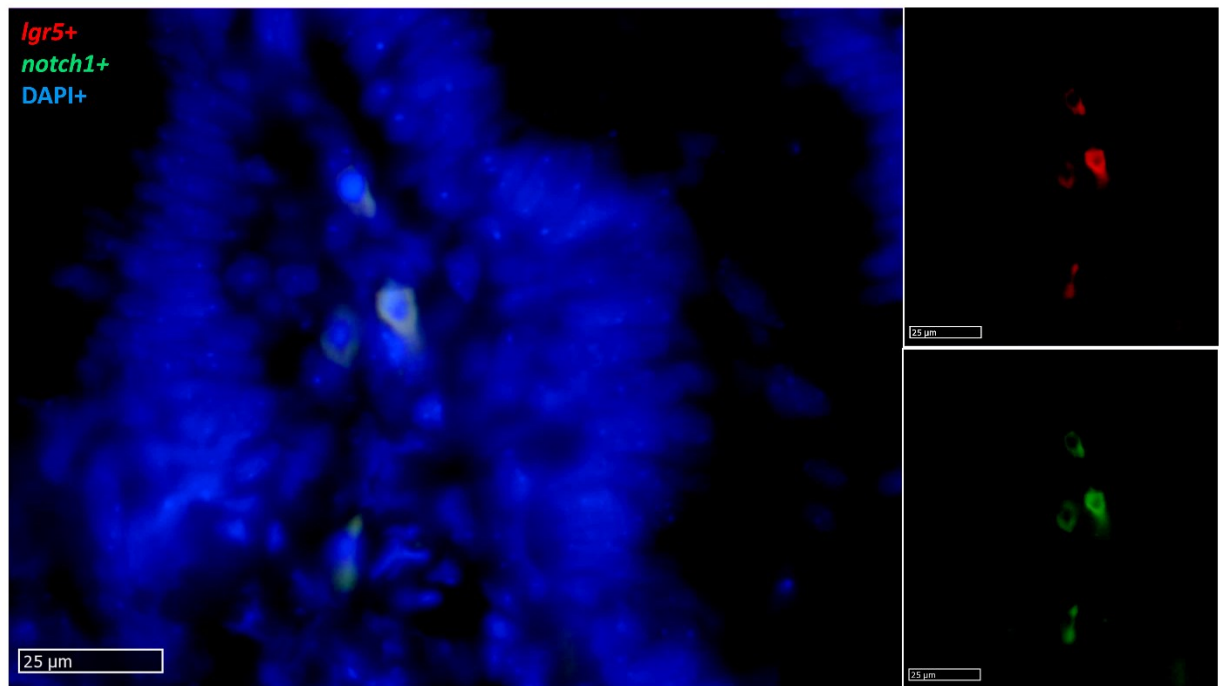
Figure 36: Multiplex *in situ* hybridization showing *lgr5⁺* cells (red) and *notch⁺* cells (green) along the folds connective axis. DAPI (blue) shows nuclei

Slender, elongated *dll1* ⁺ cells were found along the folds epithelium of all intestinal tracts but were more abundant in the pyloric caeca and in the basal part of the complex folds of the distal intestine (Figure 37). *Dll1* positive cells were also found in the lamina propria all along the intestinal tract. Interestingly, epithelial *dll1* ⁺ cells were located close to stromal *lgr5* ⁺ cells and stromal *dll1* ⁺ cells expressed also *lgr5* (Figure 38).
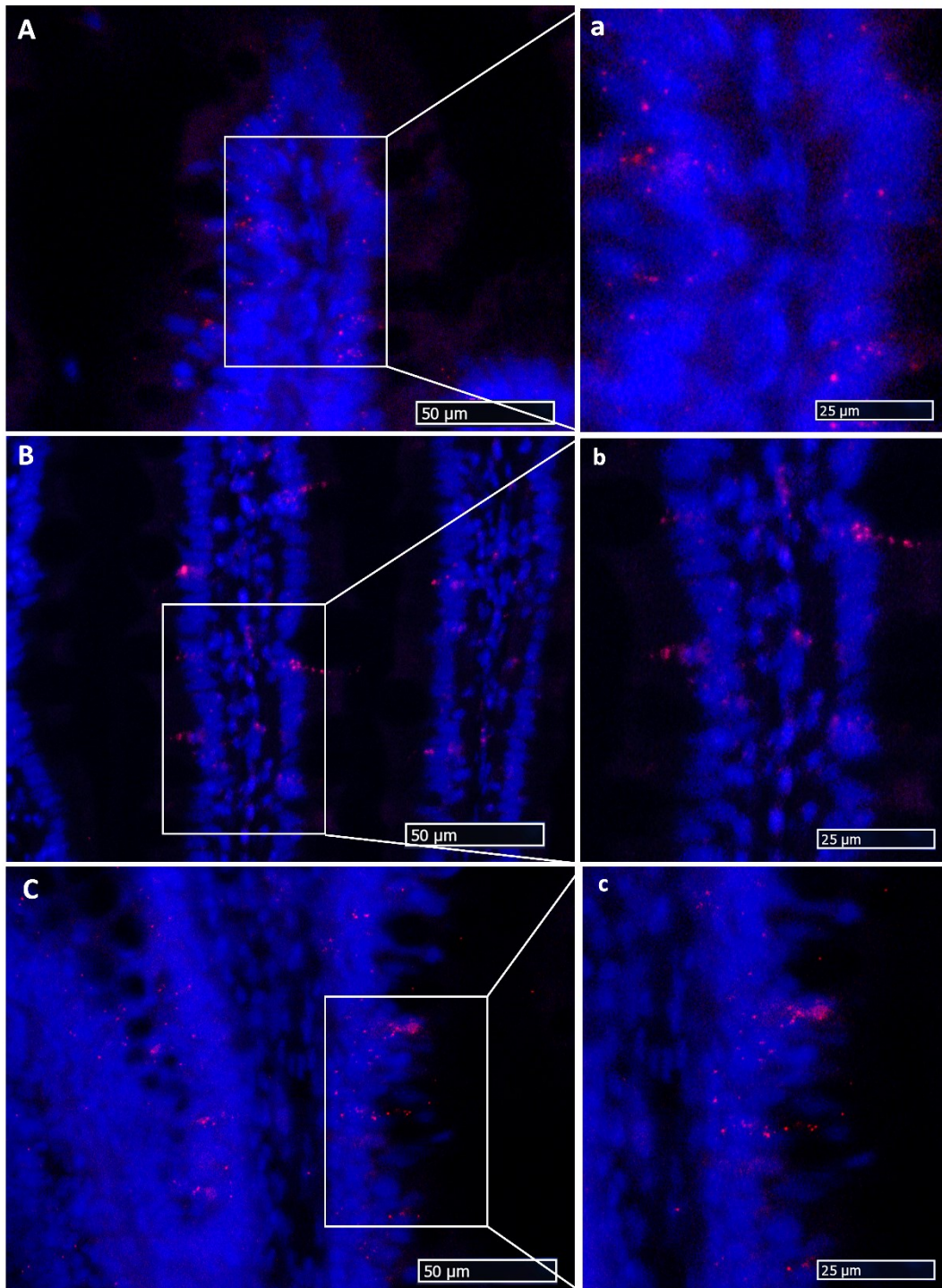
Figure 37: *In situ* hybridization showing *dll1+* cells (red). *Dll1* was observed in the connective axis and few *dll1+* cells were also found in the epithelium lining the villus length. The signal is lower in proximal intestine (A), intermediate in pyloric caeca (B) and highest in the distal intestine
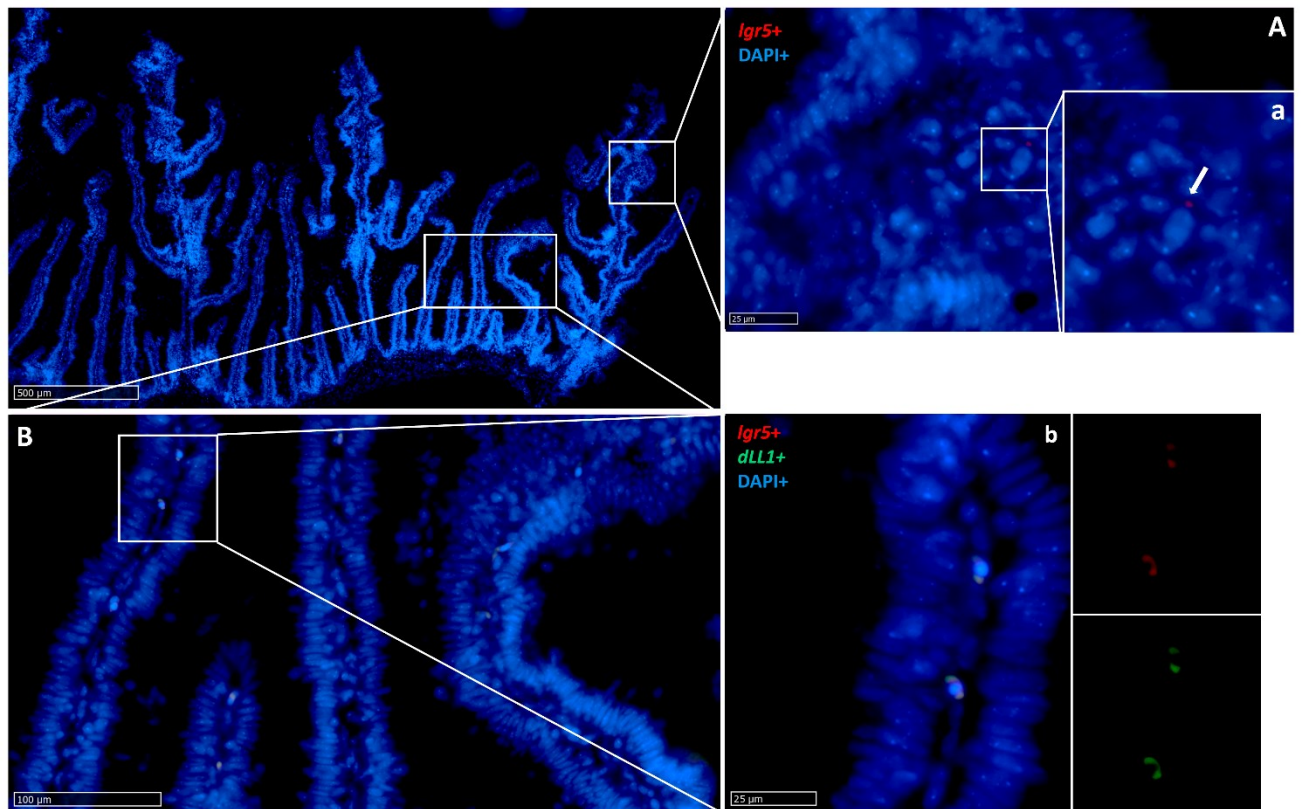
Figure 38: *In situ* hybridization of *lgr5* and *dll1* mRNA in the distal intestine. *Lgr5* (red dots) expression was low at the complex fold apex ((A,a): higher magnification, arrow) and intense at the base of the complex folds and in the rest of the distal intestine ((B,b): higher magnification). The two genes were expressed in a few cells found along the villus connective axis (b).

In rainbow trout, *wnt3a* was found in stromal cells (Figure 39) along the villus and colocalized with *lgr5* and *notch1* (Figure 40). Once again, the expression was higher in the distal intestine than in the proximal one. Pyloric caeca presented an intermediate pattern of expression.
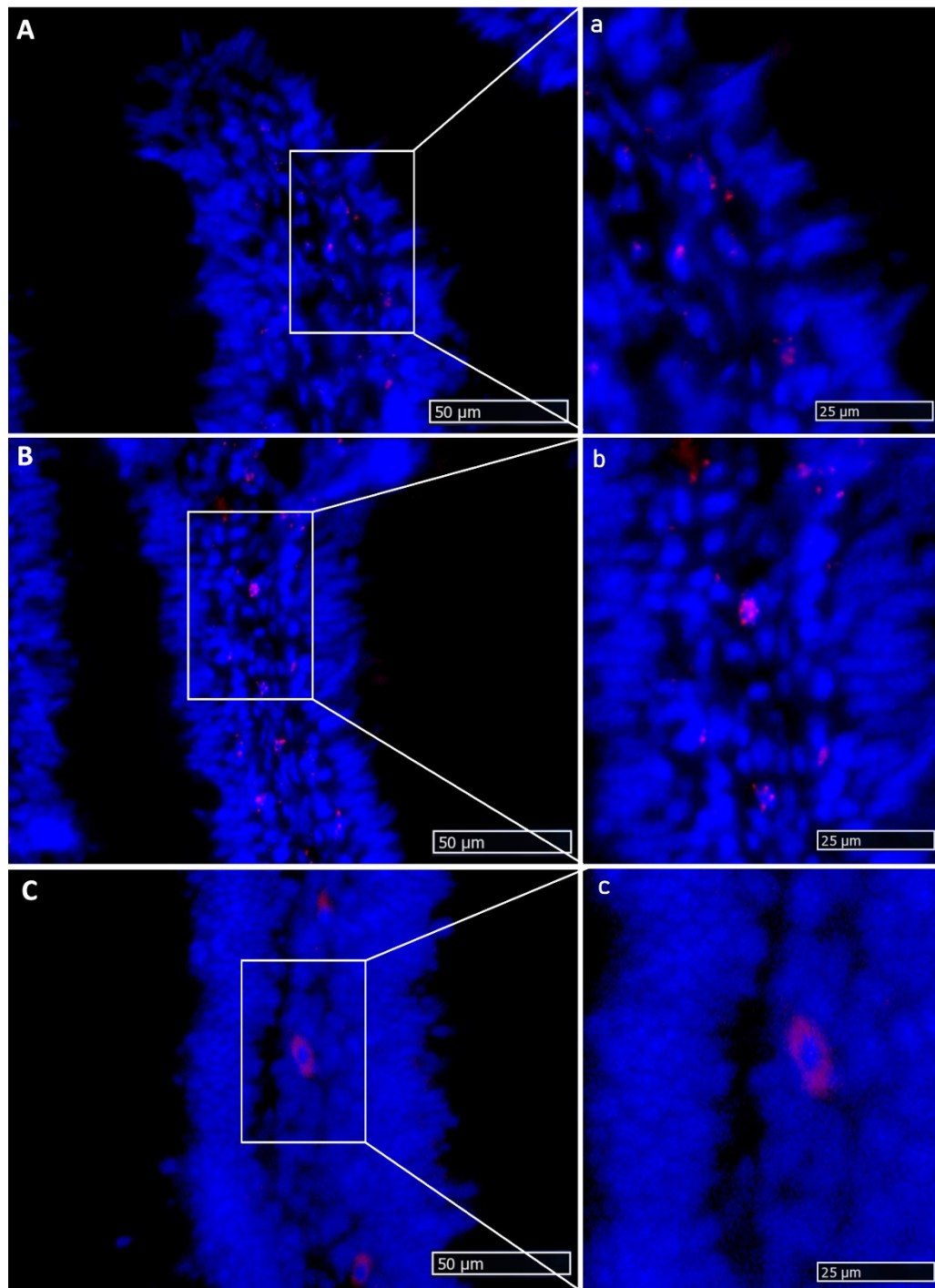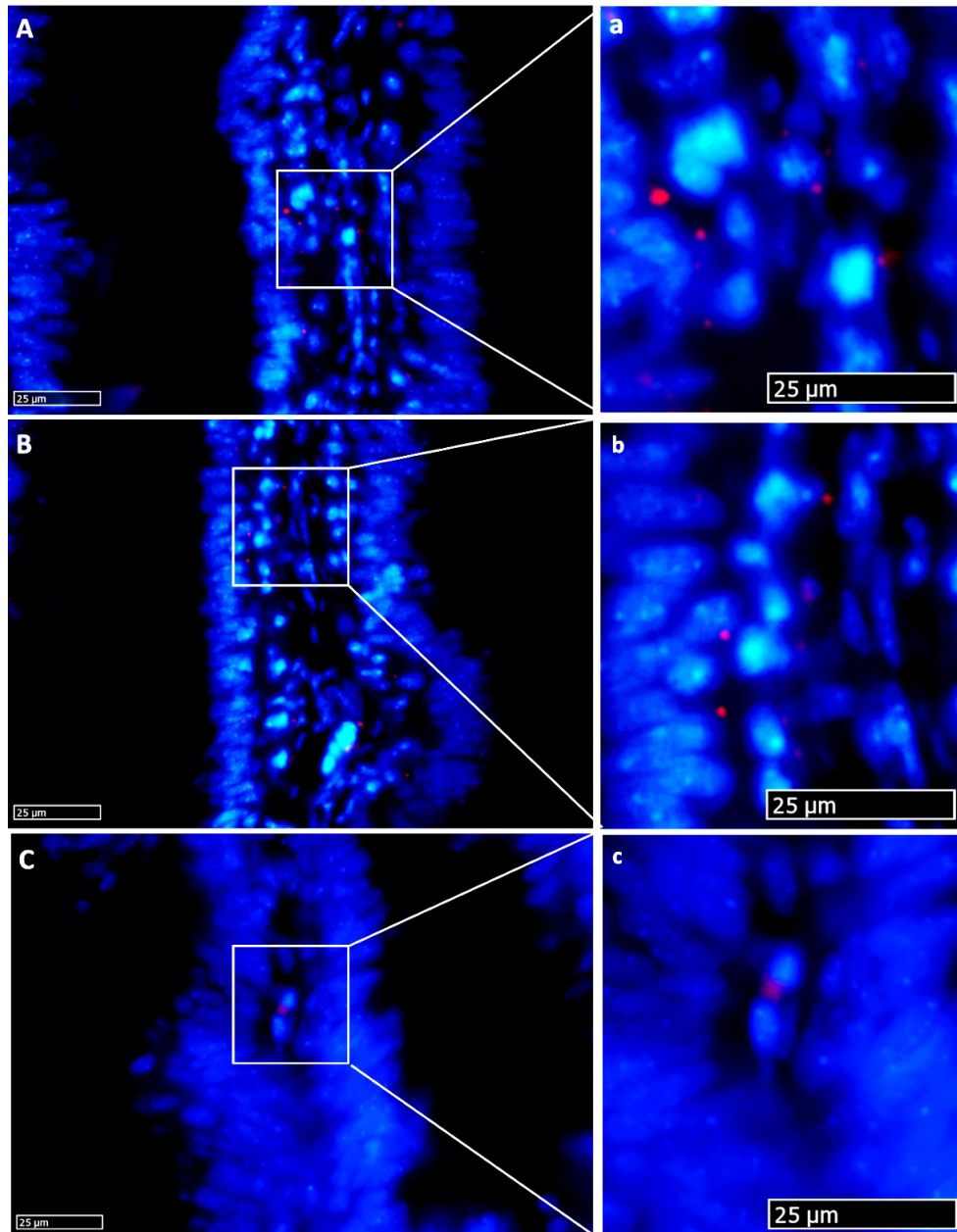

Figure 39: *In situ* hybridization showing *wnt3a⁺* cells (red). *Wnt3a* was observed in the connective axis. The signal is lower in proximal intestine (A), intermediate in pyloric caeca (B) and higher distal intestine (C). DAPI (blue) shows nuclei
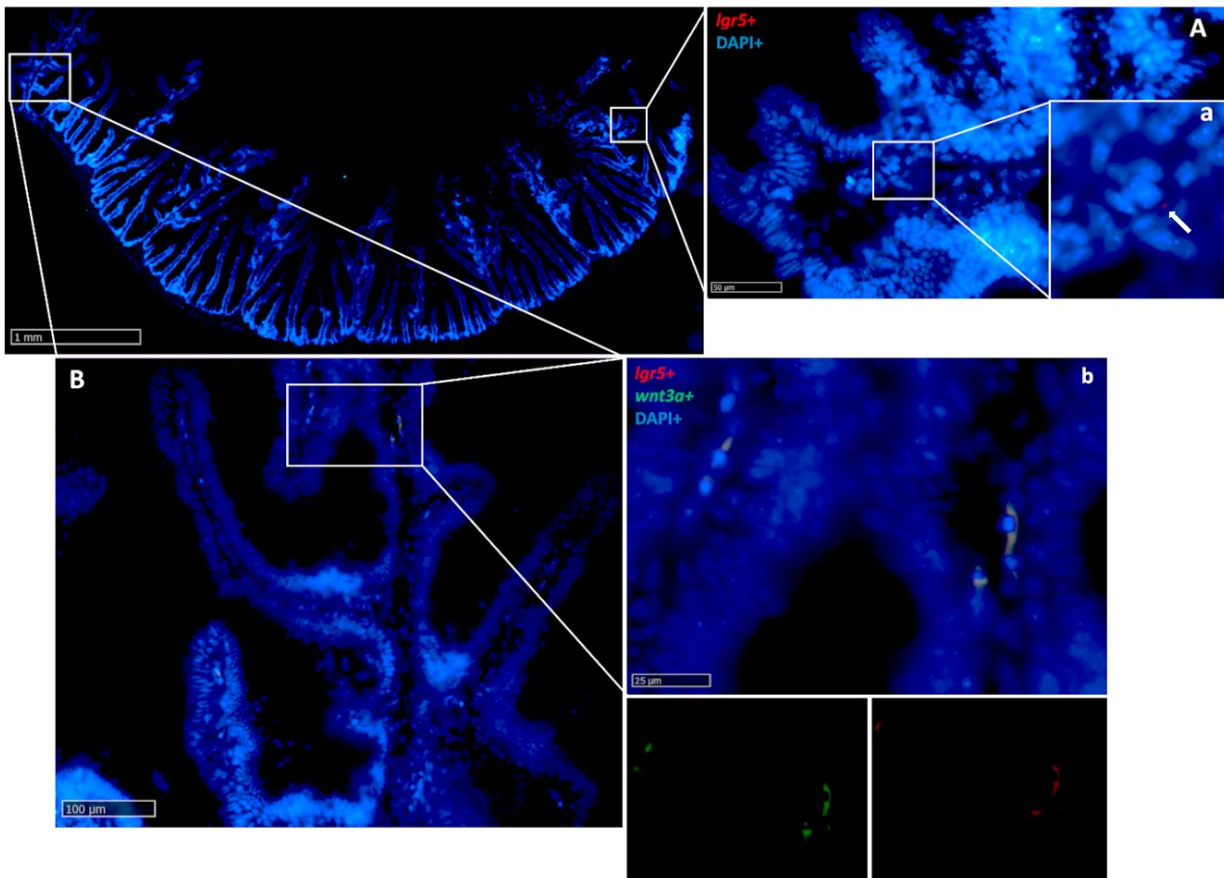
Figure 40: *In situ* hybridization of *lgr5* and *wnt3a* mRNA in the distal intestine. *Lgr5* (red dots) expression was low at the complex fold apex (A,a: higher magnification, arrow), became higher at the base of the complex fold and in the rest of the distal intestinal wall (B,b: higher magnification), where it colocalized with *wnt3a* along the folds stroma (b).

Discussion

In this chapter, I characterized the intestinal stem cells in rainbow trout *(Oncorhynchus mykiss)*, providing for the first time a detailed description of the stem cell niche architecture in this species.

Interestingly, despite the animals were raised in non-standardized conditions but rather farmed in natural-like conditions, their morphology fully matched with the one of our previous study [65]. Specifically, the apical part of the folds of the distal intestine strongly reminded the proximal intestine whereas their basal part and the pyloric caeca morphologically resembled the rest of the distal intestine. This suggests that these peculiar morphological features are species-specific rather than a consequence of intensive farming conditions or diet.

As in mammals, the intestinal epithelium of the rainbow trout is capable to completely renew itself even though more slowly. The intestinal renewal mechanisms are driven by a specific cell population known as intestinal stem cells (ISCs) located in well-defined niche. So far, a detailed description of these essential cells population in fish species has been performed only recently in the small teleost medaka, phylogenetically far from the common commercially interest species [32]. In mammals' ISCs housed in the crypts, similar invaginations are not present in fish intestine [97]. However, the folds base represents their functional equivalent.

To identify intestinal stem cells along the rainbow trout gut, I selected the classical mouse ISCs marker. At first, LGR5, the specific crypt epithelial stem cell marker was investigated. Unexpectedly, *lgr5*+ cells were exclusively expressed by a stromal, subepithelial cells population along the folds of all considered tracts, rather than restricted to the epithelium lining the folds base. However, only recently an analogous expression pattern was also described in mouse small intestine. This peculiar cell population has been identified as telocytes, a peri-epithelial specialized

cell population whose role is to regulate and preserve the folds' tip epithelium integrity. Recent evidence demonstrated that their ablation lead to the perturbation of the enterocytes' gene expression pattern [98]. Therefore, it is reasonable to assume that something similar take place also in rainbow trout intestine.

The intestinal folds base was characterized by cells expressing *sox9* at different level. As in mammals' and in medaka intestine [32,46,99], *sox9* was restricted to the epithelium covering the folds base all along the intestine. Interestingly, we observed peculiar, elongated cells expressing *sox9* at high level, and displaying the typical position and shape of mouse CBC cells. As expected, we did not observe any differences in terms of their distribution along the intestine, supporting the hypothesis that these distinctive cell populations represent the functional equivalent of mouse LGR5+ cells.

The presence of *sox9*+ cells at the bottom of the secondary folds protruding from the complex folds of the distal intestine strongly support the thesis that these typical structures are provided by numerous actively proliferating stem cells zone and thus that they are supported by local niches.

We observed also elongated, *sox9*+ cells scattered along folds epithelium. Based on our previous observations [65], these cells, specifically located around the folds length, outside of the classical stem cell compartment, do not express Pcna and thus they are not anymore proliferating cells. Experimental studies, involving the use of enhanced green fluorescent protein (Sox9EGFP) transgenic mouse in small intestine allowed authors to identified two different SOX9+ cells population. On one hand, they characterized the classical crypt base columnar cells also enriched with a high LGR5 expression. On the other, they found a SOX9+ cells population along the villus epithelium lacking the typical proliferating marker and simultaneously expressed chromogranin A, the specific marker of enteroendocrine cells [100]. Taken together, these findings support the hypothesis that in mouse SOX9 expression along the villus epithelium might detect this terminally differentiated secretory cell type.

Based on our observation, this thesis might be also translated in rainbow trout even though, we were not able to verify the expression of chromogranin A in our samples due to the lack of reactive antibody specific for this marker in rainbow trout intestine.

In mouse intestine, CBC cells are located at the crypt base and are interposed between other SOX9+ cells, similarly, in rainbow trout, these cells were located among other cells expressing a lower *sox9* signal. Moreover, the signal was highest in the distal intestine and the basal part of the complex folds, gradually decrease in the pyloric caeca and was lowest in the proximal intestine and the apical part of the complex folds. Despite *sox9*+ cells represent a subpopulation of all proliferating cells, it is interesting to note that their distribution followed coherently the one of Pcna described in our previous work [65].

Notably, *sox9*+ cells did not co-express other stem cells marker and they sharply disappeared outside the intestinal folds base, where *sox9* expression was substituted with that of *hopx* that in turn gradually decreased towards the folds apex. In mouse intestine, HOPX+ cells are rare and restricted to the +4 position of the intestinal crypt [55]. Conversely, in rainbow trout, *hopx*+ cells were abundant, absent at the villus base, and were detected in the epithelial cells along the villus. In this species, few *hopx*+ cells were also found along the villus connective axis.

Taken together, these discrepancies lead us to believe that *hopx*+ cells in rainbow trout cannot be considered the functional equivalent of HOPX in mammals' intestine, but rather, its expression fully consistent and matching with the one of Pcna suggested that in this species, *hopx*+ cells characterize the typical transient amplifying population, an undifferentiated population in transition towards differentiation present in proximity of all somatic stem cells. Once again, its expression was not homogenous along the intestine. We observed the lowest *hopx* expression in the proximal intestine and in the apical part of the complex folds of the distal intestine, the signal gradually increased in the pyloric caeca and was

highest in the distal intestine and in the basal part of the complex folds, once again, consistently with Pcna expression. Interestingly, also in piglets' intestine, HOPX expression did not follow a linear distribution along the whole intestine. In this species the highest expression was found in the large intestine [46].

Another essential marker expressed in the mouse epithelium at the crypt base and specifically by LGR5+ ISCs is NOTCH1 which induces cells to differentiate towards absorptive lineages. In rainbow trout, we observed *notch1*+ cells scattered along the folds' stroma, where it colocalizes with *lgr5*. This happens also in mouse intestine but in the epithelial cells located at the crypt base rather than in the subepithelial stromal population.

Close to *lgr5*+/*notch1*+ stromal cells, were also identified elongated epithelial *dll1*+ cells. They were located along the fold's length and its topographical nearness to the stromal population expressing *lgr5*+/*notch1*+ stromal cells, suggested a possible functional interaction. Their epithelial location did not reflect the one in mouse small intestine, where DLL1 is expressed by Paneth cells at the crypt base [101]. Despite their fundamental role, the presence of Paneth cells is still doubtful in many domestic and fish species [28,46,47,65]. Particularly, our previous works demonstrated their absence in piglets' and rainbow trout intestine. However, DLL1+ cells were also found in mouse colon, where Paneth cells are known to be absent [42]. Taken together these observations support the hypothesis that in the species in which Paneth cells are not present, another cell type functionally substitutes them actively interacting with ISCs.

Few *dll1*+ cells were also found within the stroma along the folds length, but more studies are required to understand their functional role and their implications in the intestinal stem cell niche. In mouse intestine, Paneth cells maturation and differentiation are driven and promoted by WNT signalling, the evolutionary conserved pathway that contributes to stem cells maintenance. Recent studies suggested a redundance on WNT sources, indeed it is expressed by both stromal

and epithelial cells [102]. In rainbow trout, as occurs in mouse small intestine, *wnt3a* is expressed by a subepithelial cell population. Surprisingly, while in mouse WNT3A+ cells are located in the pericryptal region throughout the lamina propria, in rainbow trout *wnt3a+* cells were scattered along the villus connective axis.

Recent studies conducted in mouse small intestine demonstrated that telocytes also express Wnt3a [60]. Interestingly, in rainbow trout, the stromal *wnt3a+* cell population co-localize with those expressing *lgr5*. The expression pattern, fully consistent with the one observed for telocytes, strongly supports our theory about the presence of this peculiar cell type also in the rainbow trout intestine (Figure 41).
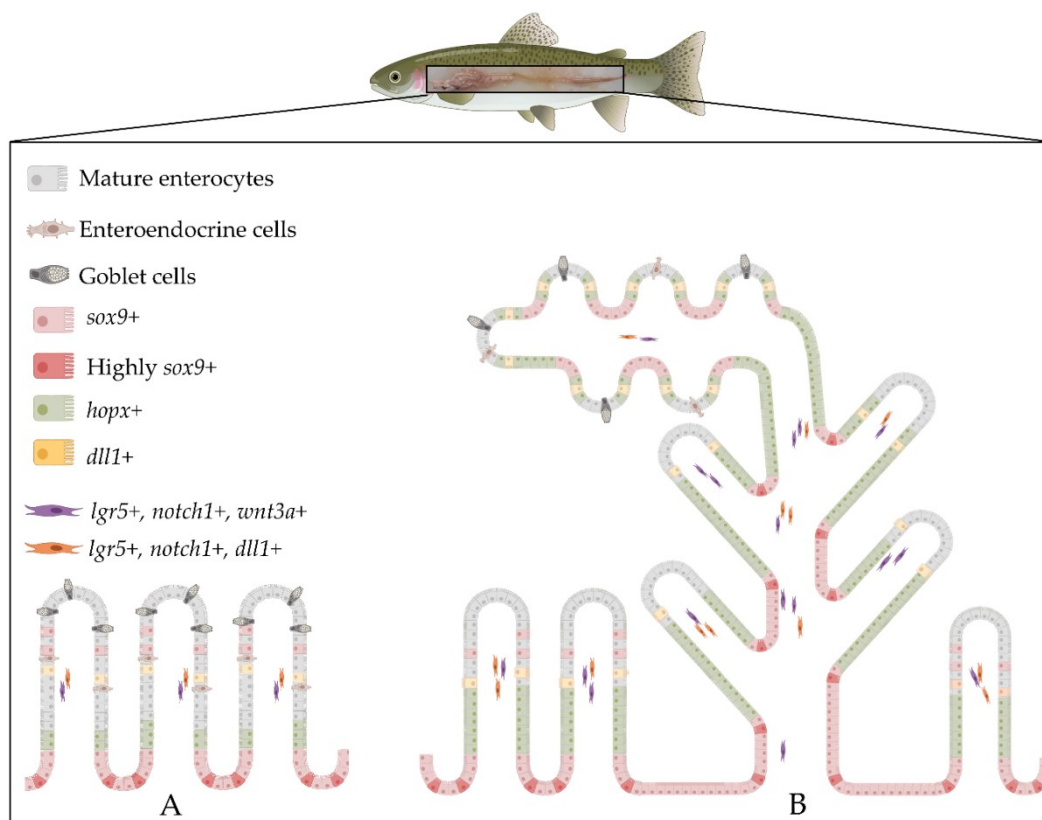
Figure 41: Schematic illustration of the architecture and the organization of the intestinal stem-cell niche in rainbow trout in the proximal (A) and distal (B) intestine. *Sox9* was expressed by the epithelial cells located at the folds base. Its signal was downregulated along the fold length, where *hopx* expression increased and then faded in the apical part of the folds. *Lgr5* was exclusively expressed in scattered cells located along the gut stroma, where it colocalized with *notch1* and *wnt3a*. *Dll1* also colocalized with *lgr5* in the lamina propria and it was expressed in the epithelium near *lgr5+* stromal cells. The distribution of these markers along the rainbow trout intestine was not homogeneous; rather, we observed the highest expression in the basal part of the complex folds of the distal intestine compared to the other intestinal regions. Illustrations created with BioRender.com.

Conclusion

Overall, our results indicated that the classical mouse intestinal stem cell markers are expressed also in the rainbow trout intestine. However, their typical localization, the niche architecture and the interactions among these markers are not conserved. In particular, in this species the functional equivalent of *lgr5* seems to be *sox9*, since *sox9*+ cells showed the peculiar location and shape of CBCs in mouse intestine. Interestingly, the present data extend our previous work, in which we described for the first time a peculiar compartmentalization of the digestive and absorptive functions along the RT intestine. Specifically, we observed that pyloric caeca and the basal part of the complex folds of the distal intestine share common morphological features and a higher renewal-rate that set them apart from the proximal intestine and the apical part of the folds of the distal intestine. Here, our data demonstrated that the high self-renewal capability displayed by pyloric caeca, distal intestine and the basal part of the complex folds previously observed, was ensured by a rich stem cell population. On the contrary, the lower renewal rate observed within the other districts, was reflected in a restricted stem cells population. Taken together, these data confirm that the RT intestinal mucosa present two different renewal-rate.

Chapter 4

Identification and Characterization of Telocytes as active player of the Stem Cell Niche in the Rainbow Trout (Oncorhynchus Mykiss) Gut

Overview

To expand and integrate our previous findings describing the organization and the architecture of the RT stem cell niche, here I performed a detailed qualitative analysis of the distribution of the stromal component of the niche and in particular of telocytes (TC) as active player of the intestinal homeostasis maintenance. To this purpose, specific histological staining for the connective tissue and ultrastructural analysis have been performed. Furthermore, since the mouse is the species in which the mesenchymal component of the niche has been studied most, I selected the typical mouse TC markers (PDGFRα and FOLX1) as target genes, and I verified their topographical localization through fluorescence *in situ* hybridization. In addition, I studied their spatial distribution in relation with the epithelial components of the stem cell niche.

Our results indicated the presence of slender elongated cells, distributed juxtaposed the enterocytes' basement membrane creating an intricate mesh extending from the folds base to their apex. TEM analysis confirmed the identity of this cell population as TC; indeed, they possessed the distinctive features of this cell type, including a voluminous nucleus and limited cytoplasm from which long thin discontinuous branches develop. Moreover, in the close proximity of telocytes, I observed extracellular vesicles suggesting their functional implication in long-distance cell-to-cell communication. *In situ* localization of *pdgfrα* transcripts highlighted two distinct *pdgfrα*+ cell populations, one displaying the typical morphology and position of TC, and another expressing *pdgfrα* at lower level and not possessing the distinctive TC morphological features and therefore considered as common fibroblasts. *In situ* localization of *foxl1* transcripts revealed that *foxl1*+ cells were rare and distributed in the peri-epithelial space both at the folds base and along the folds length. In both locations, *foxl1* was always co-expressed with *pdgfrα*, indicating the existence of a small functional telocytes subset. Basal TC were in the

proximity of actively cycling intestinal stem cells, suggesting a possible interaction through short-range signaling. Their morphology and distribution at the basal and apical portion of the intestinal folds were identical to those observed in the mouse. This allows us to infer that also in RT, as in mouse, telocytes stimulate either cell proliferation or cell differentiation depending on their topographical location. Altogether, these results substantially improve our understanding of the molecular mechanism and of the cell types involved in the maintenance of intestinal homeostasis (Figure 42) [103].
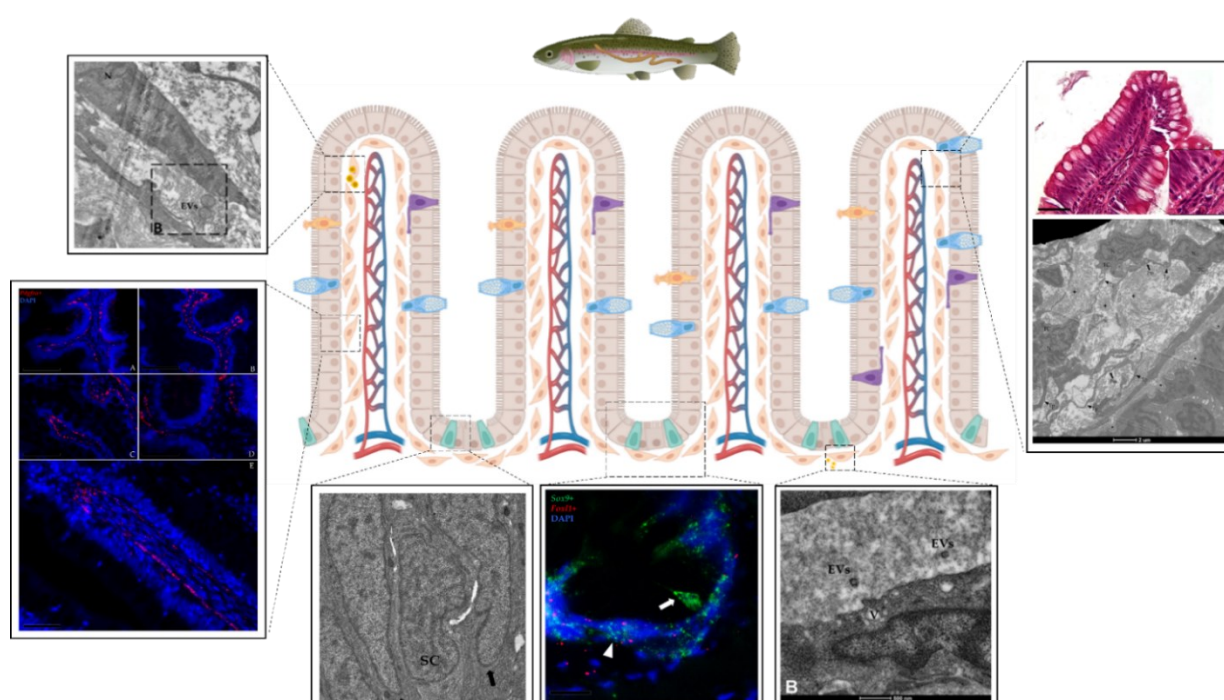
Figure 42: Schematic illustration of the rainbow trout intestinal mucosa. Telocytes (TC) were observed along the gut stroma, they were located adjacent to enterocytes' basement membrane and expressed the typical mouse TC markers (*pdgfrα* and *foxl1*). Ultrastructural studies showed that they possessed a voluminous nucleus and long, thin discontinuous branching. TC located around the folds base were distributed in the close proximity of intestinal stem cells. RT TC actively participate to cell-to cell communication through the secretion of extracellular vesicles. Image created using BioRender.com.

Introduction

Intestinal stem cells (ISCs) play a pivotal role in the mucosal homeostasis preservation. However, the thin balance between self-renewal and differentiation is ensured by the active interaction between stem cells and several extracellular signals and factors provided *in vivo* by a well-defined microenvironment called intestinal stem cell niche. These specific structures consist of different cell populations including epithelial stem cells (ISCs), supportive mesenchymal cells, adipocytes and acellular components such as growth factors, chemokines and regulatory molecules. Moreover, numerous resident immune cells also actively cooperate with the stem cell population to protect and preserve the niche. Among the different supportive stromal cell population, subepithelial telocytes , have been recently proposed to be a key source of signaling factors without which stem cells cannot proliferate and thus properly support the tissue homeostasis [55,104,105].

Telocytes are newly discovered interstitial cells, characterized by peculiar ultrastructural features exclusively appreciable under the electron microscope. They are characterized by a small cell body and by a variable number of long and thin cytoplasmic projections called telopods, generally 2-3 per cells. Overall, these extroflections allow the generation of an intricate, dense supportive 3D mesh underlying the epithelium [106]. They possess a voluminous nucleus containing condensed heterochromatin, as a consequence, the surrounding cytoplasm is scarce and include only few organelles. Mitochondria occupy approximately 5-10% of the cell volume and are generally distributed in the perinuclear region or within the cytoplasmic extensions. In this latter district, the smooth endoplasmic reticulum and the Golgi apparatus are also present representing less than 1-2% of the total cell volume. While, they have been observed in disparate tissues and organs of several mammalian species, their presence, is still unexplored in many aquatic species [106]. To date, their specific functional role is not yet fully understood but experimental

data demonstrated that these newly discovered cell population is directly involved in many key aspect of cell biology, including tissue repair and regeneration, intercellular signaling, immune response and homeostasis preservation [107]. In particular, the possibility that TC had the ability to establish direct connection with tissue-resident stem cells was originally proposed for the myocardium. Subsequently, this hypothesis has been also confirmed in the niches of other organs such as intestine, skeletal muscle, lung, and skin [60,61,108–110]. Currently, among the different stem niches of the various organs, the distribution and role of TC has aroused greater interest in the intestine where they have been studied and characterized in mice and humans [109,111–113]. Conversely, these understanding are still extremely limited in other domestic species, especially in fish. A detail characterization of the stromal population of the stem cell niche together with the evaluation of their potential relationship with its epithelial component, would be helpful to further elucidate the molecular mechanisms at play to preserve intestinal homeostasis and consequently to develop a lifelike *in vitro* model. Therefore, in this chapter of my thesis have been expanded and integrated our knowledge of the RT intestinal stem cell niche exploring also their mesenchymal component.

In particular, I verified the presence of TC along the trout gut through histochemical and ultrastructural analysis, and I evaluated their possible interaction with the epithelial constituents of the niche. To this purpose, I selected the classical mouse TC markers as target genes (*pdgfrα* and *foxl1*) and I examined their expression and topographical localization along the intestine through *in situ* hybridization individually or in combination. In addition I studied their expression in relation with *sox9* the RT epithelial stem cell marker.

Methodologies

Samples collection

A total of five adult female rainbow trout (RT), weighing approximately 500 g, were collected from fish culture ponds at the Laghi Verdi s.n.c. trout farm (Como, Italy). Individuals were euthanized according to Annex IV European Union (EU) guideline 2010/63, during non-experimental clinical veterinary practices. Immediately after sacrifice, a longitudinal incision along the ventral line was performed and the whole e gastrointestinal (GI) tract was removed (Figure 43). Small fragments of proximal and distal intestine were collected and fixed in 10% neutral buffered formalin for 24 h at room temperature, subsequently dehydrated in graded alcohols, cleared with xylene, and embedded in paraffin.
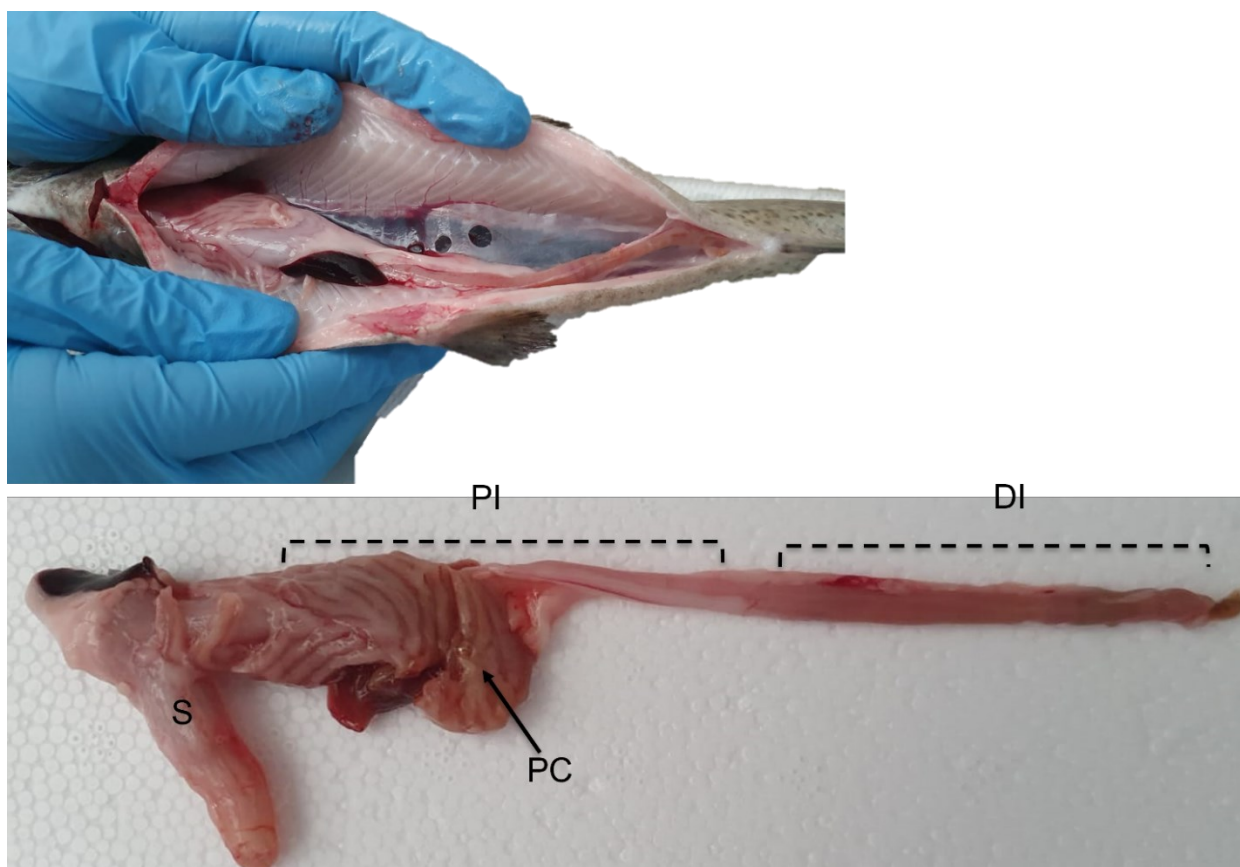

Figure 43: Gross anatomy of the digestive system of rainbow trout showing its main portions. S: stomach, PI: proximal intestine, PC: pyloric caeca, DI: distal intestine.

For transmission electron microscope (TEM) investigations, small pieces of both intestinal tract were fixed overnight with 2.5% glutaraldehyde and 4% paraformaldehyde in 0.1M sodium cacodylate buffer pH 7.4, rinsed and then postfixed with 1% osmium tetroxide diluted in 0.1M sodium cacodylate buffer. Afterwards, samples have been washed and incubate in 0.5% uranyl acetate solution at 4°C overnight. Subsequently, they have been rinsed and dehydrate through a graded series of ethanol diluted in distilled water. Ethanol was exchanged with epoxy resin mixture and embedded in fresh resin at 60°C for 48 hours. Semithin sections were cut with a RMC Boeckeler ultramicrotome and stained with toluidine blue. Ultrathin sections were examined using the Transmission electron microscope Talos L120C (Thermofisher, USA) operating at 120 KV. Images were acquired by a Ceta Camera 4K x 4K (Thermofisher, USA).

Histology and Histochemistry

Formalin-fixed paraffin embedded (FFPE) samples were used to cut thin sections of 5 μm. To evaluate the general morphology and architecture of the tissue, FFPE sections were brought to distilled water via xylene and degraded series of alcohols and subsequently stained with hematoxylin-eosin. Other sections were stained with specific histochemical staining to evidence the connective tissue as follows:

1. Periodic-acid Schiff (PAS) and Alcian blue (pH 2.5) which is a combined method used to highlight proteoglycans such as glycosaminoglycans in the extracellular matrix, in particular, this staining showed in magenta the neutral glycosaminoglycans and in blue the acid glycosaminoglycans

2. Mallory's triple stain which exploits three different dyes: carbol fuchsin for nuclear staining, aniline blue for a selective collagen staining, and orange G for cytoplasm

3. Masson's trichrome is considered the method of choice for connective tissue; highlights cell nuclei in black with Weigert's ferric hematoxylin, acid fuchsin stains the cytoplasm in red and the connective tissue in blue with aniline blue

4. Crossman's trichrome which exploits the same chemical principles as the previous staining. In brief, collagen is highlighted in blue with aniline blue, cytoplasm is made red by orange G and acid fuchsin together, while the nuclei appear black due to the presence of Weigert's ferric hematoxylin.

Immunohistochemistry

Proliferating cells were characterized through the immunolocalization of Proliferative cell nuclear antigen (Pcna). Its specific distribution was analyzed though indirect immunohistochemistry using the Avidin Biotin Complex method (VECTASTAIN® Elite® ABC, Vector Laboratories, USA) following manufacturer indications. In brief, thin sections of 5μm were brought to boiling in an antigen retrieval solution (10mM Tris Base, 1mM EDTA, 0.05% Tween20, pH 9) in a pressure cooker for 1 minute. Slides were cooled at room temperature, washed in phosphate-buffered saline (PBS, pH 7.4), and incubated with 3% H_2O_2 solution diluted in distilled water for 15 minutes to block endogenous peroxidases. Non-specific bindings were prevented incubating sections in Normal Blocking Serum Vectastain (ABC Elite KIT) at room temperature for 30 minutes and then incubated with Anti PCNA Mouse monoclonal antibody 1:1600 (Millipore Corporation, MAB424, Darmstadt, Germany) diluted in 4% BSA in PBS with 0.05% Tween20, for 60 min at room temperature in a humid chamber. Sections were then incubated with the adequate biotinylated secondary antibody for 30 minutes and later with the avidin-biotinylated horseradish peroxidase (HRP) complex (Vectastain ABC Elite KIT) for another 30 minutes. Sections were exposed to 3,3'-diaminobenzidine solution (ImmPACT® DAB, SK-4105 Vector Laboratoris, USA), counterstained with Mayer's hematoxylin, dehydrated and permanently mounted.

Target probe design and in situ hybridization

Since the mouse is the species in which telocytes (TC) have been studied most, the two following well-defined mouse TC markers have been selected as targes: Platelet-derived growth factor receptor α (*Pdgfrα*) and Forkhead Box L1 (*Foxl*1) [60,114]. PCR confirmed their expression also along the rainbow trout gut, later the amplification product (Table 6) has been sent to Advanced Cell Diagnostics (ACD) for the design and synthesis of *ad hoc* custom probes.

Table 6: Probe targets and corresponding conjugated channels

Species	Gene	Channel		Target Region	Number Of Pairs	Cat. Number
Rainbow Trout	*pdgfrα*	3	LOC110499401	4757 - 6512	19	1029301-C3
Rainbow Trout	*Foxl1*	2	LOC110530975	1910 - 3262	20	1039271-C2
Rainbow Trout	*Sox9*	3	LOC100135781	28-972	14	847751-C3
Rainbow Trout	*Ppib*	1	LOC110491579	178-1096	19	540651
Rainbow Trout	*DapB*	1	EF191515	414-862	10	312038

Fluorescent *in situ* hybridization was performed using Multiplex Fluorescent Reagent Kit V2 (RNAscope technology, Advanced Cell Diagnostics, San Francisco, CA, USA) according to the manufacturer's instructions. Briefly, 4 μm sections were heated and immediately immerse in xylene to encourage paraffin removal. Slides were exposed to hydrogen peroxide (Advanced Cell Diagnostics, San Francisco, CA, USA) and brought to boiling in a target retrieval solution (Advanced Cell Diagnostics, San Francisco, CA, USA). Subsequently, sections were incubated with Protease III (Advanced Cell Diagnostics, San Francisco, CA, USA) to allow probes

to reach their defined target. Afterward, samples were incubated with diluted probes 1:50 in diluent buffer in a HybEZ oven (Advanced Cell Diagnostics, San Francisco, CA, USA) for 2 h at 40° C. Probes were conjugated with different channels in order to allow multiplex comparison. Signal amplification was performed incubating sections in three signal amplification solutions, whereas signal development was performed incubating the slides with the adequate fluorophore (OPAL 520 or OPAL 570, Akoya biosciences, Marlborough, MA, USA) diluted 1:750 in tyramide signal amplification (TSA) buffer.

Moreover, to explore the relation between the stem cells and the stromal cell population, the two selected markers, were combined to *sox9* (probe: om-Loc100135781-C3, cat. No. 847751-C3). Sections were then counterstained with DAPI for 30 seconds and mounted with ProLong™Gold Antifade Mountant (ThermoFisher Scientific, Waltham, MA, USA).

mRNA quality and integrity within FFPE samples were checked using a constitutive control gene (*PPiB-Peptidylprolyl Isomerase B*), while negative controls were performed incubating slides with *Bacillus subtilis* dihydrodipicolinate reductase (dapB) gene. Samples were analyzed under an Eclipse E600 microscope (Nikon) equipped with a digital camera (Nikon). Images were acquired with NIS-Elements Software (Version 4.6; Nikon).

Results

Identification and Characterization of Telocytes in the Rainbow Trout Gut

Morphological analysis of the connective tissue of the trout gut revealed the presence of cells exhibiting a peculiar slender and thin morphology. They were localized around the folds' base and along the folds' length within the stromal space adjacent to the intestinal epithelium. Hematoxylin-eosin staining evidenced a typical distribution generating a dense supportive mesh juxtaposed the enterocyte's basement membrane (Figure 44).

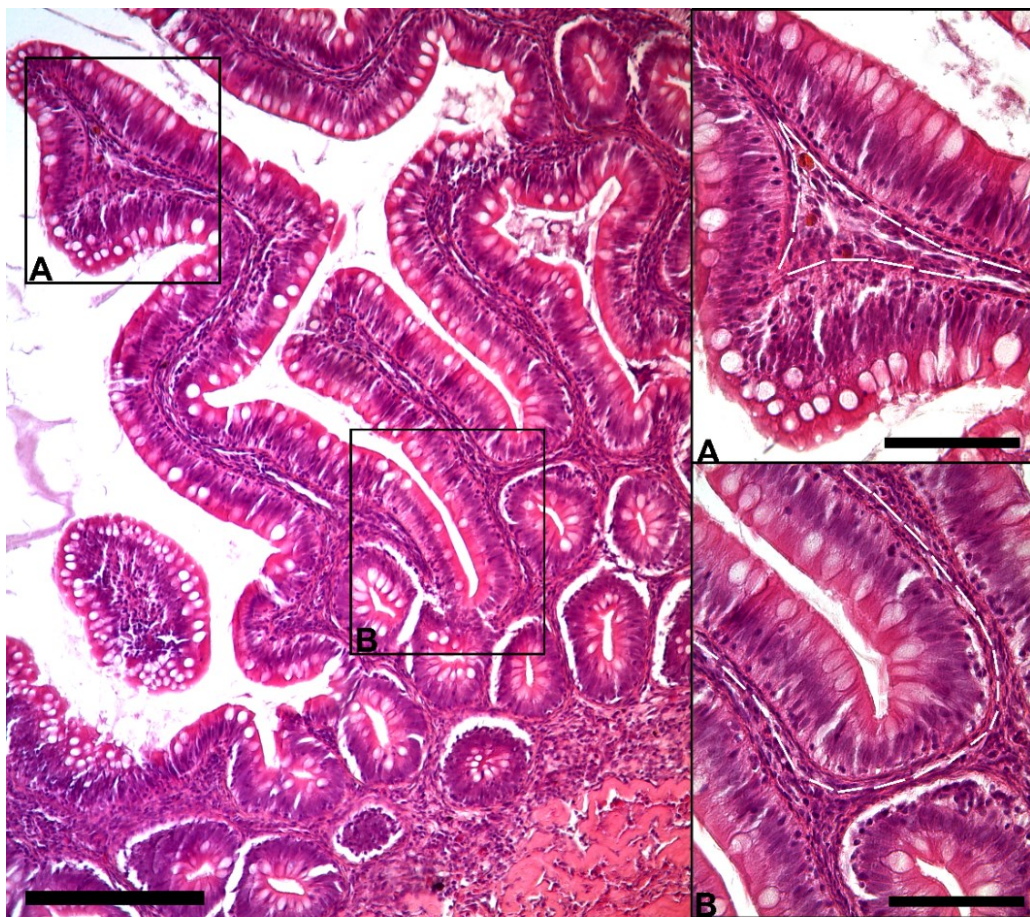**Figure 44**: Hematoxylin-eosin stained section of proximal intestine showing the organization of slender, elongated cells distribute along the enterocytes' basement membrane.

Optical microscope investigation at high magnification reveled that these cells were characterized by a distinctive moniliform shape by *virtue* of its slender and stretched nucleus and long thin cytoplasmic projections (Figure 45).
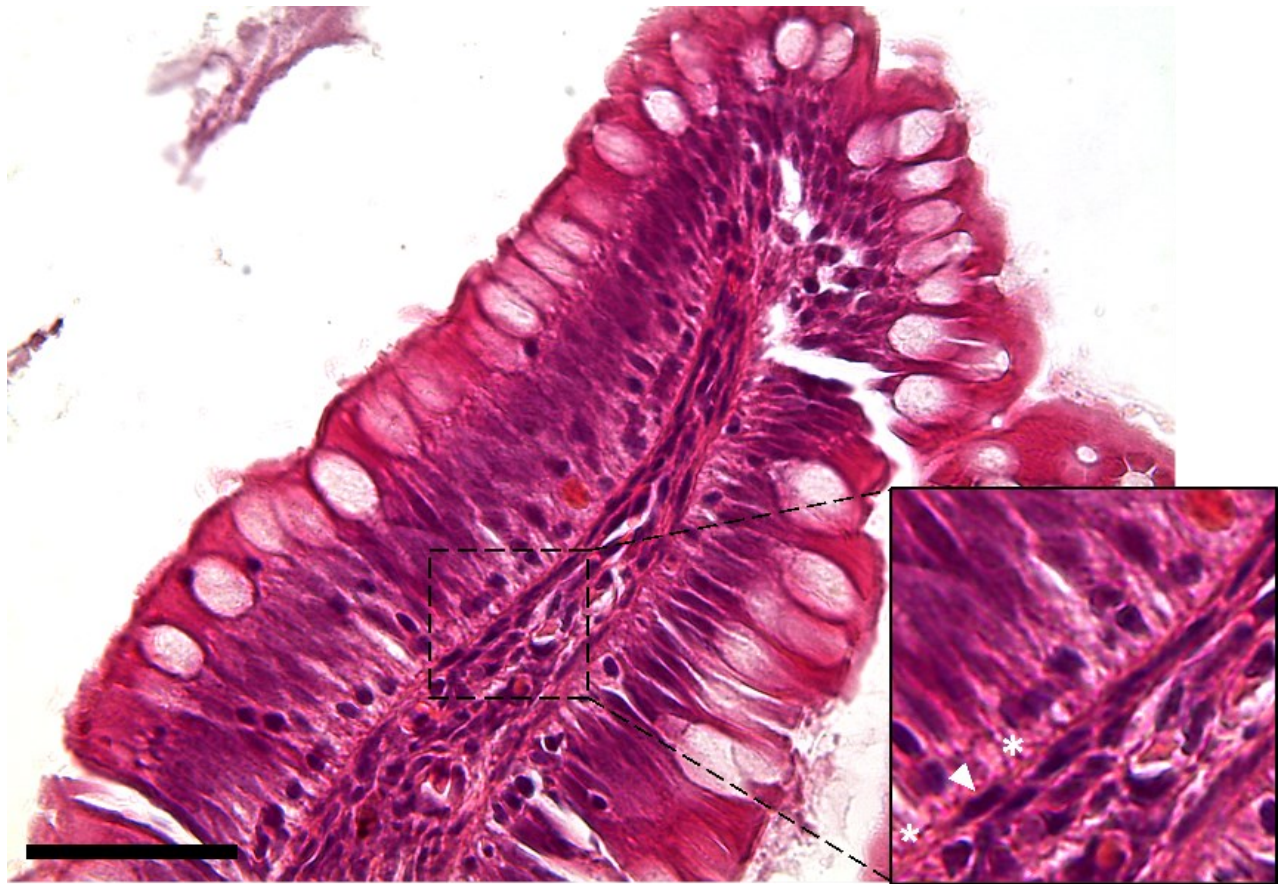
Figure 45: Hematoxylin-eosin of proximal intestine showing peculiar stromal cells having an elongated nucleus (arrowhead) and long and thin branches (asterisks).

Moreover, histochemical staining specific for the connective tissue including Periodic-acid Schiff (PAS) and Alcian blue (pH 2.5), Mallory's triple stain, Masson's trichrome and Crossman's trichrome (Figure 46-47) and toluidine blue (Figure 48) performed on semi-thin sections, further affirm the presence of an intricate and continuous network underlining the epithelium.
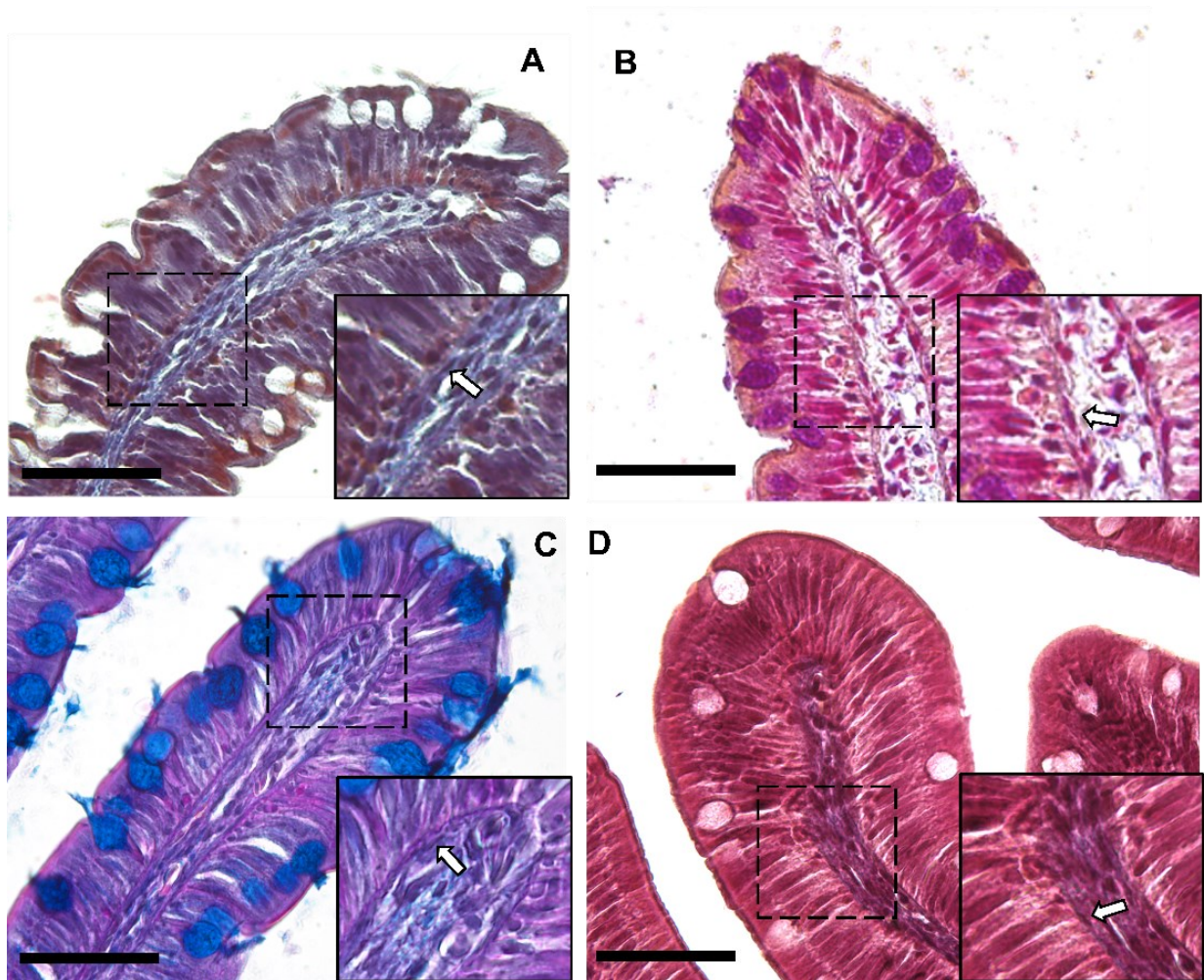
Figure 46: Representative figures of proximal intestine stained with Crossman's trichrome (A), Mallory's triple stain (B), Periodic Acid Schiff-Alcian Blue at pH 2.5 (PAS-AB 2.5) (C) and Masson's trichrome (D) emphasizing the generation of the elaborate network adjacent to the intestinal epithelium (arrows). Scale bar 50µm.
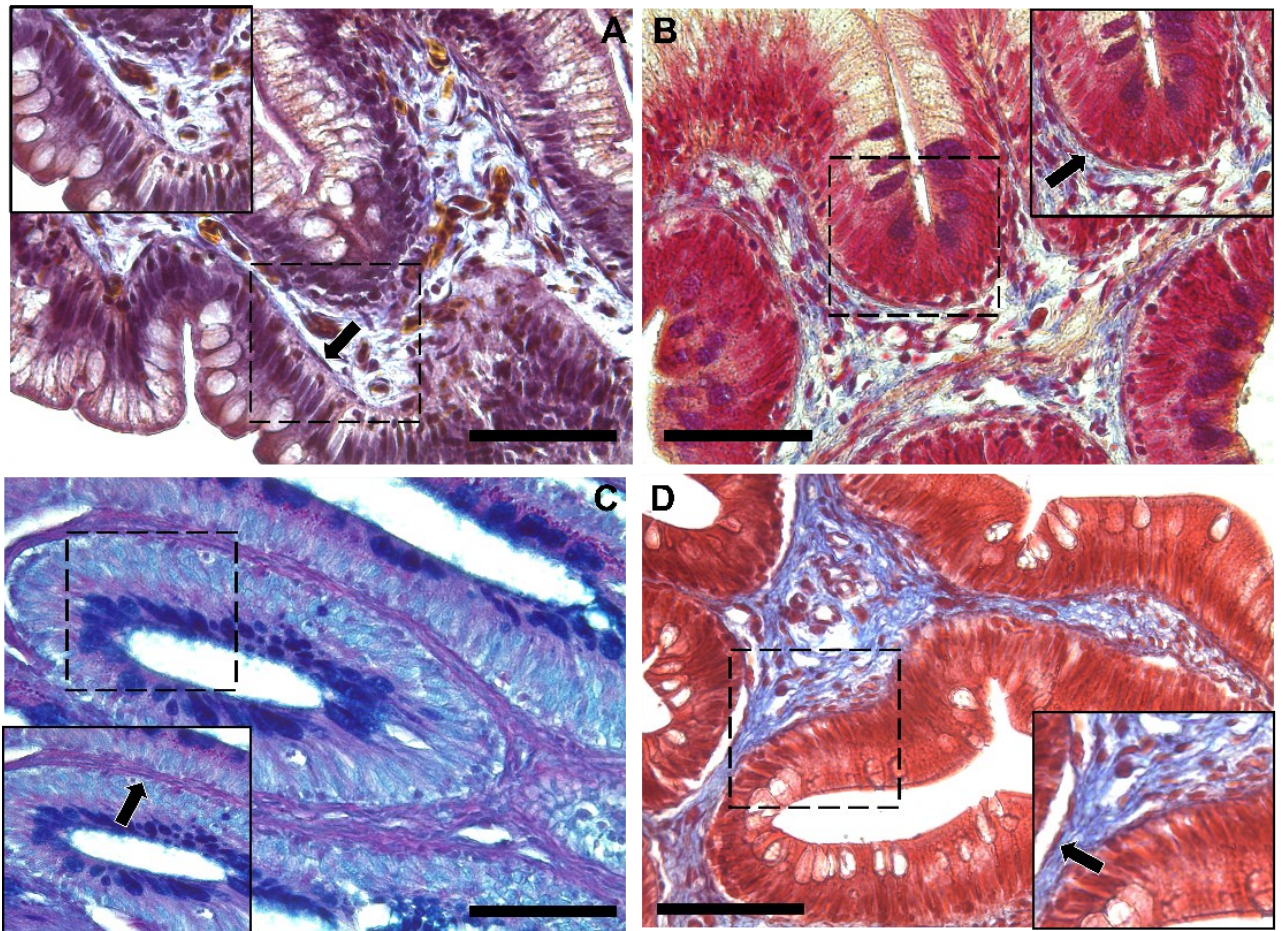
Figure 47: Representative figures of distal intestine stained with Crossman's trichrome (A), Mallory's triple stain (B), Periodic Acid Schiff-Alcian Blue at pH 2.5 (PAS-AB 2.5) (C) and Masson's trichrome (D) emphasizing the generation of the elaborate network adjacent to the intestinal epithelium (arrows). Scale bar 50μm.
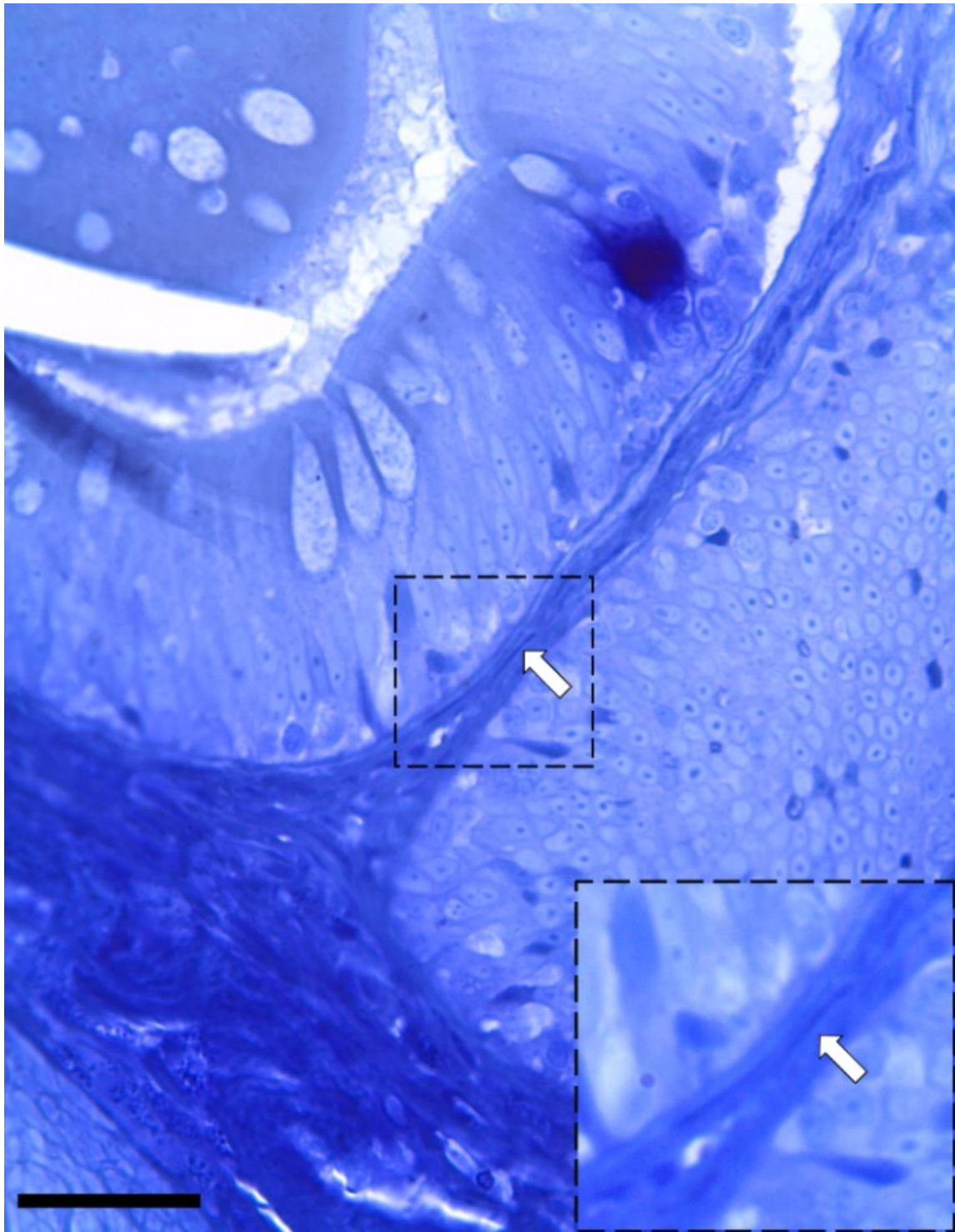
Figure 48: Representative semi-thin section of proximal intestine stained with toluidne blue highlighting the presence of slender cells just below the enterocyte's basement membrane (arrow) (Scale bar 25μm).

TEM investigation confirmed the presence of mesenchymal cells disposed along the enterocytes' basement membrane easily distinguishable from the fibroblasts that commonly are localized within the lamina propria. They possessed an irregular shape, a voluminous nucleus containing heterochromatin cluster mainly located on the nuclear periphery, and a scarce and restricted cytoplasm from which originated long and discontinuous branches in a variable number (generally 2-3 per cells). These cytoplasmic projections known as telopds (Tp) developed in a non-linear fashion and presented peripheral dilatation called podoms (Pm) hosting vacuoles and cellular organelles (Figure 49-50-51). Altogether, histological and ultrastructural examination confirmed the identity of this cell population as telocytes.
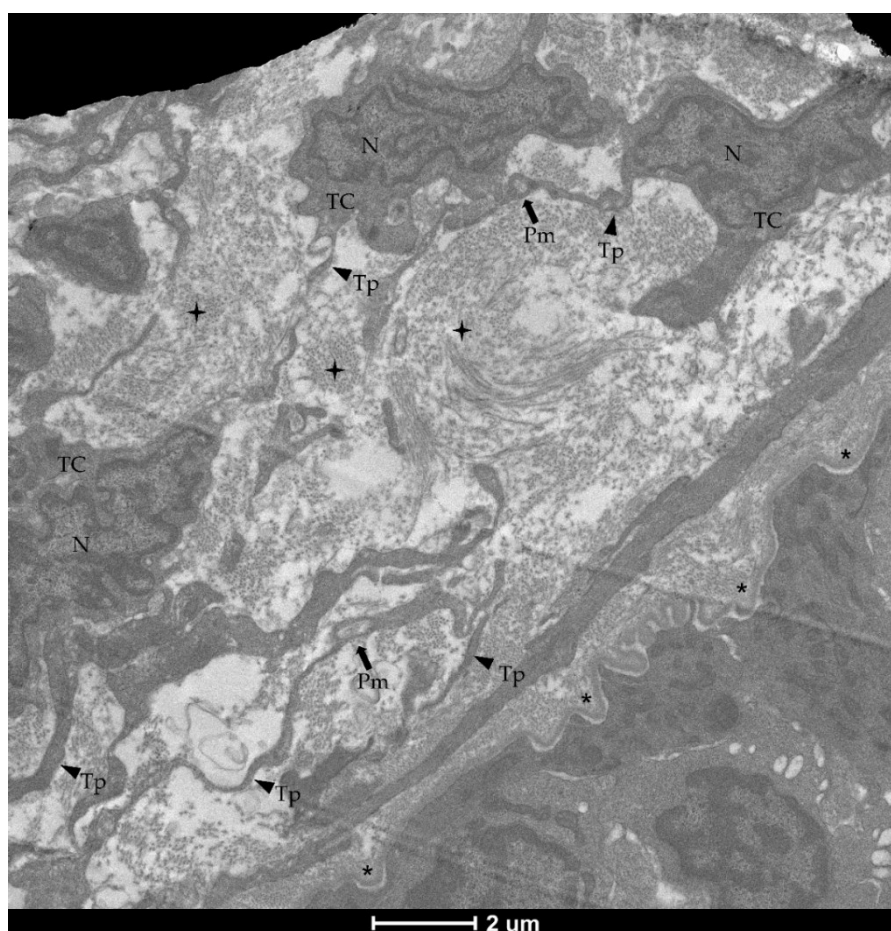
Figure 49: Transmission electron microscope image of proximal intestine showing the presence of telocytes (TC) located juxtaposed the epithelium (asterisks) with voluminous nucleus (N), long and thin cytoplasmic prolongations called telopods (Tp) immersed in collagen fibers (cross) which dilate in their periphery originating podoms (Pm).
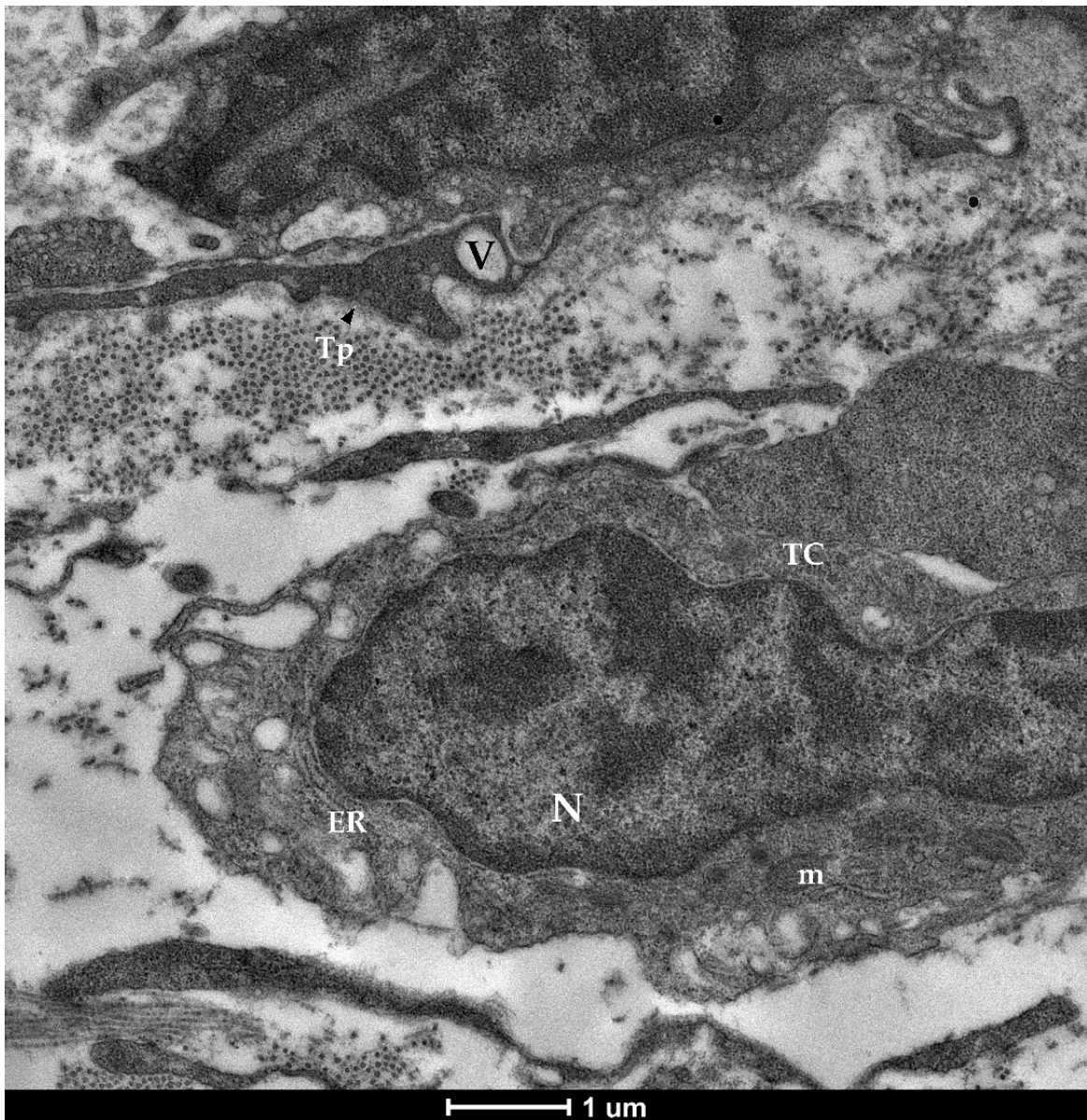
Figure 50: Representative transmission electron microscope image showing telocytes (TC) with an expanded nucleus and limited cytoplasm hosting cellular organelles (ER: endoplasmic reticulum, m: mitochondria).
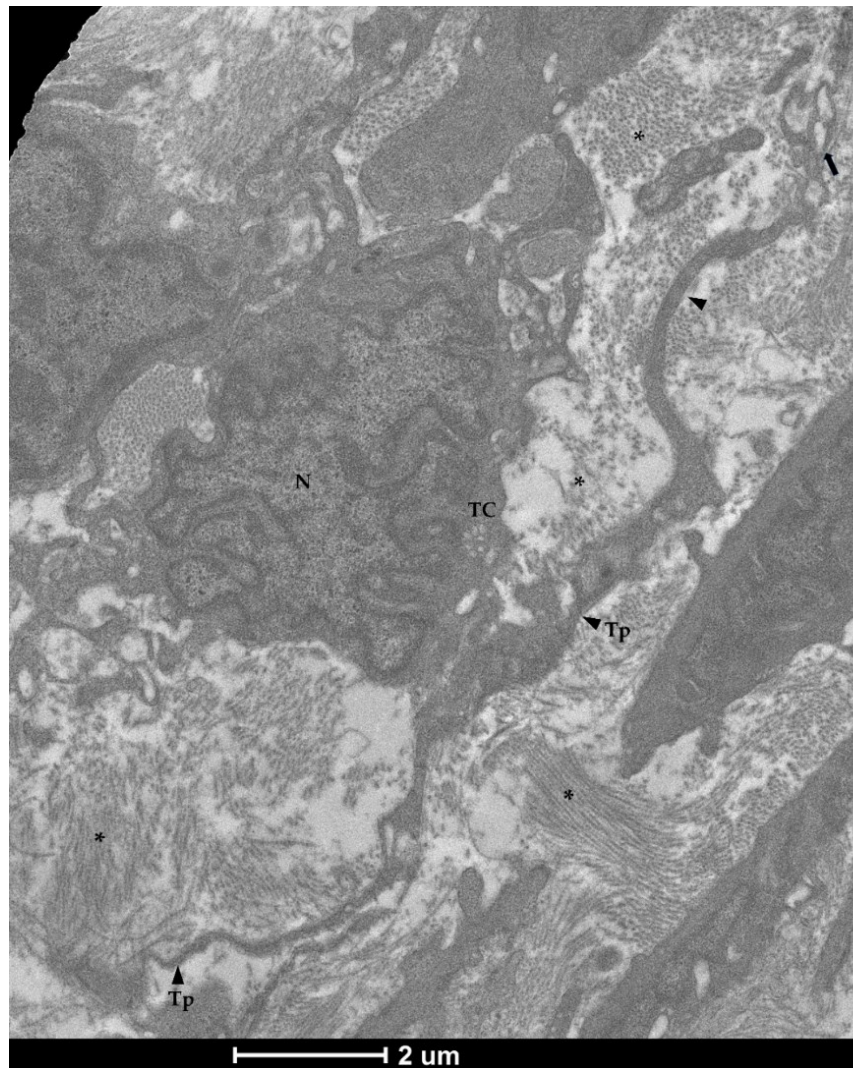
Figure 51: Transmission electron microscope figure showing typical telocytes features: voluminous nucleus (N) and long and discontinuous telopods (Tp).

In situ hybridization of *pdgfra* showed that *pdgfra⁺* cells were abundant and located exclusively along the gut stroma. In this location, two different *pdgfra⁺* cell populations were recognizable. The first displayed high level of *pdgfra* expression, presented thin and elongated nucleus and was selectively distributed underlining the intestinal epithelium. This cell population generates a continuous plexus spanning from the folds' bases towards their tips. *Pdgfra* expression was more intense at the folds apex and along the fold's length compared to the one located around the folds' base. The other *pdgfra⁺* cell population was localized in the innermost region of the lamina propria and was characterized by a low label-intensity (Figure 52).
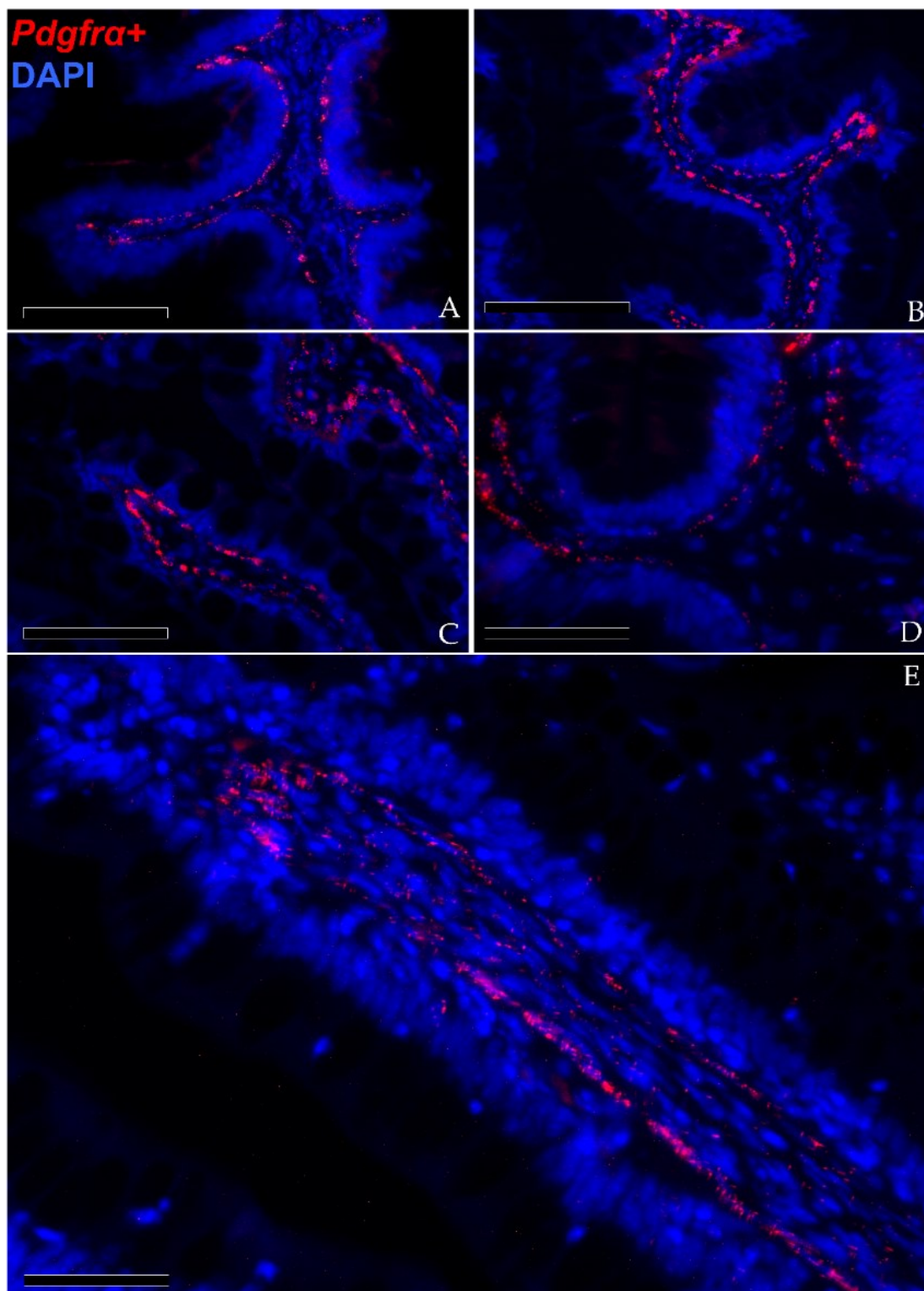
Figure 52: *In sit*u hybridization of *pdgfrα* (red dots) along the rainbow trout intestine. *Pdgfrα*+ cells were located along the intestinal stroma. Two different *pdgfrα⁺* cell populations have been detected: the first displayed high *pdgfrα* expression and was distributed immediately below the enterocytes' basement membrane. This, generated a complex network underlying the folds epithelium (A-B; Scale bar 100 μm). Moreover, the signal was less intense around the folds base compared to the one along the folds length and apex (C-D; Scale bar 50μm). The other, shower a lower *pdgfrα* expression and was found in the innermost region of the lamina propria (E; Scale bar 50μm). Nuclei were counterstained with DAPI (blue).

In both proximal and distal intestine, *foxl1*+ cells were rare and located along the gut stroma. In particular, few *foxl1*+ cells were distributed in the peri-epithelial space enwrapping the folds base. Interestingly, *foxl1*+ cells have been found also encircling the folds base of the secondary folds emerging from the complex *plicae* characteristic of this tract. Scattered mRNA dots of *foxl1* were also present in the epithelium lining the base of the folds (Figure 53). Dual-label fluorescence *in situ* hybridization showed that some *pdgfra*+ cells located beneath the enterocyte's basal membrane simultaneously expressed *foxl1* suggesting the presence of small functional telocytes subset (Figure 54).
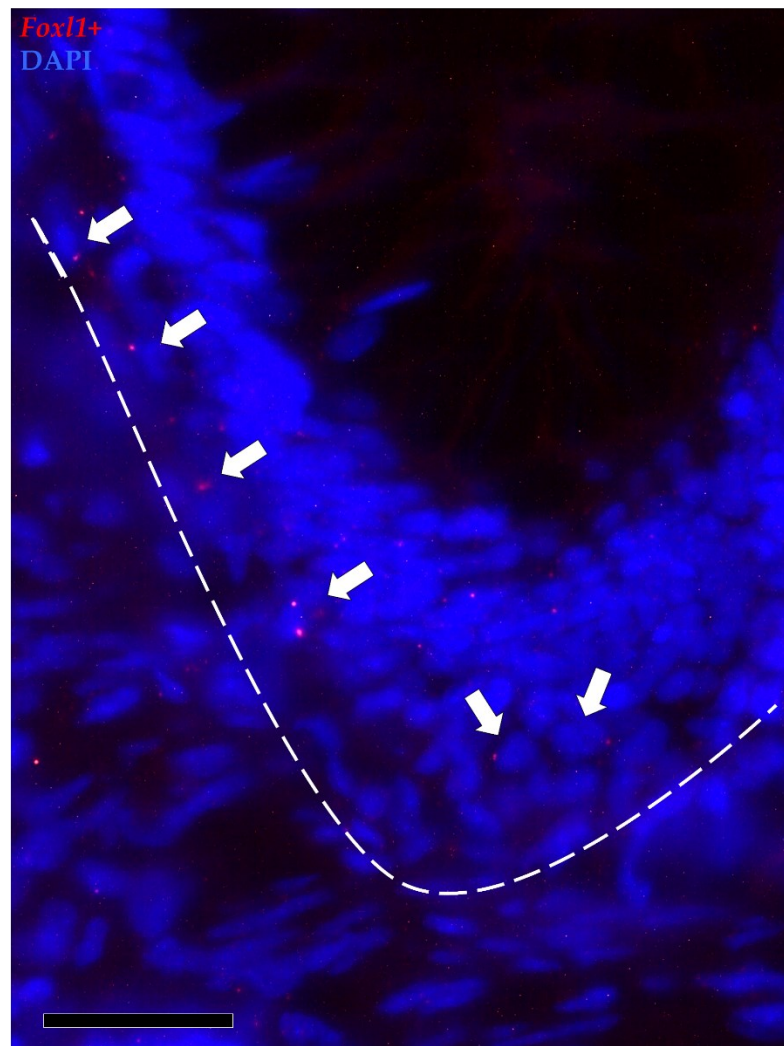
Figure 53: Representative image showing *in situ* hybridization of *foxl1* (red dots) in the proximal intestine. *Foxl1*+ cells were rare and located preferentially within the gut stroma. Scattered mRNA dots were also found in the epithelial cells lining the folds base (scale bar 50μm). Nuclei were counterstained with DAPI (blue).

Figure 54: Representative image of dual-fluorescence *in s*itu hybridization of *foxl1* (red dots) and *pdgfrα* (green dots). Stromal *foxl1*+ cells simultaneously expressed *pdgfrα*+ indicating the presence of small functional subsets. They were distributed along the folds length (A) and surrounding the folds base (B) (scale bar 50μm). Nuclei were counterstained with DAPI (blue).

Telocytes as Stromal Component of The Stem Cell Niche

We previously observed that *sox9⁺* cells in RT intestine display common features with the well-known crypt base columnar cells (CBCs) widely described in mouse small and large intestine, included a typical slender morphology and a topographical localization limited to the epithelium lining the folds base. Here, we integrated those results evaluating also their ultrastructural characteristics. TEM examination showed the presence of few epithelial cells characterized by a nucleus to cytoplasm ratio unbalanced in favor of the nucleus containing loose decondensed heterochromatin, a distinguishing mark of the stem cell population (Figure 55). These observations confirmed their identity as stem cells and their equivalent functional role of CBCs. They were located among other epithelial cells defined by a cell nucleus containing heterochromatin clusters with a compact appearance.
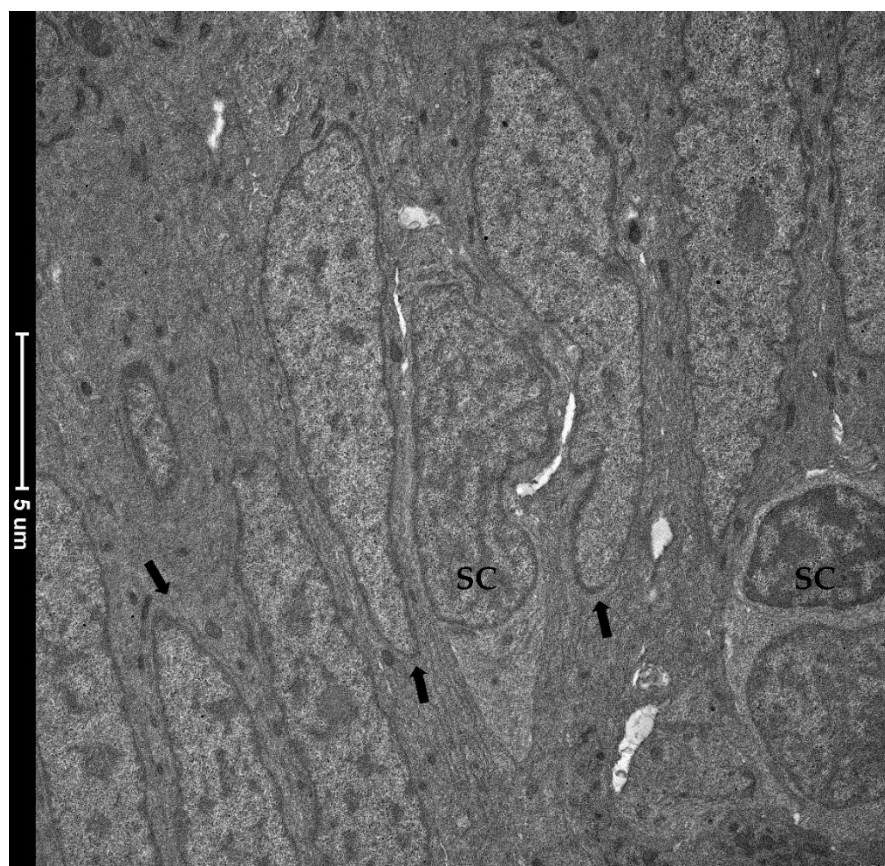
Figure 55: Representative transmission electron microscope image showing intestinal stem cells (SC) characterized by the typical loose decondensed heterochromatin and located among other common epithelial cells (arrows).

Immunolocalization of Pcna showed that TC were not active proliferating cells. However, they enwrapped the proliferative compartment located at the folds' base and thus they probably established a direct connection with proliferating cells (Figure 56).
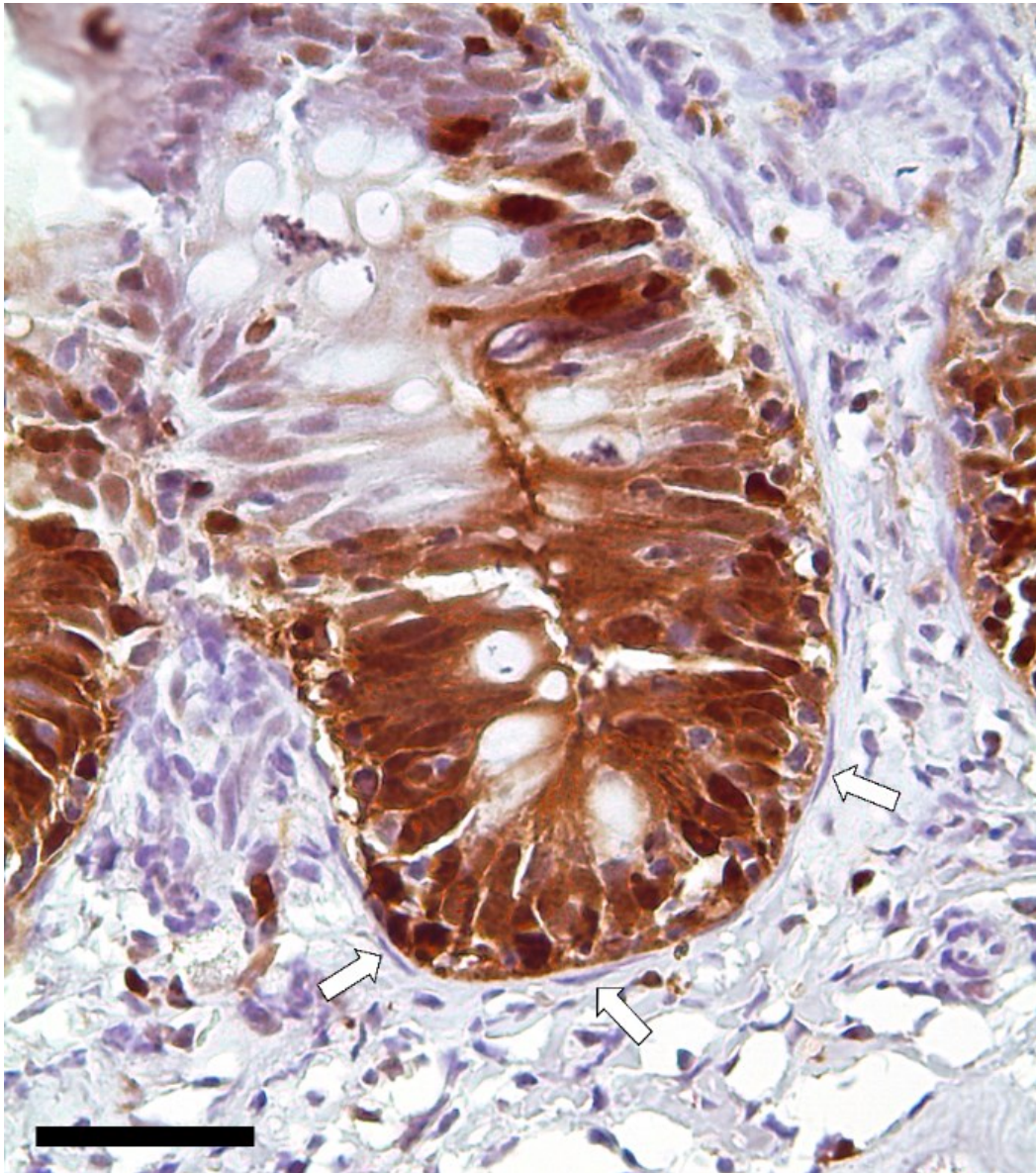
Figure 56: Immunolocalization of Pcna as marker of proliferating cells. Its expression was high in the epithelial cells lining the folds base, whereas no expression was found in the nearby stromal cells (arrows) Nuclei were counterstained with Mayer's hematoxylin.

To further investigate the possible relationship between TC and stem cells, we performed the combined *in situ* hybridization of *foxl1*[+] and *sox9*, telocytes' and stem cells markers' respectively. Results showed that *foxl1*[+] TC were distributed in the close proximity of *sox9*[+]. Moreover, these two markers colocalized in a few epithelial cells expressing *sox9* at a low level (Figure 57). These cells were recognizable as progenitor's cells namely cells at the beginning of their differentiation process [103].
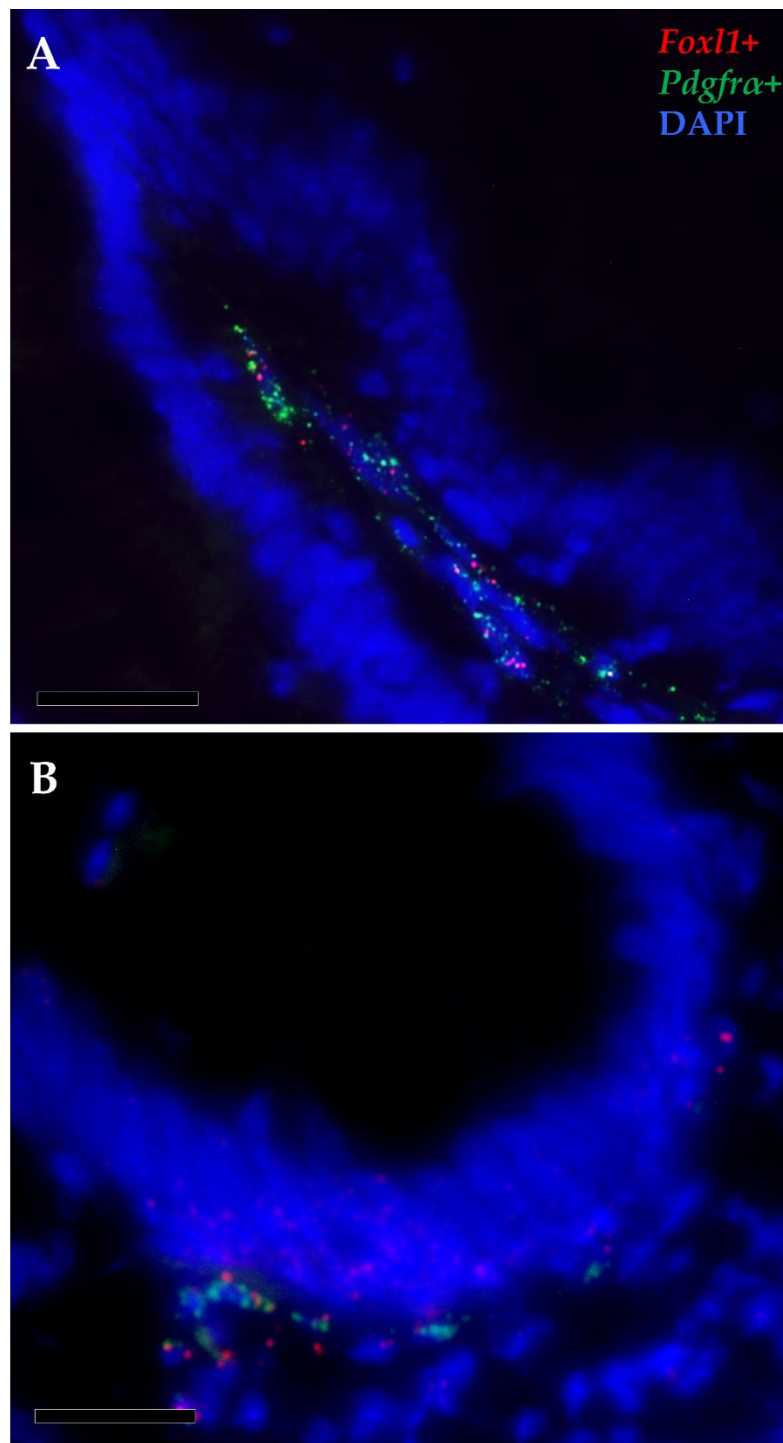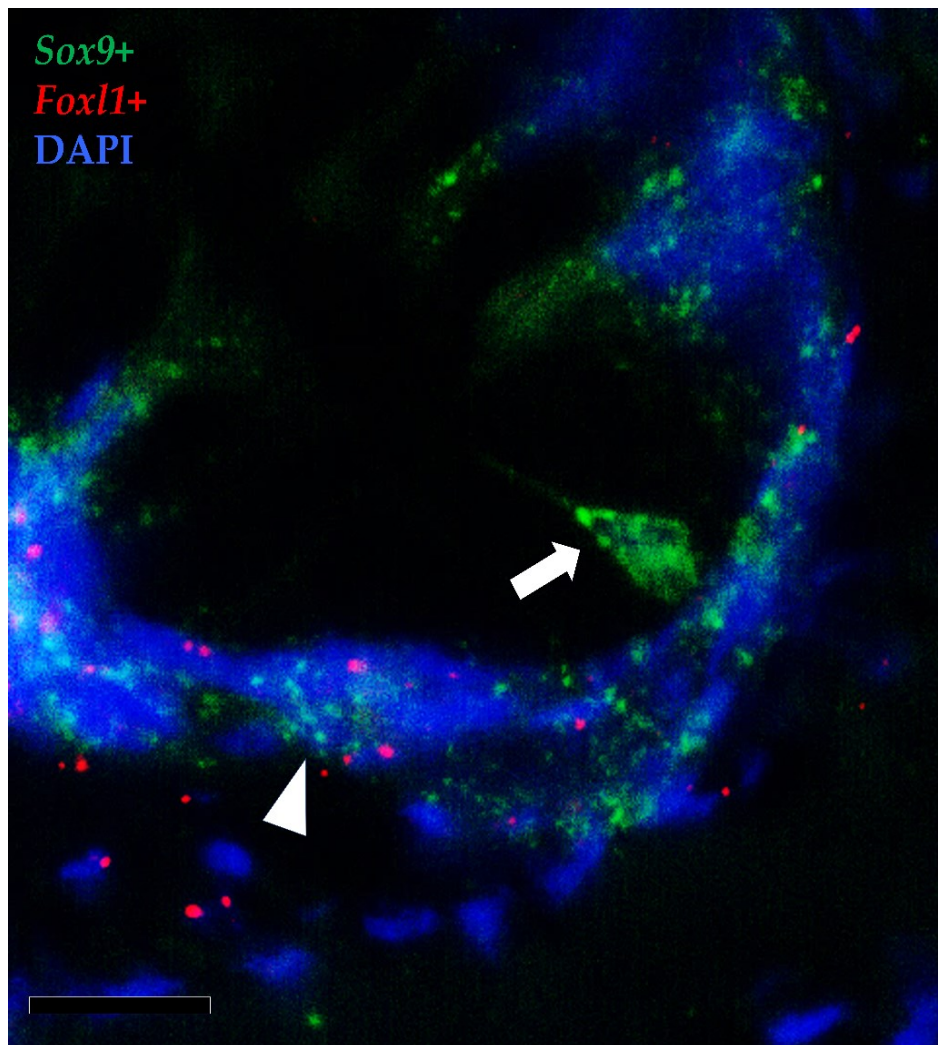

Figure 57: Representative image of dual-fluorescence *in s*itu hybridization of *sox9* (green dots) and *foxl1* (red dots). Stromal f*oxl1*^{+} cells were located in the close proximity of *sox9*[+] *cells* (arrow). Epithelial *foxl1*^{+} cells colocalized with cells expressing *sox9* at low level (arrowhead) (scale bar 50μm). Nuclei were counterstained with DAPI (blue).

Moreover, within the extracellular space, nearby of TC, were observed spherical vesicles displaying the typical position, shape, membrane morphology and size of extracellular vesicles. Therefore they have been considered as such. Interestingly, while TCs located along the folds length released EVs large in size (310-450 nm), those found encircling the folds base were smaller in diameter (120-130 nm) (Figure 58-59).
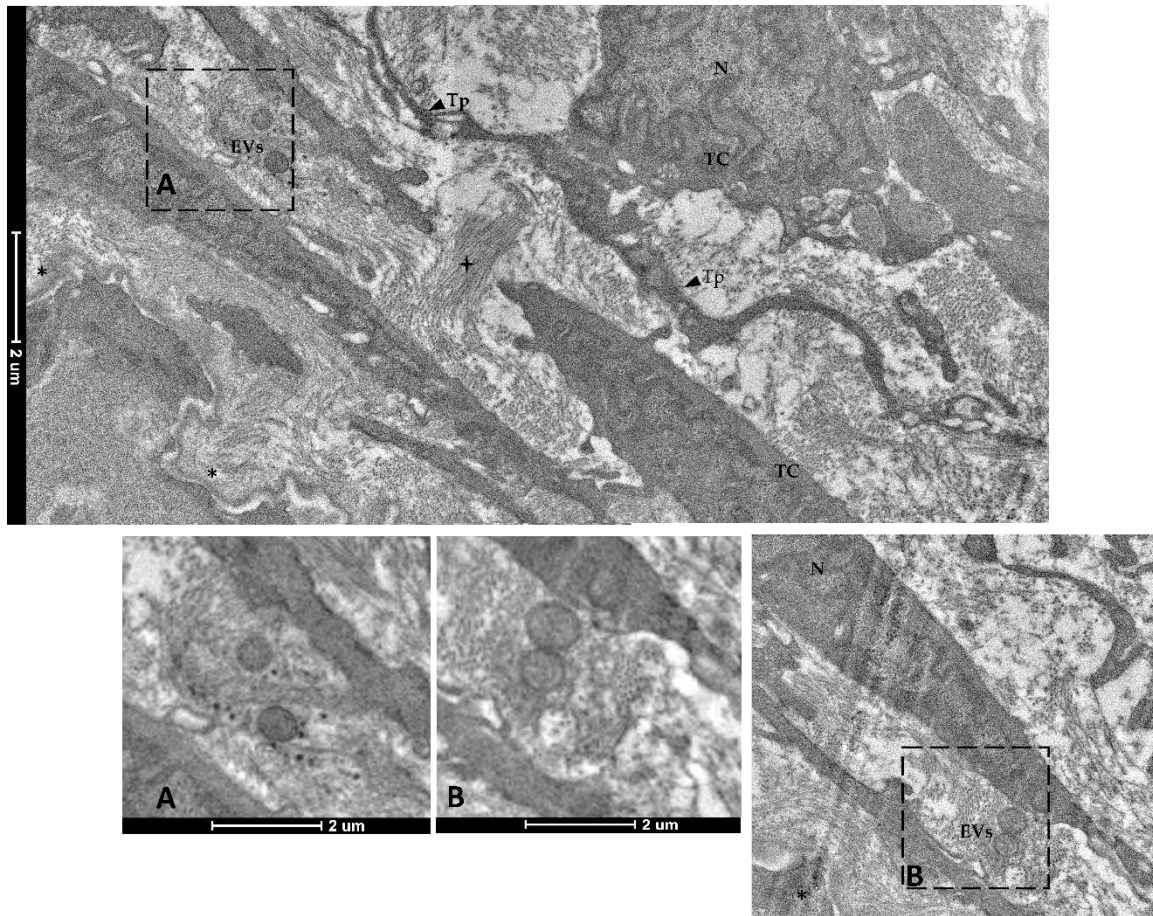
Figure 58: Representative transmission electron microscope (TEM) image showing extracellular vesicles (EVs) located within the extracellular space nearby telocytes (TC) found along the folds length ; (N-Nucleus, Tp-telopods, Cross- collagen fibers, asterisk-basement membrane).
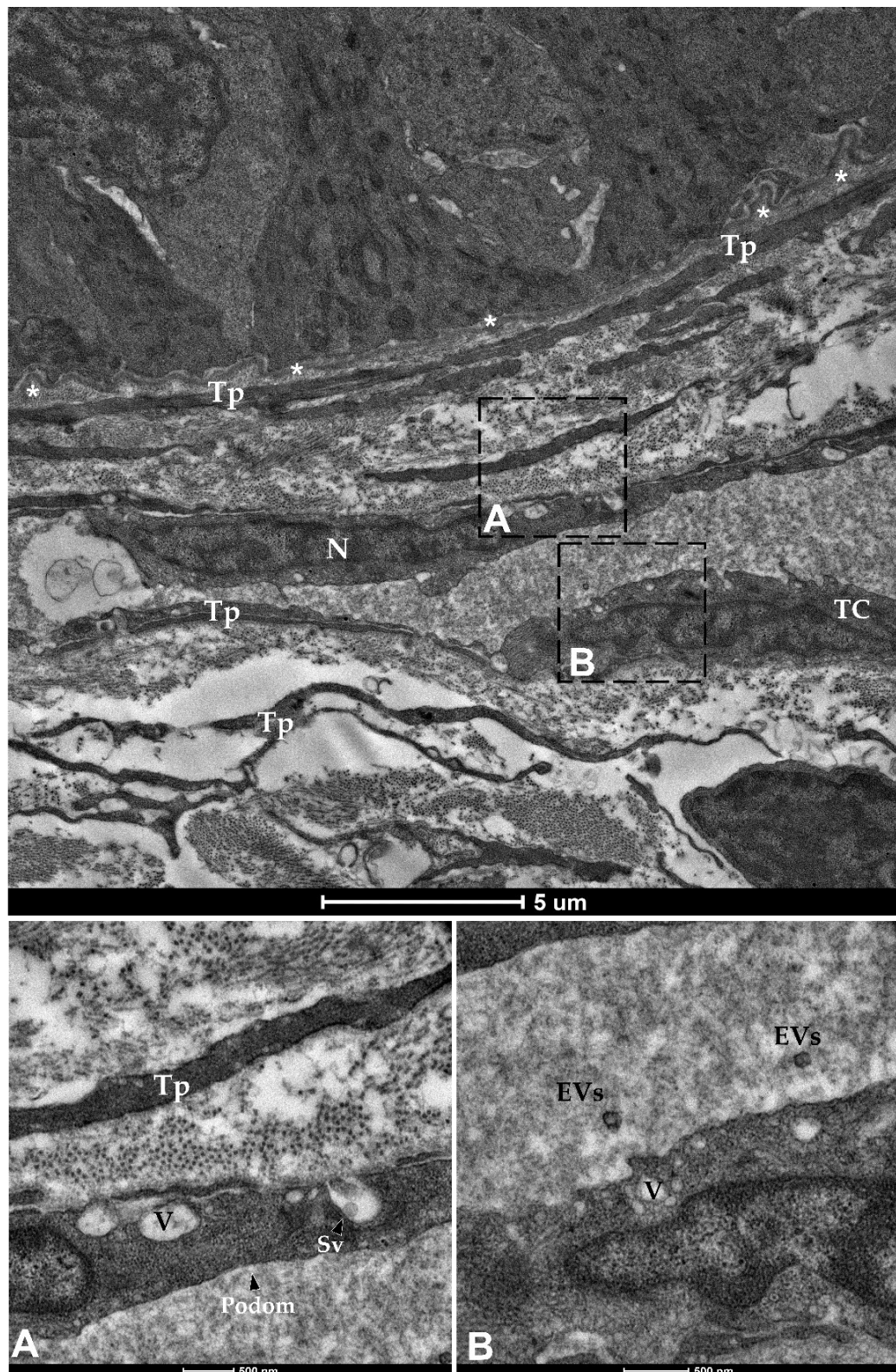
Figure 59: Transmission electron microscopy (TEM) showing telocytes (TC) encircling the folds base defined by extended nucleus and long and thin prolongations. Shedding vesicles (Sv) and extracellular vesicles (EVs) secreted within the extracellular space are appreciable in higher magnification (A-B). N-Nucleus, Tp-telopods, V-Vacuoles, asterisks-basement membrane).

Discussion

Previously, I characterized the organization and the specific structure of the epithelial stem cell niche along the rainbow trout (RT) intestine [93]. In this chapter of my thesis, I extended and integrated those observation examining also its mesenchymal component. In particular, I dedicated my efforts to the identification and characterization of TC due to their recently discovered role as active player of the niche microenvironment. This work represent the first detailed description of the stromal component of the stem cell niche in an aquatic species with a great commercial interest.

Morphological analysis showed the existence of peculiar mesenchymal cells localized just beneath the intestinal epithelium. This specific cell population displayed the typic moniliform shape distinguishable of telocytes (TC). Moreover, they possessed a stretched nucleus and long and thin cytoplasmic branches and were juxtaposed the enterocyte's basal membrane [108,115–117]. Different histochemical staining specific for the connective tissue, further highlighted that overall, the distribution of these cells allow the generation of a dense, continuous and elaborate mesh underlining the intestinal epithelium. Their morphology, position, and peculiar organization were fully consistent with those previously described for TC in mouse and human intestine [60,112]. However, to confirm our findings, ultrastructural examination has been performed since to date is the generally accepted methodology for the identification of this cell type [106,118,119]. TEM investigation revealed that they possessed a voluminous nucleus with limited cytoplasm, arranged in long thin discontinuous projections, and an irregular shape variable according to the branches number. These specific features allow us to clearly distinguish this cell population from the fibroblasts the regularly are located in the gut stroma. Overall, they presented all the distinguishable mark which are described for telocytes in the intestine and in other organs of disparate species

[113,115,119–122], including their ability to secrete extracellular vesicles (EVs). Based on their diameter size, EVs have been classified as microvesicles (MVs) or exosomes [123]. In humans, MVs play a central role in cellular communication, by conveying proteins, messenger RNA and microRNA (miRNA) to far cells modifying gene expression, proliferation, and differentiation of the receiving cell [124]. Our findings support the thesis that RT TC these exploit these intercellular means of communication to transfer biological information and to assure long-range cell-to-cell signaling. Interestingly, MVs and exosomes were not homogeneously distributed within the stromal space, but rather, the firsts were found in the close proximity of TC located along the folds length, whereas the other, were observed in the vicinity of TC encircling the folds' base. This observation suggest that TC take advantage of different forms of cell-cell communication based on their topographical localization along the gut stroma [103]. Recently, in mouse and humans, telocytes have arousing increasingly interest due to their central role as key component of the stem cell niche microenvironment. A growing amount of data demonstrated a direct connection between TCs and the stem cell niches of heart, lungs, skeletal muscle and intestine [60,108–110,118]. In this latter, experimental data conducted in mouse have demonstrated that interstitial telocytes represent a fundamental source of Wnt ligands and growth factors essential to assure a proper equilibrium between stem cells renewal and differentiation [60]. Despite, the high impact that an accurate characterization of the mechanisms that meticulously control the intestinal homeostasis would have for nutritional studies, these mechanisms are still scarcely investigated.

I evaluated the expression of *pdgfrα*, a well-defined marker that in mouse and human identify the mesenchymal cell population, including telocytes [112]. Its expression is essential for an adequate physiological development and for the small intestinal mucosa morphogenesis [108,125]. Moreover, I also assessed the topographical localization of *foxl1* as specific marker of intestinal telocytes, recently

discovered to be a key component of the mouse intestinal stem cell niche [60,108,126].

Pdgfra$^+$ cells have been exclusively found in the stromal space along the entire intestine. This is in agreement with other previous observation in both mouse and humans [112,127]. Mesenchymal cells express *pdgfra* at different level. In particular, those showing a high label-intensity, elongated nuclei, distributed just beneath the enterocytes' basement membrane, and creating a complex network extending from the folds' base towards the folds apex were ascribable to telocytes. The generation of this intricate mesh has been proposed to be essential to establish a direct connection with the overhead epithelium and critical to preserve the mucosa architecture [108]. Subepithelial telocytes' localized along folds length showed a higher *pdgfra* expression compared to those enwrapping the folds base. This expression pattern was fully coherent to the one described in mouse [125,126]. In particular, in this species, single-cell RNA sequencing studies proved that telocytes encircling the folds' base preserve the stem cell reservoir whereas, those distributed in the peri-epithelial space around folds' base promote cell differentiation assuring an effective and efficient epithelium [126]. Since we observed fully correspondent expression pattern between mouse and rainbow trout it is reasonable to assume that also in RT telocytes exert different function based on their topographical localization. Conversely, mesenchymal *pdgfra* expressing cells at low level, possessed a rounded nucleus and were located in the innermost region of the lamina propria therefore they lack the distinguishing features that characterize telocytes. Based on these observation, these cells should be considered as common fibroblast that reside within the stromal space and thus do not directly implicated in the regulation of the stem cell function and behavior but rather involved in connective tissue regeneration and remodeling [128].

In mouse, *Foxl1*-expressing subepithelial telocytes have been recently proposed to be a critical component of the stem cell niche [60,126]. Indeed, they

represent a crucial source of Wnt ligands essential for epithelial stem and progenitor cells lining the crypt base, to the extent that, *Foxl1* ablation rapidly lead to intestinal mucosa architecture impairment followed by animal death [129]. Precisely, as reported in mouse, *foxl1+* cells were rare and preferentially located encircling the folds base. Despite we were not able to evaluate their specific functional role since genetic ablation studies are unfeasible in RT, the fact that we observed exactly the same expression pattern and distribution, prompt us to assume that also RT *Foxl1*-expressing subepithelial telocytes represent an essential constituents of the stem cell niche. The combined *in situ* hybridization of *pdgfrα* and *foxl1* showed that *foxl1* is expressed by a small, functional *pdgfrα+* TC subpopulation localized both around the folds base and along the *plicae* length. The same pattern has been observed in mouse intestine, in which has been proved that TC express a diverse transcriptome according to their spatial distribution within the lamina propria [114]. Overall, these findings further emphasize the elaborate network that preserve the equilibrium between proliferation and differentiation.

Immunolocalization of proliferating cell nuclear antigen (Pcna), revealed that RT TC are not actively replicating cells. Moreover, they had a typic and well-defined phenotype indicating their terminally differentiate state. Nevertheless, RT TC distributed around the folds base were located in the close proximity of the epithelial proliferative compartment suggesting a direct interaction between the epithelial and the mesenchymal component. Furthermore, dual-fluorescence *in situ* hybridization of *foxl1* and *sox9* proved that peri-epithelial telocytes, were juxtaposed to *sox9+* cells.

We previously speculated that in RT *sox9+* cells could be considered the functional equivalent of the well-defined crypt base columnar cells (CBCs) in mouse. Here, we integrated our previous hypothesis demonstrating that these cells present the peculiar decondensed heterochromatin arrangement which characterize intestinal stem cells (ISC) [130]. Therefore, considering the spatial close proximity

between TC and ISC, it is reasonable to assume that peri-epithelial TC that enwrapped the stem cell compartment, promote their proliferation providing short-range signaling.

In addition, *Foxl1*-expressing subepithelial telocytes were also observed surrounding the base of the secondary and tertiary folds which develop from the complex *plicae* distinguishing of the more distal tract [93], supporting the hypothesis that also these folds are maintained by a sort of a local niche.

Conclusion

Overall, our results proved for the first time the presence of telocytes along the rainbow trout gut. They generate an intricate mesh extending from the basal to the apical portion of the intestinal folds. Their position, morphology, their typical distribution as well as their gene expression pattern are basically identical to those described in the mouse. Therefore, it is reasonable to infer that as in mouse, RT telocytes promote cell proliferation or cell differentiation depending on their topographical location.

This represent the first detailed description of the mesenchymal cell population in a fish species with a great commercial interest. These findings, substantially improves our knowledge of the renewal mechanism at play in the intestine which drive the intestinal homeostasis.

Chapter 5

Derivation And Characterization Of Two Novel Primary Intestinal Cell Lines From The Rainbow Trout (Oncorhynchus Mykiss) Gut

Overview

As mentioned above, despite the complexity organization of the RT mucosa, the development of an *in vitro* tool able to retain similarities with the *in vivo* counterpart, would be a helpful tool for the rapid screen of several alternatives feeds implied in aquaculture. After several attempts, two novel cells line belonging from proximal (RTpi-MI) and distal (RTdi-MI) intestine of RT were successfully derived and characterized. Therefore, based on the extensive morphological and functional characterization of the RT mucosa *in vivo*, in this thesis several efforts have been also dedicated to the derivation of new stable cell lines. Then, they have been compared with the only continuous cell line that so far has been established from rainbow trout intestine (RTgutGC). Gene expression analysis demonstrated that all the cell line presented both epithelial and mesenchymal components. However, despite all of them displayed an epithelial component, this was significantly higher in the RTpiMI. Moreover, they also expressed the typical enterocytes' functional markers (PepT1 and Sglt1) suggesting their suitability as a model of *in vitro* absorption. Furthermore, all the cell lines preserved both stem cells and differentiating cell types. High seeding density induced their differentiation into more mature phenotypes, as indicated by the simultaneously downregulation of intestinal stem cell-related genes (i.e., *sox9*, *hopx* and *lgr5*) and upregulation of alkaline phosphatase activity. Nevertheless, among the three cell lines most parameters that we analyzed were conserved, some significant differences were observed. Therefore, this suggests that some typical features that characterize the two main intestinal portions are also preserved *in vitro*. Moreover, since only a mild stimulus was able to induce their differentiation it would be interesting to further explore these mechanisms using more controlled and sophisticated culture systems (Figure 60).
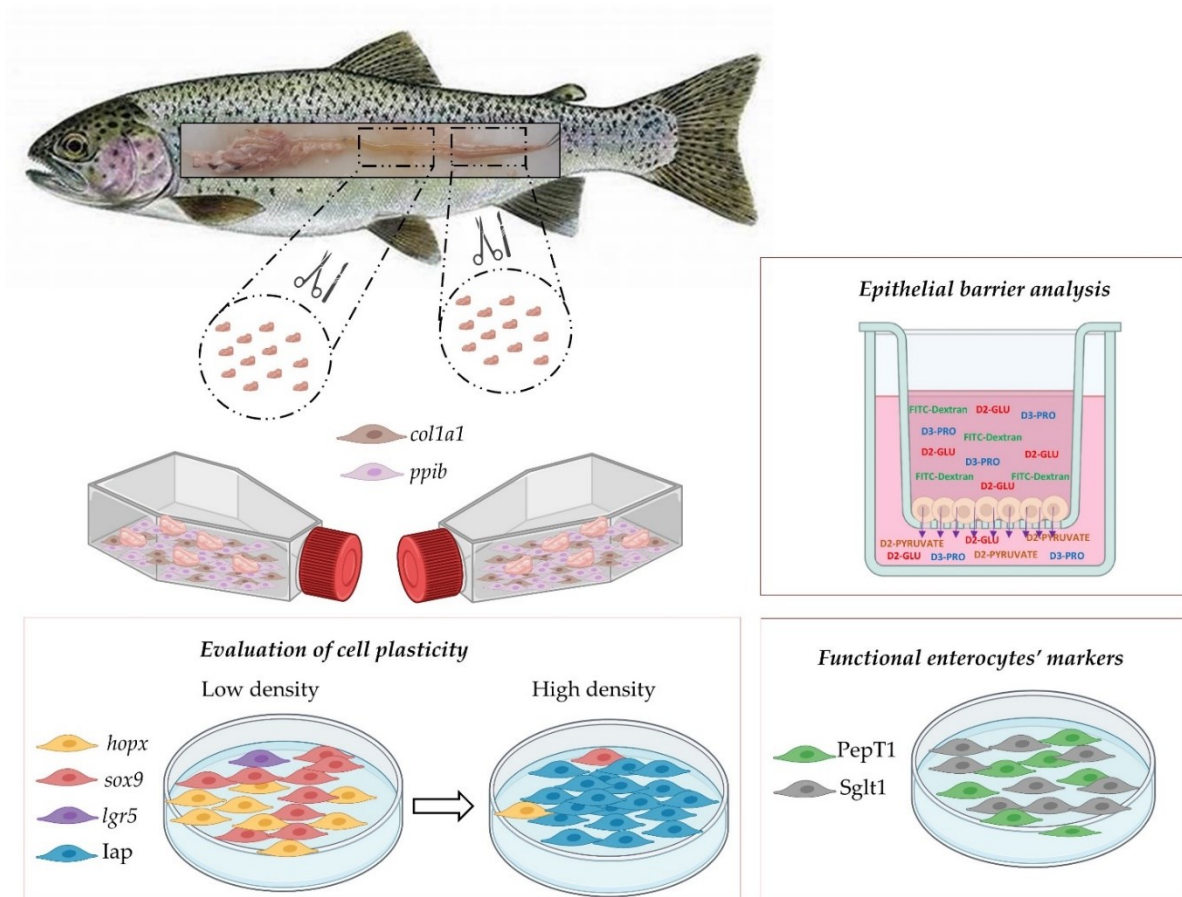
Figure 60: Graphical abstract summarizing the main results obtained in this chapter. Two novel stable cell lines have been derived from proximal and distal intestine. They were characterized for their stemness properties and for their ability to differentiate in vitro. Image created using BioRender.com

Introduction

To improve aquaculture sustainability, the search for viable and efficient feed formulations as alternatives to the common marine-derived protein and lipids is required [131,132]. The potential effect on these novel feed formulation on the digestive system health, need to be tested through extensive *in vivo* feeding trails. In this perspective, the development of a predictive *in vitro* model which accurately mimics the fish intestinal mucosa would be a helpful *tool* to limit exclusively the most promising formulations to *in vivo* studies. At present, immortalized human (e.g. Caco-2) or rat cell lines are main models to study intestinal absorption mechanisms. They offer many advantages, indeed they easily grow and propagate in culture but since they originated from tumours lack of cell heterogeneity and of fully differentiated phenotype [9,10]. Therefore, they are not considered a reliable *in vitro* model of the physiological environment. A similar cell line RTgutGC cell line has been also established from the distal portion of the rainbow trout gut [13]. However, its aneuploid karyotype probably correlates with their immortalized state and consequently with their unlimited proliferative capability *in vitro*.

Recently, progression and improvement in 3D cultures system and stem cell research has allowed the establishment of specialized tissue *in vitro* consisting of primary non-transformed cells as potential alternative to the classical immortalized cell lines [133,134]. These structures, called *enteroids*, present a spheric architecture and are made of both stem progenitors cells as well as of fully mature and heterogenous cell types. However, their typical structure severely limits functional absorption *in vitro* studies. This because, their lumen is enclosed within a thick mass of hydrogel as a consequence, the substances that have to be tested have difficult to reach the luminal compartment which is located inside the structure rather than easily exposed. In this perspective, the objective of this chapter was to derive novel stable cell lines from RT gut that preserve properties that define the intestinal mucosa *in vivo.* Trout-derived cell lines have been characterized evaluating whether they preserve stem cells and fully mature cell types as well as

to assess their ability to differentiate *in vitro* applying only a mild differentiation stimulus.

Methodologies

Samples collection

A total of 17 rainbow trout (RT) weighing approximately 500g, were collected at Laghi Verdi s.n.c. trout farm (Como, Italy). This stage corresponds to the classical commercial weight. We collected samples of proximal and distal intestine.

Derivation of primary intestinal cell line from proximal and distal intestine of rainbow trout

Intestinal fragments for cell culture experiments were gently rinsed with Mg_2 and Ca_2 free Dulbecco's phosphate-buffered saline (PBS) supplemented with antibiotic. Proximal and distal intestinal segments of RT were cut longitudinally and gently washed using PBS+ 2% antibiotic to completely remove the intestinal content. Tissues were then diced into small pieces and transferred in 25-cm^2 culture flasks (3-4 pieces/flask) precoated with 0.1% gelatin derived from pig skin (Figure 61). Cells were then cultured in Leibovitz's (L-15) medium supplemented with 5% Foetal Calf Serum (FCS), 2mM L-glutamine, and 1% penicillin/streptomycin and maintained at 20 C° in the incubator under ambient atmosphere. Cell culture medium was replaced once a week and once cells reached their confluence state, intestinal explants were carefully removed from flasks surface by gently aspirating them using a micropipette tip (Figure 60). To assess their doubling time, 70.000 cells were seeded in each well of a 4well-dish in complete medium, cultured for 6 days and was then calculated via cell counting method according to the following formula:

$$\text{Doubling time} = \frac{\text{duration} * log(2)}{\log(Final\ Concentration) - \log(Inital\ Concentration)}.$$

In which, duration = 6 days, Log = 10 based Log, final concentration = cell count at day 6th, initial concentration = cell count at day 1st.

To study the effect of low and high seeding density on growth and differentiation, cell lines were seeded in 4-well plates at 100.000 or 200.000 cells/cm² respectively as previously described [13] and cultured for 7 days.
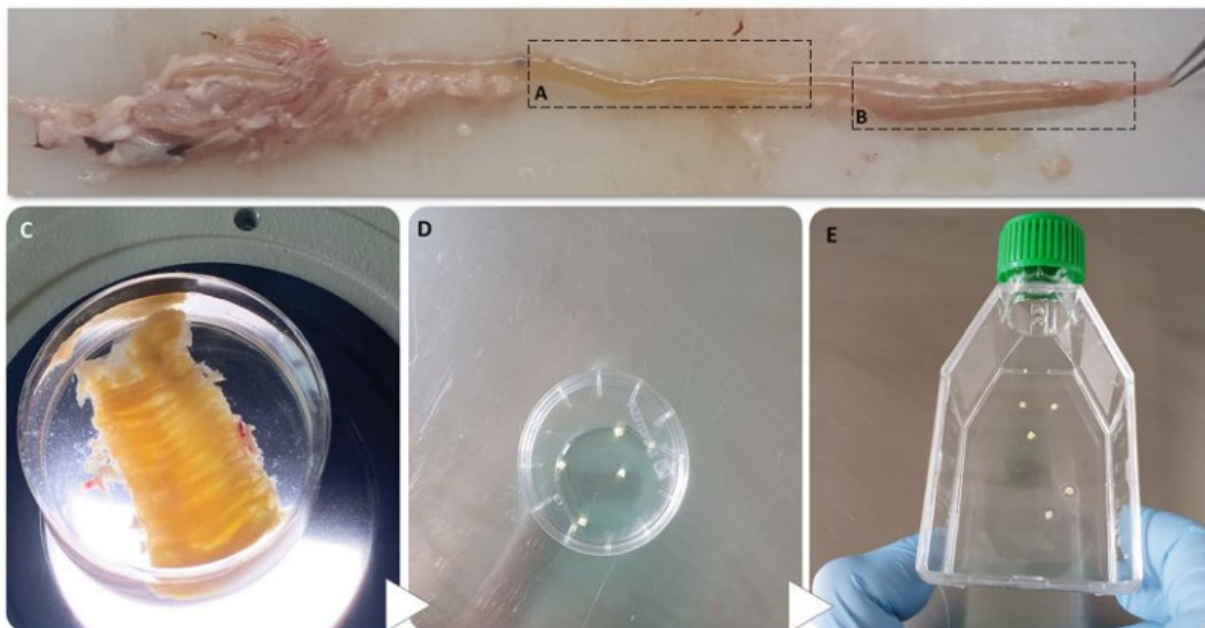
Figure 61: Images showing selected regions for the samples collection (A: proximal; B: distal) and describing the main steps of primary cell culture isolation; c: distal intestine devoid of mucus after several vigorously wash in PBS, d: small intestinal pieces diced; e: explants inserted in a 25-cm² culture flask precoated with of 0.1% gelatin derived from pig skin [135]

Gene expression analysis

At 90-95% confluency, cells were detached using trypsin-EDTA solution, cell suspension was centrifuged at 800x g for 5 min, pellets were washed twice in PBS, snap frozen in liquid Nitrogen and stored at -80°C until RNA extraction and gene expression analysis. We analyzed the expression of the following genes, representative of different cell sub populations:

- *SRY-box 9* (*sox9*): as marker of intestinal stem cells
- *Leucine-rich repeat-containing G-protein-coupled receptor 5* (*lgr5*): as marker of the mesenchymal stem niche component

- *Homeodomain-only protein* (*hopx*): as marker of the transient amplifying population

- *Zonula occludens 1* (*zo-1*), *Claudin-3* (*clnd3*), *E-cadherin* (*E-cad*): as markers of epithelial cells

- *Type I Collagen* (*col1a1*) and *Vimentin* (*vim*): as markers of stromal component

- *Intestinal alkaline phosphatase* (*iap*): as marker of fully differentiated enterocytes

- *Peptide transporter 1* (*pept1*), *sodium - glucose/galactose transporter 1* (*sglt1*): as markers of enterocytes' functionality m

- *mucin 1* (*muc1*): as goblet cell marker.

Poly(A)mRNA samples were obtained using Dynabeads mRNA DIRECT micro-kit (Deutsche Dynal, Hamburg, Germany) following manufacturer indications. RNA samples were then transcribed into cDNA using iScript Advanced cDNA Synthesis Kit for RTqPCR (Bio-Rad). The synthesis was completed in accordance with the manufacturer's instructions and the resulting cDNA was stored at -20°C. Qualitative PCR was performed using GoTaq® G2 Flexi DNA Polymerase kit (Promega). The PCR program was: 95°c for 2 min for first cycle of denaturation, followed by 40 cycles of 95°C for 30s (denaturation), 60°C for 30 s (amplification) and 72°C for 5 min (extension), and final extension at 72°C for 5 min. For each PCR reaction, a negative control was always run to exclude contaminations. PCR products were analyzed using electrophoresis on a 2% agarose gel that was stained using ethidium bromide (ThermoFisher Scientific, Waltham, MA, USA). A molecular marker of 50 base pair (bp) gaps (ThermoFisher Scientific, Waltham, MA, USA) was run for each gel to confirm the length of PCR fragments. Primers specifications are listed in table 6.

Table 6: List of primer sequences used for gene expression analysis. Gene ID, amplicon size in base pairs (bp), accession number ID, forward and reverse primer sequences are reported for each gene.

Gene ID (amplicon size in base pairs (bp))	Accession Number ID	Forward (F) and reverse (R) Primer Sequence (5->3)
sox9 (366bp)	NM_001124179.1	F:TGCAGGAGTGCATCTTTGTC R:GGTCAGCCTTCTTGAACTCG
hopx (231bp)	XM_021584037.1	F:AGTAGAGCTTTCACACGGTCG R:AGCTCTCAGCCACAGAAGTC
lgr5 (202bp)	XM_021576530.1	F:ACTCAACGGAGCCACAGATA R:TTCTGGATCTTTCTGCAACCAC
zo-1 (99bp)	XM_021607172.1	F:GCTGTTCCTCCTAGACCTT R:TCACCCACATCTGACTCTAC
cldn3 (112bp)	XM_021587920	F:AGGCAACGACGCTACATCAA R:CCCTGGGAATCTACGTCAAA
e-cad (107bp)	XM_021607117	F:ACTATGACGAGGAGGGAGGT R:TGGAGCGATGTCATTACGGA
col1a1a (214bp)	NM_001124207	F:CTTTGCTGCTCAGTTTGATGG R:GTTACCATCCTCACCAGGTTT
vim (203bp)	NM_001124729.1	F:AGGAAGGTGGAGTCTCTTCA R: TCTTCAGAGTCCTGGAGGTT
iap (157bp)	XM_021606337	F:TTGGCACGGAAAGAGAGTCC R:CATGGGAAAGCTACCAGGCA
pept-1 (161bp)	XM_031818746.1	F: CCTGTCAATCAACGCTGGT R: CACTGCCCATAATGAACACG
sglt1 (208bp)	XM_021591066.2	F:ATCGCTGAGTTTGCCTATGG R:TCTCCTCTGTGTGGTTCCT
muc1 (263bp)	XM_021578564.1	F:GTCTGCCACATGCCAAATATC R:CCCTCCATGAATGAGTCACATA

Immunofluorescence

Cells were quickly fixed in 4% paraformaldehyde (PFA) solution in in phosphate-buffered saline (PBS) for 30 minutes at room temperature. Non-specific bindings were prevented by incubating cells with blocking buffer containing 5% bovine serum albumin (BSA), 0,3% Triton X-100 in PBS for another 30 minutes at room temperature. Subsequently, cells were incubated with a FITC conjugated anti-Zo-1 (anti-ZO1, 339188) antibody diluted 1:100 in PBS. Nuclei were counterstained with ',6-diamidino-2-phenylindole (DAPI). Peptide transporter 1 (Pept-1) sodium–glucose co-transporter-1 (Sglt-1) or with collagen type I (colA1) were characterized through indirect immunofluorescence. In brief, cells were promptly fixed in 4%

paraformaldehyde (PFA) solution in in phosphate-buffered saline (PBS) for 30 minutes at room temperature. Aspecific bindings were prevented incubating cells in 10% goat serum in PBS for another 30 min at room temperature. Later samples were incubated with anti-PEPT1 mouse monoclonal antibody, (Santa Cruz Biotechnology, sc-373742, Heidelberg, Germany) with anti-SGLT-1 rabbit polyclonal antibody (Millipore Corporation, 07-1417, Darmstadt, Germany) 1:100 diluted in PBS or with for anti-collagen type I antibody diluted 1:40 for 60 minutes at room temperature. Primary antibody specificity was previously validated in rainbow trout intestine. Subsequently, cells were incubated with appropriate secondary antibody Alexa FluorTM 594 goat anti-mouse (Life Technologies Corporation, A11058 Willow Creek Road, OG, USA) or with goat anti-rabbit diluted 1:250 in PBS for 30 minutes at room temperature. Samples were then counterstained with 4′,6-diamidino-2-phenylindole (DAPI).

Fluorescent in situ hybridization

As mentioned above, due to the lack of commercially available fish-specific antibodies, the identification of cells expressing genes specific for intestinal stem cells (*sox9* and *lgr5*) and transient amplifying cells (*hopx*) has been performed using fluorescent *in situ* hybridization (FISH) using Multiplex Fluorescent Reagent Kit V2 (RNAscope technology, Advanced Cell Diagnostics, San Francisco, CA, USA) according to the manufacturer's instructions. Specific probes were previously validated in RT intestine.

Briefly, cells were firstly fixed in 10% neutral buffered formalin for 30 minutes at room temperature and were later incubated with hydrogen peroxide (Advanced Cell Diagnostics, San Francisco, CA, USA) Subsequently, samples were exposed to Protease plus for 10 minutes (Advanced Cell Diagnostics, San Francisco, CA, USA) and then incubated with specific probes diluted 1:50 in diluent buffer in a HybEZ oven (Advanced Cell Diagnostics, San Francisco, CA, USA) for 2 h at 40

°C. Afterward, signal was amplified incubating cells in signal amplification solutions 1, 2, and 3 and was later developed applying the fluorophore OPAL 570 or OPAL 520 (Akoya biosciences, Marlborough, MA, USA) diluted 1:750 in tyramide signal amplification (TSA) buffer. Samples were then counterstained with DAPI and observed under a fluorescence inverted microscope. Negative controls were performed by incubating cells with a probe specific for the *Bacillus subtilis* dihydrodipicolinate reductase (dapB) gene. At least 7-8 representative images and homogenously distributed within the wells (n = 3 replicates/well per each gene) of low and high seeding density for each cell line were acquired. Cells were considered positive for the target genes if expressed at least one dot as recommend by RNAscope technology guideline. For all the genes, the percentage positive cells was calculated as ratio between positive cells for the specific target and the total cells counted for each field of vision. For *sox9*, gene expression level was also measured using the H-score as suggested by the manufacturer. Briefly, expression was quantified using a five-level scoring system (0, no staining; 1, 1 – 3 dots/cell; 2, 4 – 10 dots/cell; 3, > 10 dots/cell; 4, >15 dots/cell with > 10% of dots in clusters). The H-score was calculated following the formula: (% of grade 1 cells × 1) + (% of grade 2cells × 2) + (% of grade 3 cells × 3) + (% of grade 4 cells× 4) [136].

Alkaline phosphatase detection

Alkaline phosphatase (AP) was detected using alkaline phosphatase kit (Millipore Corporation, 86R-1KT, Darmstadt, Germany) following the manufacturer's indications. Briefly, cells were promptly fixed in a citrate and acetone (1:3) based solution for 30 seconds at room temperature. Later, cells were incubated with the appropriate substrate solution consisted of Naphthol AS-BI Alkaline Solution (Millipore Corporation, 86R-1KT, Darmstadt, Germany) combined with diazonium salt for 30 minutes and were washed using deionized water. Nuclei were counterstained applying Mayer's hematoxylin (Millipore Corporation, 86R-1KT, Darmstadt, Germany) for 10 minutes.

Statistical Analysis

Results are showed as mean ± standard deviation from at least three independent experiments. One-way ANOVA followed by Tukey's post hoc tests were performed to perform multiple comparisons using PRISM version 8.2.1. (GraphPad Software, San Diego, CA, USA). Results were considered statistically significant if $P < 0.05$.

Results

Derivation of primary intestinal cell line from proximal and distal intestine of rainbow trout

After 5-10 days culture, cells started to grow out from proximal and distal intestinal tissue fragments. In the early culture stages, cells showed a heterogeneous morphology including fibroblast-like cells, dendritic-like cells, multipolar-like cells and epithelial-like cells (Figure 62). After around 3 months of culture, fibroblast, dendritic and multipolar-like cells disappeared, probably entering in a senescence state, leaving a quite uniform population of epithelial-like cells. At this stage, the tissue explants were removed, and cells began to grow vigorously reaching the confluent state.
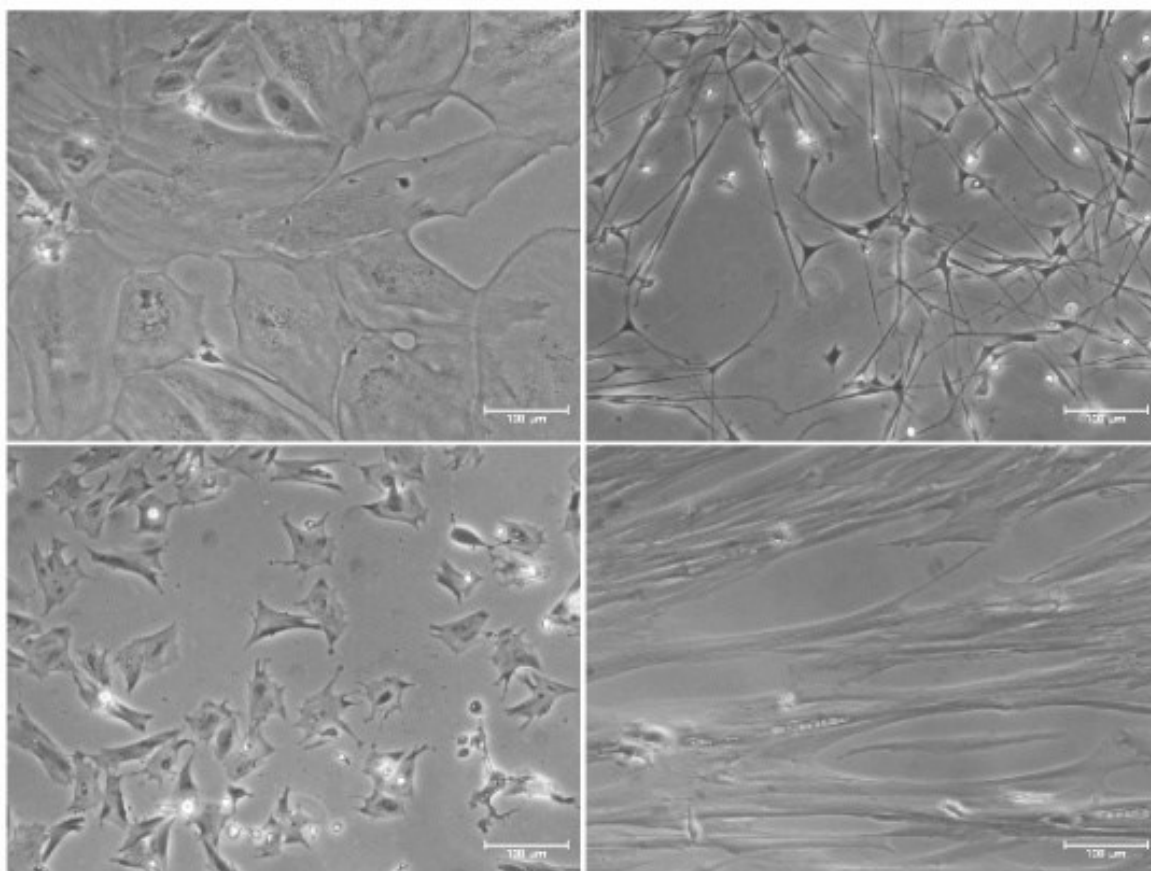

Figure 62: Representative pictures showing culture morphology of different primary cells isolated from intestinal explants.

However, despite several attempts were performed, only two primary cells lines were successfully established and at the time of the experiments were at passage 30. They have been named RTpi-MI and RTdi-MI that stands for Rainbow Trout proximal intestine Milan Italy and Rainbow Trout distal intestine Milan Italy, respectively, to indicate the intestinal portion of origin. (Figure 63-A). Cells were also successfully cryopreserved at different passage with 10% DMSO as a cryoprotectant.

The RTpi-MI cell line displayed a slower proliferation rate (doubling time: 4.4 days) compared to RTdi-MI (doubling time: 3.0 days) and RTgutGC (doubling time: 2.9 days) cell lines (Figure 63-B). Interestingly, RTpi-MI is the only cell line currently available derived from the more proximal portion of the rainbow trout intestine since RTgutGC, the only other intestinal cell line established from this species, has been derived from the distal intestine .
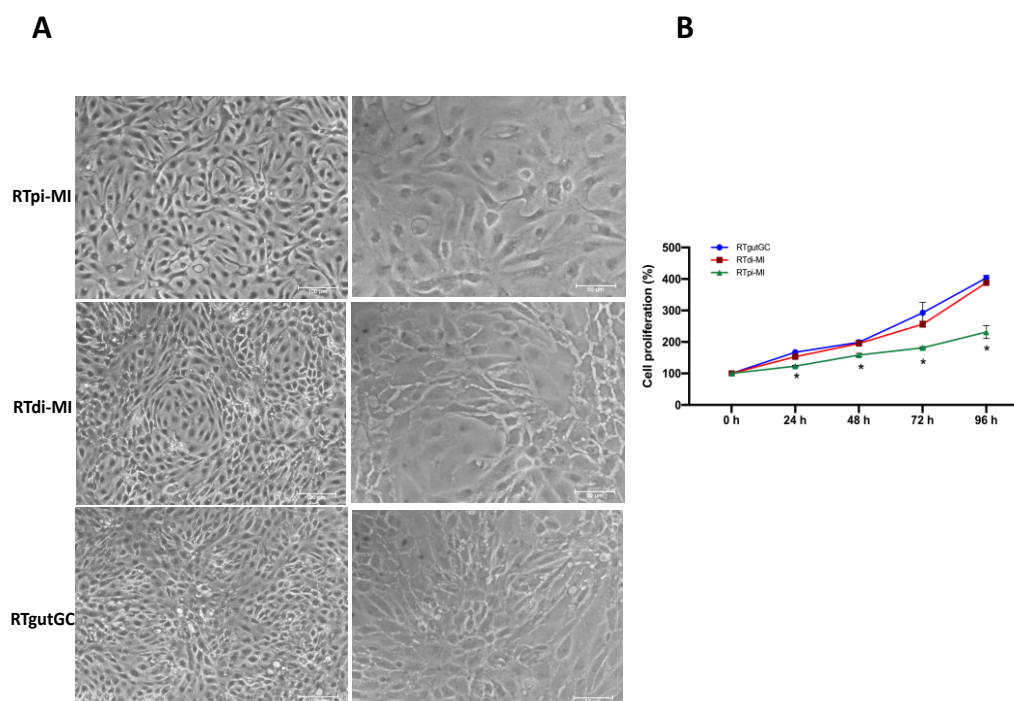

Figure 63: Representative images showing different cell lines morphology at low and high magnification (panel A), and graph illustrating the growth curve of RTgutGC (blue line), RTdi-MI (red line) and RTpi-MI (green line) from 24 h (day 1) to 96 h (day 4) of culture. RTpi-MI displayed a significantly lower proliferation rate compared to the other two cell lines.

Gene expression analysis

All the cell lines expressed both typical epithelial (*ppib, zo-1, cdh1e cldn3*) and mesenchymal markers (*Collagen type 1 and Vimentin*). The presence of the epithelial component has been further confirmed by the formation of occluding-junctions and through the detection of the zonula occludens protein. Immunodetection of Col1a1 proved the presence of mesenchymal components (Figure 64 A-B).
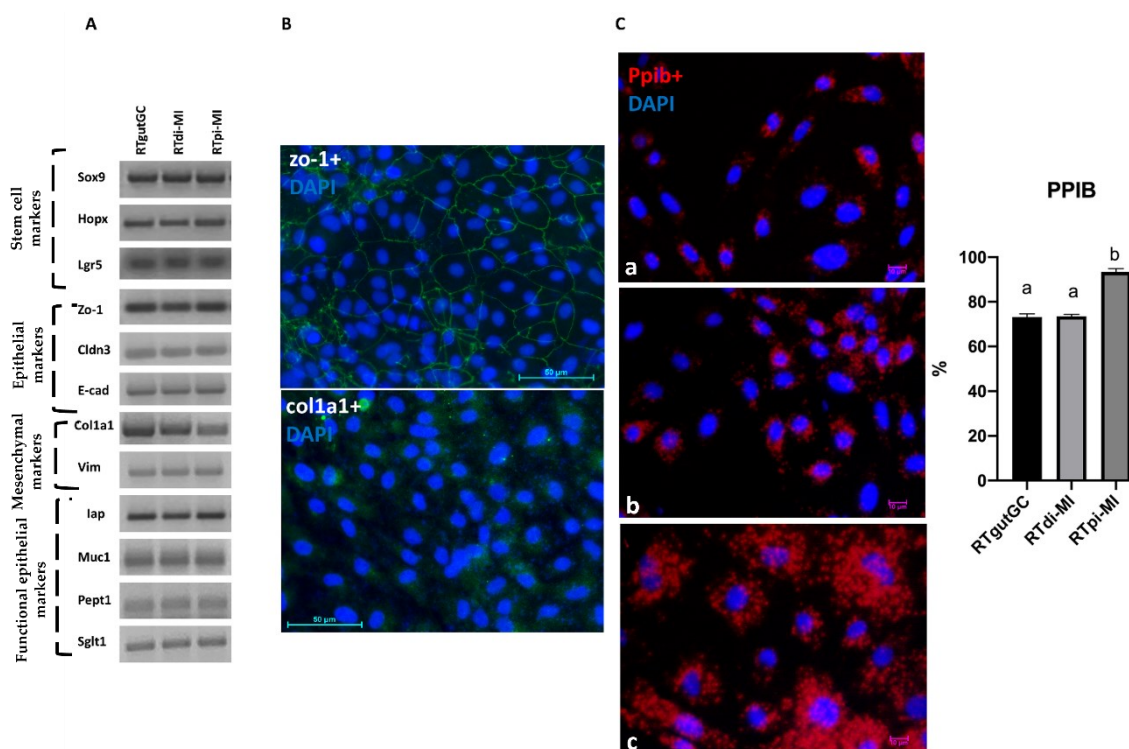
Figure 64: RTpi-MI, RTdi-MI and RTgutGC cell lines were made up by an heterogeneous cell population as shown in the panel A: *sox9*, *hopx* and *lgr5*: stem cell markers; *zo-1*, *cldn3* and *e-cad*: epithelial markers; *col1a1* and *vim*: mesenchymal markers, *iap*: enterocyte, *muc1*:goblet cells. Representative image showing immunolocalization of zonula occludens (Zo-1) and collagen type 1 (Col1a1). Nuclei were counterstained with DAPI (blue). (C) Representative images of *ppib in situ* hybridization (red dots) in RTdi-MI (a) and RTgutGC (b), RTpi-MI (c). The bar chart showed the percentage of *ppib*-expressing cells in RTpi-MI, RTdi-MI and RTgutGC cell lines. Values are expressed as mean± SD from 3 independent experiments. Different superscript in the same graph indicate statistical significance.

In situ hybridization

As described above, *in situ* hybridization of the *ppib* marker allowed the quantification of the epithelial component related to entire cell population in the three cell lines. Interestingly, although the epithelial component was high in all of them (RTgutGC: 73.2 ± 1.5 %, RTdi-MI: 73.9 ± 0.7, RTpi-MI: 92.8 ± 1.8), the one isolated from the proximal tract showed a significantly higher percentage of epithelial cells (more than 90%) compared to the others (Figure 63-C).

As reported in the methodologies section, the experiment for the evaluation of the enterocytes' functional markers, stem cell component as well as fully mature cell types, was carried out at two different seeding densities, to verify whether or not it would affected their expression.

Our results indicated that all the cell lines expressed Sglt1 and Pept1 proteins, responsible for the transport of glucose/galactose and peptides respectively (Figure 65 A-B). In all cell lines we observed an abundant signal of both markers. However, no differences in terms of expression were observed among different cell lines and between the two seeding densities considered.
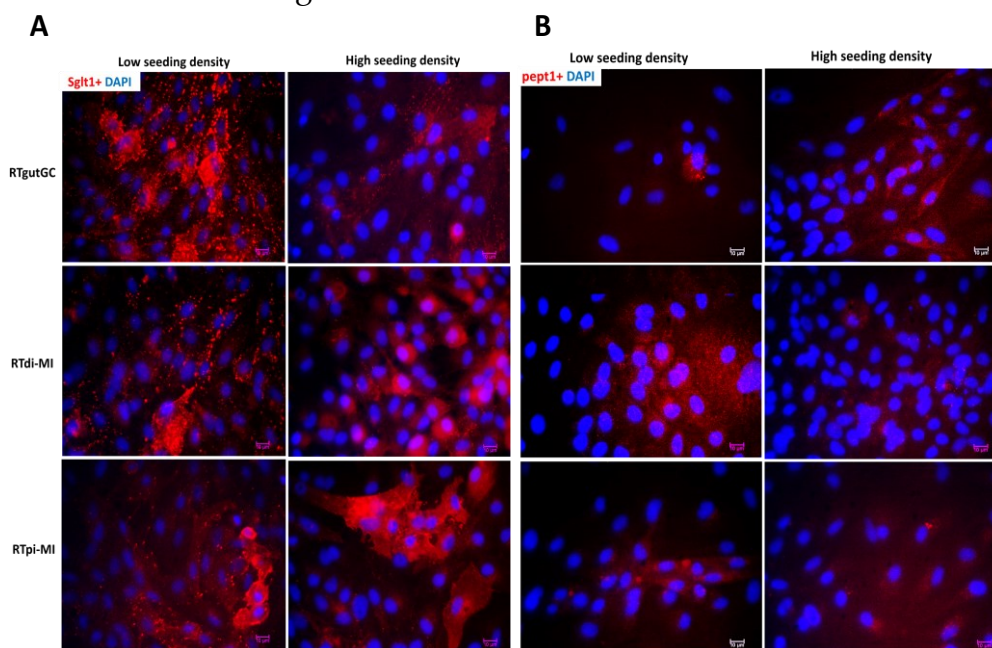
Figure 65: Representative images showing immunolocalization of Sglt1 (A) and Pept1 (B) in the considered cell lines seeded at two different seeding densities. Nuclei were counterstained with DAPI. Scale bar, 10 μm.

At low density, just over a third of all lines expressed *sox9*, without significant variations between different cell lines (RTgutGC: 34.7±2.2%; RTdiMI: 35.4±4.6%, RtpiMI:36.0±7.6%).   The percentage of *sox9⁺* cells was close to 50% (RTdiMI: 48.1±6.7%;   RTdiMI: 47.0±5.1%, RtpiMI:38.5±7.8%) when we considered only epithelial cells identified as positive to *ppib*. High seeding density resulted in a significant reduction in the percentage of *sox9⁺* cells exclusively in RTpiMI cell line, (Figure 66).
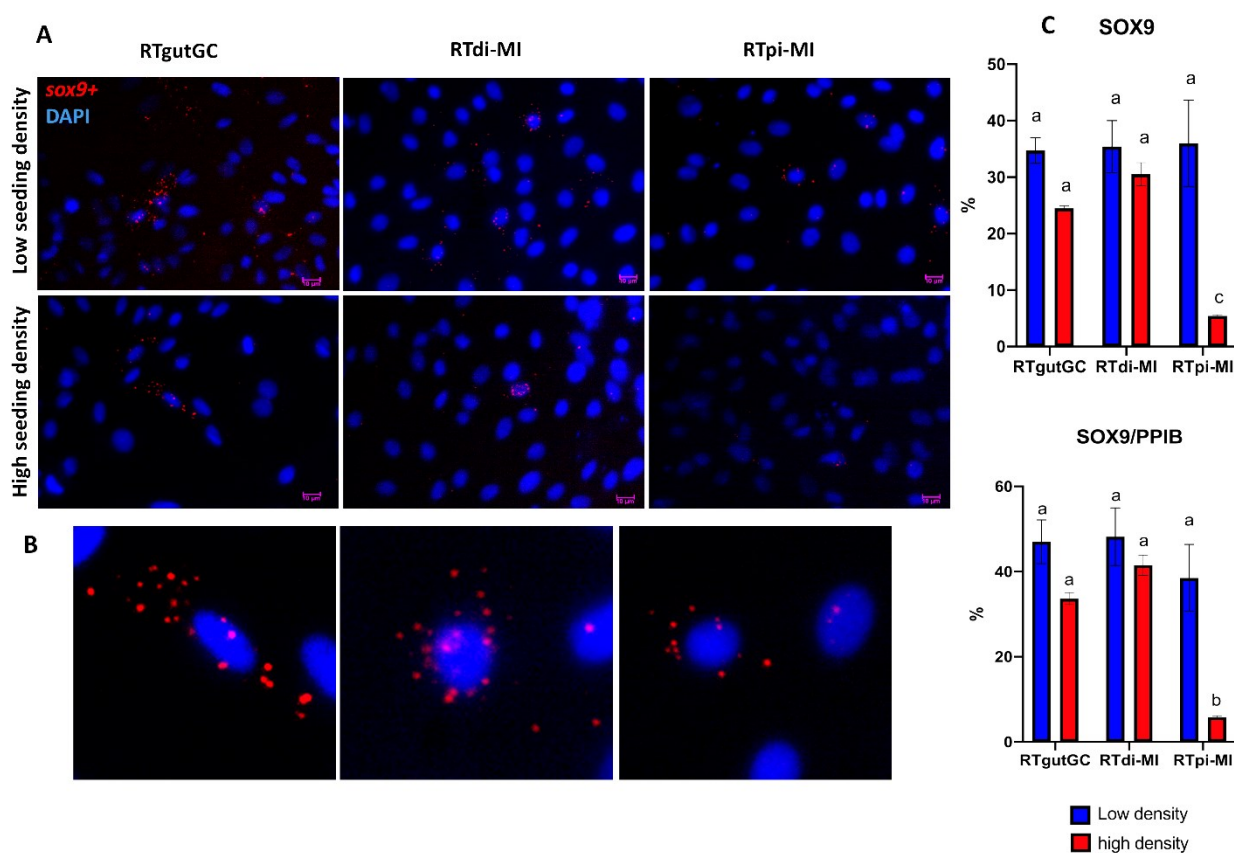
Figure 66: Representative panel showing *in situ* hybridization of *sox9* and their estimated percentage considering both high and low seeding density and related to the epithealil cell component (*ppib*) (A-C). Representative images of cells displaying *sox9* at high level (>10mRNA dots/ nucleus-B).

Hopx was used as a marker for partially differentiated precursors (Figure 67-A). Also for this gene, we did not observe significant difference between the percentages of positive cells in the different lines when they were seeded at low density (RTgutGC: 28.3 ± 1.4%, RTdi-MI 27.7 ± 1.5%, RTpi-MI: 29.8 ± 1.8%). Conversely, a high seeding density significantly reduced the percentage of positive cells in all lines (RTgutGC: 18.8 ± 4.3, RTdi-MI: 16.0 ± 1.1, RTpi-MI: 11.9 ± 1.2) as shown in figure below (Figure 67-B). Only a few cells expressed both *sox9* and *hopx* simultaneously (Figure 68).
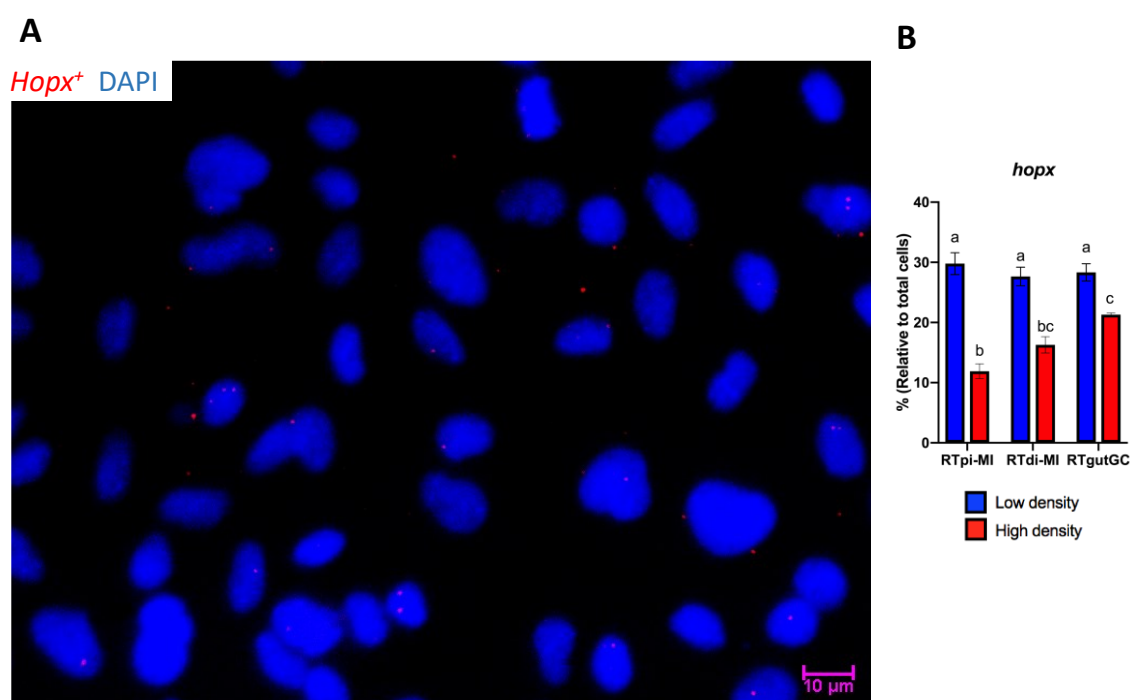
Figure 67: Representative image showing *in situ* hybridization of *hopx*+ cells (red dots) (A), and bar chart of the percentage of *hopx*+ cell seeded at low and high density (B). Nuclei were counterstained with DAPI (blue). Scale bar, 10 μm.
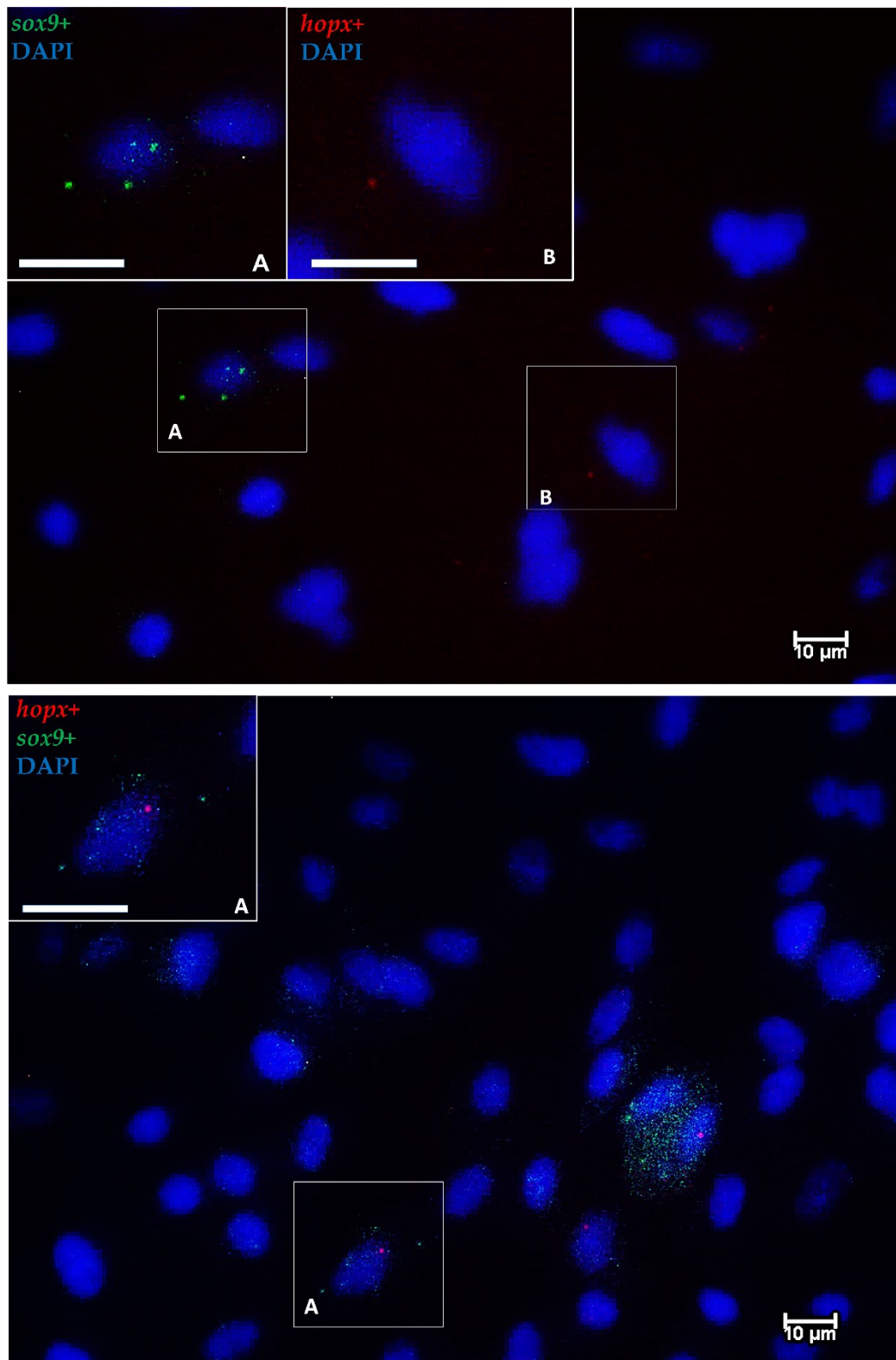
Figure 68: Representative image of dual-fluorescence *in situ* hybridization of *sox9* and *hopx* showing that the two markers evidence two different cell population. However, few *hopx+* cells expressed at the same time *sox9*.

In vivo, lgr5 is expressed in rare stromal cells spread at folds' apex. As *in vivo*, *in vitro* only few cells expressed *lgr5*. In addition they were only weak positive (1-2 mRNA dots/nucleus). Their percentage was variable between 10.6 and 3.3% when the cells were seeded at low density. Its expression was further reduced when they were seeded at high density (2.5-0.3%) as shown in figures 69 A-B.

A

B
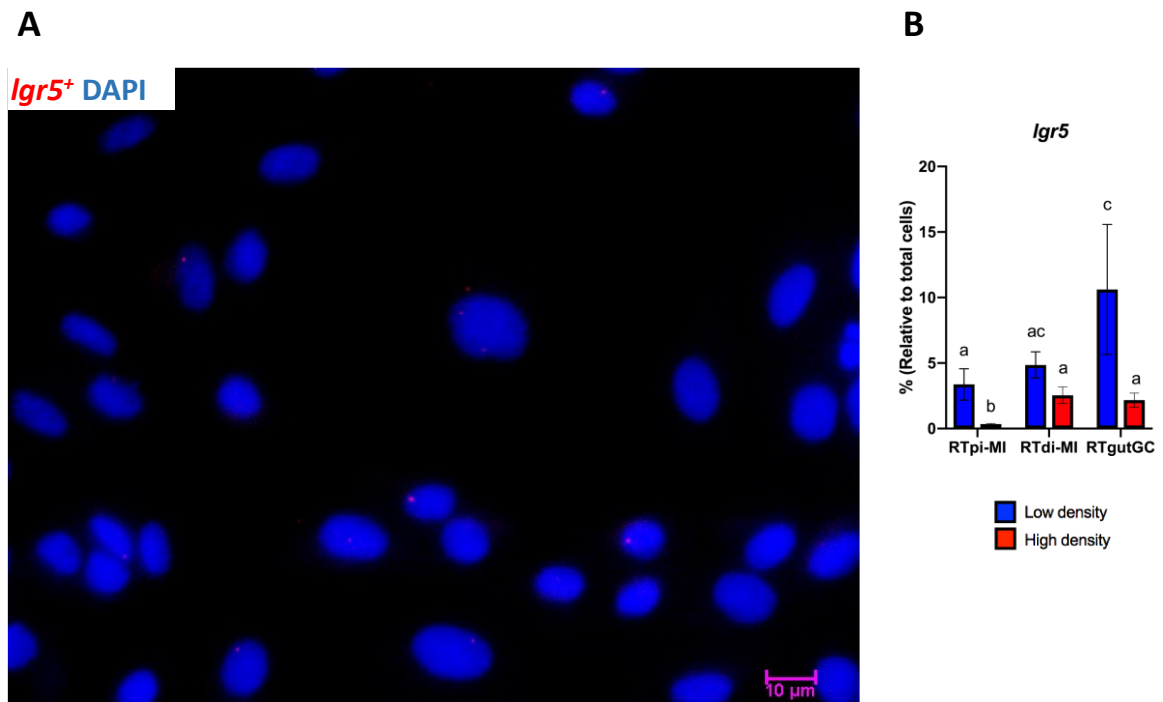
Figure 69: Representative image of *lgr5* (red dots) *in situ* hybridization (A), bar chart reporting the percentage of *lgr5*+ cells seeded at high a low densities in the different cells line (B). Nuclei were counterstained with DAPI. Scale bar, 10 μm.

The histochemical detection of the alkaline phosphatase (AP) enzyme activity was used to identify terminally differentiated epithelial cells. Iap was undetectable in all cells line seeded at low density, whereas a clear signal was found at high seeding density exclusively in the RTpi-Mi (Figure 70-71). Interestingly, this latter, was the only cell line in which has been also observed a significant reduction of the stem cell components.
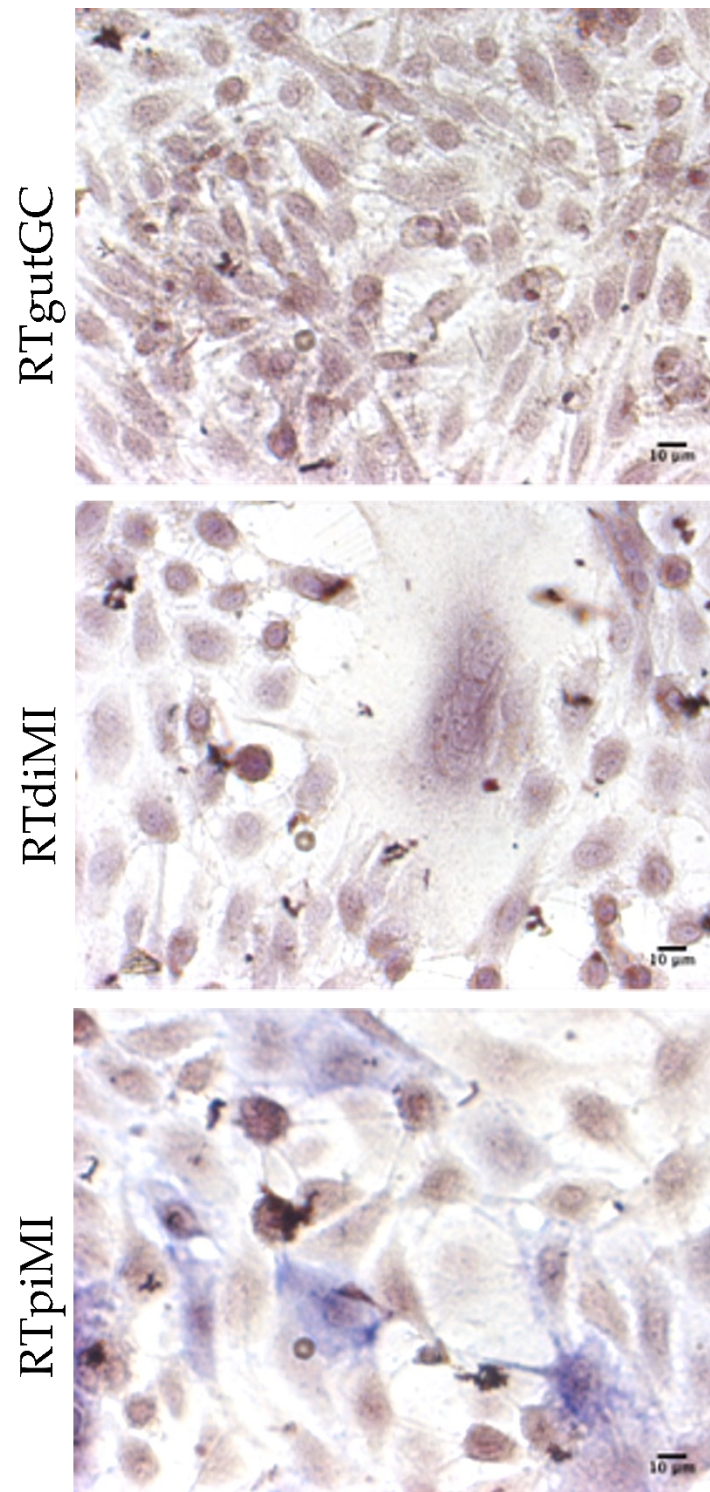
Figure 70: Representative images showing a clear alkaline phosphatase (AP) signal (blue) in RTpiMi cell line seeded at high density. AP was instead absent in the other two cell lines even after a high seeding density. Nuclei were counterstained with Mayer's hematoxylin. Scale bar, 10 μm.
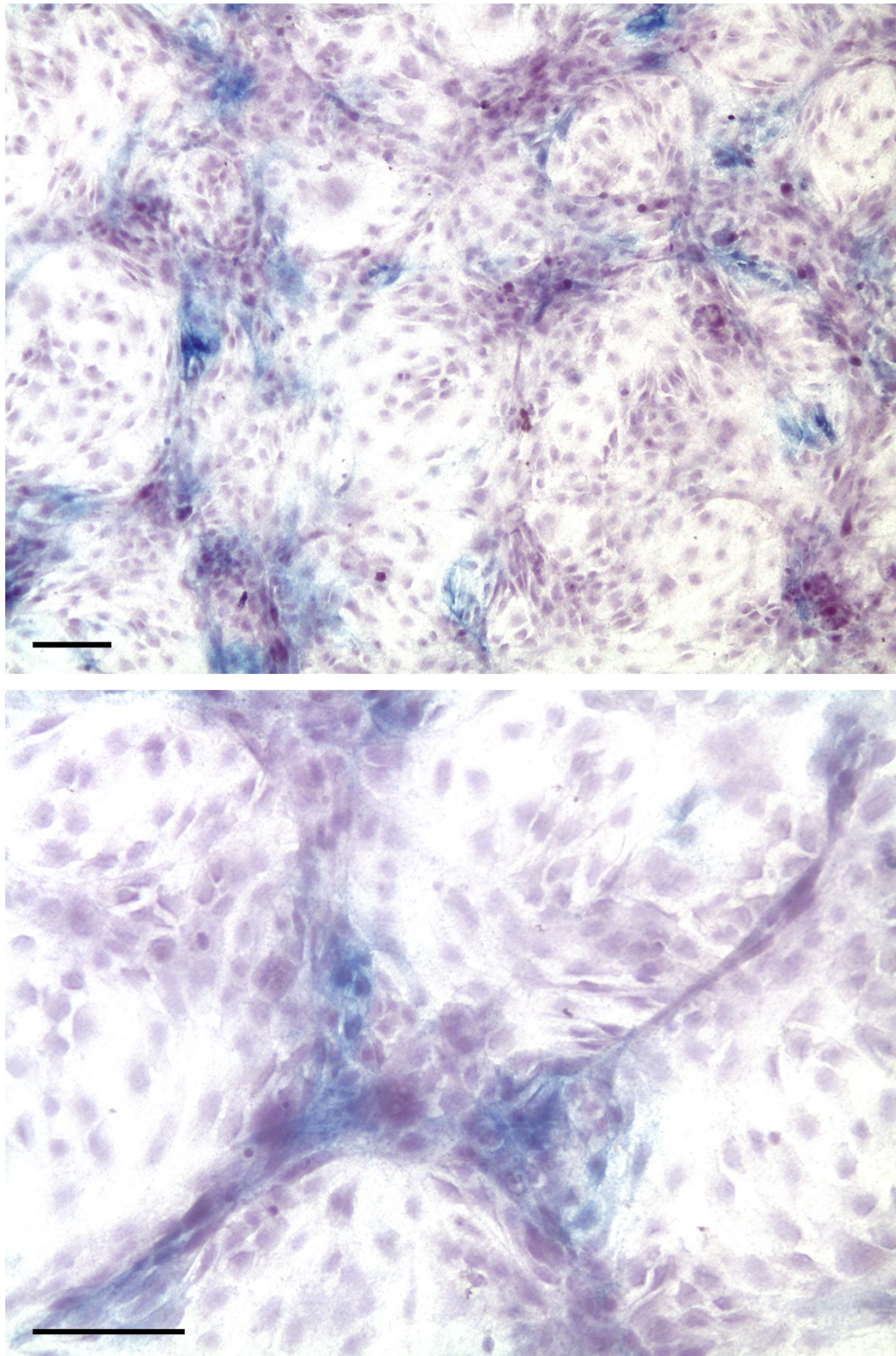
Figure 71: Representative images of the histochemical detection of alkaline phosphatase (AP) (blue signal) in RTpiMi cell line seeded at high density. Nuclei were counterstained with Mayer's hematoxylin. Scale bar, 100 μm

Discussion

Here, I successfully characterized the two novel, stable cell lines derived from the two main portions of the trout gut. They have been successfully cryopreserved and passaged more than 30 times. As mentioned before, RTgutGC cell line has been obtained from the more distal portion [13], consequently to the best of our knowledge, RTpiMi is the only cell lines that has been established from the proximal tract. Since our extensive morphological and functional characterization of the *in vivo* intestinal mucosa highlighted several substantial differences between the two main districts, it is reasonable to assume that have available of two cells lines, representative of these two districts, substantially improved our possibility to generate lifelike *in vitro* models.

To provide an *in vitro* model that shares functional similarities with the intestinal microenvironment, cell lines also need to preserve a heterogeneous cell population, including stem and progenitors as well as terminally differentiated cells.

All the considered cell lines expressed specific transcripts related to cell-junctions formation, essential structures for the maintenance of cellular polarity and epithelium integrity. In particular, they expressed E-Cadherin marker, a well-characterized anchored-protein whose key role is to preserve the epithelial barrier function [137]. Moreover, all cell lines expressed the specific transcript as well as the related structural protein Zonula Occludens-1, which, interacting with the proteins belonging to the classes of the Cadherin and Claudine, contributes to the maintenance of the structural barrier and to signal transduction [138]. Overall, their presence suggests not only an epithelial component in the considered cell lines but also the formation of a functioning barrier. However, the identification of Vimentin and of the Collagen type 1, fibroblast-specific markers, indicated also the presence of a mesenchymal population. *In vivo*, it is known that among the different stromal

components, fibroblasts actively participate in the preservation of tissue homeostasis producing growth factors, cytokines, and extracellular matrix proteins [139]. Consequently, ideally, *in vitro* models need to preserve both components in order to mimic the native intestinal mucosa [140].

The epithelial component was not homogeneous among the cell lines. *Ppib* is generally considered the most accurate marker when examining the intestinal epithelium [141], its expression has been also observed in other *in vitro* intestinal models such as IEC-6 cells (epithelial intestinal line derived from rat duodenum) [141]. In the rainbow trout intestinal mucosa, *ppib* was abundantly expressed in the epithelial cells, demonstrating its reliability as epithelial marker in the trout-derived cell lines. Therefore, it has been used to estimate the percentage of epithelial cells. Although the epithelial component was high in all cell lines, the line derived from the proximal tract displayed a significantly higher percentage.

Sglt1 is the protein responsible for the active transport of glucose through the enterocytes' membrane in the small intestine. Due to its essential role *in vivo*, this specific transport system must also be preserved in the *in vitro* models. However, to date, the available intestinal cell lines, such as Caco2 cells, express this protein only at low levels [142]. In particular, data demonstrated that despite this immortalized cell line shows typical characteristics of mature enterocytes such as polarization, tight-junction and microvilli formation, expression of enterocyte-specific enzymes (disaccharidase, peptidase and alkaline phosphate), and glucose and galactose transporters (SGLT1), their expressions are extremely variable [143] and in any case lower to those of the enterocytes *in vivo* [144]. This high variability is related to several external factors such as cellular source, passage and culture conditions [145]. In addition, great variability and low expression, make it difficult in *vivo*/*in vitro* correlation studies [143]. In all cell lines isolated from rainbow trout and considered in this thesis, instead, we observed an abundant and homogeneous expression of Sglt1, independent of the seeding density. It is therefore possible to

assume that these lines are more suitable to in *vivo*/*in vitro* correlation studies rather than Caco2.

As described above, academia and aquaculture feed industries are continuously looking for alternative formulations to the classical marine-derived protein. Therefore, it is necessary to develop a predictive model for the *in vitro* absorption of protein components. Pept1, is an essential peptide transporter, selectively expressed in the apical part of the enterocyte cytoplasm [86], involved in the absorption of di- and tri-peptides across the brush border membrane [146]. In Caco2 cell line, its expression increases significantly within the first two weeks of culture while different seeding densities do not affect its expression [145]. Interestingly, trout-derived cell lines expressed Pept1, suggesting their capacity to actively participate in peptide absorption. *In vivo*, we previously demonstrated that both Sglt1 and Pept1 are abundantly expressed in the proximal intestine, while they are weakly represented in the distal trait [93]. However, this typical feature has not been preserved *in vitro* since we did not observe any significant difference in terms of expression.

All the cell lines expressed *sox9* marker, some of which showed a high expression level, comparable to that observed at the folds' base *in vivo*. Based on our previous observation, this strongly suggests the presence of RT stem cells [93]. The percentage of *sox9*+ cells was quite high and homogeneous in all the cell lines, representing about a third of the total population that was approached to 50% when only epithelial cells were considered. This, indicated an excellent plastic capacity of the *in vitro* models. While the percentage of *sox9*+ cells was unchanged when cells were cultured at low seeding density, it significantly decreased exclusively in RTpi-MI when cultured at high seeding density.

Partially differentiated precursors have been selectively detected using *hopx* marker, it was interesting to note that the high seeding density has led to a significant reduction in its expression in all cell lines. Since *hopx*+ identifies cells in

transition towards differentiation [93], it is reasonable to assume that this cell population is the first to undergo the differentiation process. The presence of few cells co-expressing *sox9* and *hopx* in the RT cell lines indicates that the two cell populations remain fully distinct *in vitro* as observed *in vivo*, suggesting a high degree of maturation.

Finally, *lgr5* was used as marker to evaluate the presence of a mesenchymal component that regulates the differentiation of the intestinal tip epithelium. As *in vivo*, *lgr5*+ were rare and displayed only a weak expression [93]. These data confirmed the presence of a limited stromal component, but indicated that this population had played a potentially relevant functional.

Terminally differentiated cells have been characterized through the demonstration of the activity of alkaline phosphate, generally considered as mature enterocytes' marker [13]. Although all cell lines did not express this marker at low seeding density, high density induce the differentiation of the sole cell line derived from the proximal intestine. This latter was characterized by a distinct positive signal, suggesting the presence of a population of mature and functional enterocytes.

Conclusion

These results suggest that due to the mixed origin (epithelial/mesenchymal) of the cell lines it would possible to develop advanced *in vitro* models which will allow the evaluation of the functional interactions between the epithelium and stroma. In addition, the formation of a functional barrier together with the abundant expression of typical enterocytes' functional markers make these models compatible for both absorption and *in vivo*/*in vitro* correlation studies. Moreover, their high plastic properties make them potentially suitable to be differentiated specifically towards the functional cell types which constitute the intestinal mucosa. Finally, results of the experiment performed at two different seeding density, led us to believe that the stimulus used to induce cell differentiation was most effective on the cell line derived from the proximal intestine, in which we observed a significant reduction in the stem components and a simultaneously expression of the terminally differentiate enterocytes marker. However, the same stimulus was not enough to produce a similar effect on the two cell lines isolated from the distal tract. Considering that, *in vivo* the differentiated compartment is more extended in the proximal than in the distal tract, it is possible to hypothesize that *in vitro*, cells isolated from the proximal tract are more predisposed to differentiation.

Overall, the cell lines partially preserved the typical features that distinguish the intestine *in vivo*, leading us to believe that they represent a promising starting material to generate more representative and complex *in vitro* intestinal absorption models.

Overall Conclusion

The detailed morphological characterization of the rainbow trout (RT) intestinal mucosa architecture and of the different cell populations, substantially expanded and integrated the current anatomical and physiological knowledge of the RT intestine. Interestingly, I highlighted several differences between the two main gut portions, I confirmed that the proximal RT intestinal mucosa is arranged in simple folds while the one belonging to the more distal portion is characterized by complex *plicae* from which secondary and tertiary folds branch-off. I also provided new evidences showing the existence of two mingled, but well-distinct morphological and functional compartments along the trout intestine: the first includes the proximal intestine and the apical part of the complex folds of the more distal tract, whereas the second, consists of the basal portion of the complex *plicae* and the pyloric caeca.

I also investigated the mechanisms regulating the epithelium renewal and the maintenance of intestinal homeostasis, exploring the organization and the structure of the epithelial component of the stem cell niche. Since no crypts are present all along the trout gut, the folds base can be considered their functional equivalent, namely the functional and anatomical unit in which stem and progenitor's cells are housed. I discovered that despite all the classical mouse intestinal cell markers are expressed in rainbow trout, their typical localization, the niche architecture and the interactions among these markers are not conserved. In particular, in this species the functional equivalent of *lgr5*, the selective marker of the mouse actively cycling stem cells, seems to be *sox9*, since *sox9*$^+$ cells showed the same peculiar location and shape of *lgr5*$^+$ cells in mouse intestine. Conversely, *lgr5* which in mammals is generally considered a crypt epithelial stem cell marker, in this species is exclusively expressed by stromal cells distributed along the folds constituting a specific cell subpopulation, probably capable of supporting epithelial integrity and efficiency. Furthermore, since mounting evidence demonstrate that the epithelial component of the niche cannot exert properly their functional role

without the active cooperation of a supportive stromal cell population, I integrated these findings evaluating also the mesenchymal niche constituent. In particular, I proved, for the first time, the presence of telocytes (TC) within the RT gut stroma generating an intricate 3D mesh underneath the epithelium. I also observed that this peculiar cell population establishes direct connection to the close epithelial stem cells, providing short-range signalling and, at the same time, it exploits extracellular vesicles as means to convey biological information to more distant cells. This suggests their active implication in the regulation of the stem cell niche, as well as, more in general, in the intestinal homeostasis.

The accurate morphological and functional characterization of the rainbow trout intestine will be instrumental for evaluating how faithful to its physiological counterpart are *in vitro* intestinal models. Indeed, the substantial differences observed between the anterior and the posterior intestine, suggested that it would be very helpful to generate two *in vitro* models representing both the proximal and the distal intestine as long as they could preserve the typical distinguishing features of both. Moreover, the detailed characterization of the stem cell niche *in vivo* showed that, given the considerable phylogenetic distance between mouse and rainbow trout, is not advisable to directly extrapolate the knowledge from one species to the other.

In parallel, our group has successfully derived and established two cell lines, belonging to the two intestinal tracts, enriching the RT *in vitro* models availability. They have been characterized and compared with the only RT cell line currently available (RTgutGC) which has been isolated from the distal intestinal region. Interestingly, they partially shared similarities with the *in vivo* intestinal mucosa environment. Indeed, they preserved both epithelial and mesenchymal cell populations, expressed typical enterocyte's functional markers, and exhibited a stem cell component. This work represents the first detailed characterization of the

stem cell population of RT intestinal cell lines and demonstrates their high plasticity properties and consequently their suitability to *in vitro* differentiation studies.

In conclusion, the experiments conducted in parallel both *in vivo* and *in vitro* proved to be a successful strategy to properly compare, evaluate and monitor the *in vitro* models. In addition, since the trout-derived cell lines retained several of the distinguishing features that characterize the *in vivo* intestinal mucosa, in the future, they will represent a valuable tool to be combined with appropriate scaffolds to develop advanced and predictive models of intestinal absorption.

List of Abbreviations

AB: Alcian blue

ABC: Avidin biotin complex

ANOVA: Analysis of Variance

AP: Alkaline phosphatase

AP-DI: Apical part of the complex folds of the distal intestine

BCIP/NBT: 5-bromo-4-chloro-3-indolyl-phosphate

BMPs: Bone morphogenetic proteins

BP-DI: Basal part of the complex folds of the distal intestine

Caco2: Cancer coli-2

CASP3: Cleaved caspase 3

CBCs: Crypt base columnar cells

CLND3: Claudin- 3

COL1A1: Collagen type I

DAB: Diaminobenzidine

DapB: *Bacillus subtilis* dihydrodipicolinate reductase

DAPI: 4′,6-diamidino-2-phenylindole

DI: Distal intestine

DLL1:Delta-like protein 1

DMSO: Dimethyl sulfoxide

E-CAD: E-cadherin

ECM: extracellular matrix

EDTA : Ethylenediaminetetraacetic acid

EGCs: eosinophilic granule cells

EVs : Extracellular vesicles

FABP2: fatty acid binding protein 2

FFPE : formalin fixed-paraffin embedded

FISH: Fluorescence in situ hybridization

FOXL1: forkhead box l1

GI: Gastrointestinal tract

GLUT2: Glucose transporter 2

H_2O_2: Hydrogen peroxide

HE: Hematoxylin -esoin

HOPX: Homeodomain-only protein

HRP: Horseradish peroxidase

IAP: intestinal alkaline phosphatase

IECs: Intestinal epithealil cells

IESCs: Intestinal epithelial stem cells

LCFA: Long chain fatty acids

LFABP: Liver fatty acid-binding protein

LGR5:Leucine-rich-repeat-containing G-protein-coupled receptor 5

LPS: Lipopolysaccharides

LZY: lysozyme

MUC1: mucin 1

NOTCH1:Notch receptor 1

PAS: periodic acid Shiff

PBS: Phosphate-buffered saline

PC: Pyloric caeca

PCNA: proliferating cell nuclear antigen

PDGFRA: platelet-derived growth factor receptor A

PEPT1: peptide transporter 1

PI: Proximal intestine

PPIB : peptidylprolyl isomerase B

RT: Rainbow trout

RTdiMI : Rainbow trout Distal intestine Milan Italy

RTgutGC: Rainbow trout gut Guelph Canada

RTpiMI : Rainbow trout Proximal intestine Milan Italy

SC: Stem cells

sFRPs: Secreted frizzled related protein

SGLT1: Sodium - glucose/galactose transporter 1

SOX9:SRY-box 9

TA: Transit-amplifying cells

TC: Telocytes

TdT: terminal deoxynucleotidyl transferase

TEM : Transmission electron microscopy

TP : Telopodes

TRIS BASE : Trizma® base

Tris HCL: Tris hydrochloride

TUNEL: terminal deoxynucleotidyl transferase dUTP nick end labeling

VIM: Vimentin

Vv: Volume densities

WNT3A: Wnt family member 3A

ZO-1: Zonula occludens 1

Acknowledgements

The realization of this work could not have been possible without the time, the support and the dedication of so many people.

First and foremost, I am extremely grateful to my supervisor Prof. Fulvio Gandolfi for his constant presence, continuous support, for his advice and suggestions, for believing in me more than I have ever believed in myself, for trusting me every time, for sharing his knowledge, experience and skills with me and last but not least for giving me opportunities and deserve.

I would like to express my gratitude to Prof. Tiziana Brevini for her precious help, constant encouragement, and for guiding me professionally and confidently in the daily life of my Ph.D.

I also would like to thank all the UNISTEM members, Dr. Georgia Pennarossa, Dr. Rolando Pasquariello, Dr. Sharon Arcuri and Dr. Teresina De Iorio.

A special thanks goes to NOLIMITS, the advanced imaging facility established by the "Università degli Studi di Milano". In particular, my sincere gratitude goes to Dr. Laura Madaschi for sharing with me her experience and for always working hard and incessantly to help me.

A special thanks go to Daphne, Federica, Marta, Lodovico, Barbara, Matilde, for their precious support and for having actively participated in the realization of this work, sharing with me both difficult and harmonious moments.

Bibliography

1.	Unfpa The World at Seven Billion Seven Billion People – Counting On Each Other. *J. Econ. Surv.* **2019**, *19*, 561–586.

2.	Brunner, E.J.; Jones, P.J.S.; Friel, S.; Bartley, M. Fish, human health and marine ecosystem health: Policies in collision. *Int. J. Epidemiol.* **2009**, *38*, 93–100, doi:10.1093/ije/dyn157.

3.	FAO *The State of World Fisheries and Aquaculture 2020*; FAO, 2020;

4.	Fao Small-scale rainbow trout farming.

5.	Le Boucher, R.; Dupont-Nivet, M.; Vandeputte, M.; Kerneïs, T.; Goardon, L.; Labbé, L.; Chatain, B.; Bothaire, M.J.; Larroquet, L.; Médale, F.; et al. Selection for Adaptation to Dietary Shifts: Towards Sustainable Breeding of Carnivorous Fish. *PLoS One* **2012**, *7*, 3–9, doi:10.1371/journal.pone.0044898.

6.	Bell, J.G.; Henderson, R.J.; Tocher, D.R.; Sargent, J.R. Replacement of dietary fish oil with increasing levels of linseed oil: Modification of flesh fatty acid compositions in atlantic salmon (Salmo salar) using a fish oil finishing diet. *Lipids* **2004**, *39*, 223–232, doi:10.1007/s11745-004-1223-5.

7.	Gouseti, O.; Bornhorst, G.M.; Bakalis, S.; Mackie, A. *Interdisciplinary approaches to food digestion*; Springer International Publishing, 2019; ISBN 9783030039011.

8.	Barker, N.; van Oudenaarden, A.; Clevers, H.; van Oudenaarden, A.; Clevers, H. Identifying the Stem Cell of the Intestinal Crypt: Strategies and Pitfalls. *Cell Stem Cells* **2012**, *11*, doi:10.1016/j.stem.2012.09.009.

9.	Keemink, J.; Bergström, C.A.S. Caco-2 Cell Conditions Enabling Studies of Drug Absorption from Digestible Lipid-Based Formulations. *Pharm. Res.* **2018**, *35*, doi:10.1007/s11095-017-2327-8.

10.	Vázquez, M.; Vélez, D.; Devesa, V. In vitro characterization of the intestinal absorption of methylmercury using a caco-2 cell model. *Chem. Res. Toxicol.* **2014**, *27*, 254–264, doi:10.1021/tx4003758.

11.	Maqsood, M.I.; Matin, M.M.; Bahrami, A.R.; Ghasroldasht, M.M. Immortality of cell lines: Challenges and advantages of establishment. *Cell Biol. Int.* 2013, *37*, 1038–1045.

12.	Le Ferrec, E.; Chesne, C.; Artusson, P.; Brayden, D.; Fabre, G.; Gires, P.; Guillou, F.; Rousset, M.; Rubas, W.; Scarino, M.L. In vitro models of the intestinal barrier. The report and recommendations of ECVAM Workshop 46. European Centre for the Validation of Alternative methods. *Altern. Lab. Anim.* **2001**, *29*, 649–68.

13.	Kawano, A.; HAIDUK, C.; SCHIRMER, K.; HANNER, R.; LEE, L.E.J.; DIXON, B.; BOLS, N.C. Development of a rainbow trout intestinal epithelial cell line and its response to lipopolysaccharide. *Aquac. Nutr.* **2011**, *17*, e241–e252, doi:10.1111/j.1365-2095.2010.00757.x.

14.	Date, S.; Sato, T. Mini-Gut Organoids: Reconstitution of the Stem Cell Niche. *Annu. Rev. Cell*

Dev. Biol. **2015**, *31*, 269–289, doi:10.1146/annurev-cellbio-100814-125218.

15. Merker, S.R.; Weitz, J.; Stange, D.E. Gastrointestinal organoids: How they gut it out. *Dev. Biol.* **2016**, *420*, 239–250, doi:10.1016/j.ydbio.2016.08.010.

16. Sato, T.; Clevers, H.; Flier, L.G. van der; Clevers, H.; Cheng, H.; Leblond, C.P.; Barker, N.; Potten, C.S.; Sangiorgi, E.; Capecchi, M.R.; et al. Growing Self-Organizing Mini-Guts from a Single Intestinal Stem Cell: Mechanism and Applications. *Science (80-.).* **2013**, *340*, 241–260, doi:10.1126/science.1234852.

17. Garibaldi Luca, Simon Funge-Smith, Xiaowei Shou, J.C. *The state of world fisheries and aquaculture 2018 : meeting the sustainable development goals.*; 2018; ISBN 9789251305621.

18. Fagundes, K.R.C.; Rotundo, M.M.; Mari, R.B. Morphological and histochemical characterization of the digestive tract of the puffer fish Sphoeroides testudineus (Linnaeus 1758) (Tetraodontiformes: Tetraodontidae). *An. Acad. Bras. Cienc.* **2016**, *88*, 1615–1624, doi:10.1590/0001-3765201620150167.

19. Olsson, C.; Aldman, G.; Larsson, A.; Holmgren, S. Cholecystokinin affects gastric emptying and stomach motility in the rainbow trout Oncorhynchus mykiss. *J. Exp. Biol.* **1999**, *202*, 161–170, doi:10.1242/jeb.202.2.161.

20. Egerton, S.; Culloty, S.; Whooley, J.; Stanton, C.; Ross, R.P. The gut microbiota of marine fish. *Front. Microbiol.* **2018**, *9*, 1–17, doi:10.3389/fmicb.2018.00873.

21. Ostos Garrido, M. V.; Nuñez Torres, M.I.; Abaurrea Equisoain, M.A. Histological, histochemical and ultrastructural analysis of the gastric mucosa in Oncorhynchus mykiss. *Aquaculture* **1993**, *115*, 121–132, doi:10.1016/0044-8486(93)90363-4.

22. Buddington, R.K.; Diamond, J.M. Pyloric ceca of fish: A "new" absorptive organ. *Am. J. Physiol. - Gastrointest. Liver Physiol.* **1987**, *252*, doi:10.1152/ajpgi.1987.252.1.g65.

23. Kiela, P.R.; Ghishan, F.K. Physiology of intestinal absorption and secretion. *Best Pract. Res. Clin. Gastroenterol.* 2016, *30*, 145–159.

24. Blanco, A.M.; Bertucci, J.I.; Ramesh, N.; Delgado, M.J.; Valenciano, A.I.; Unniappan, S. Ghrelin Facilitates GLUT2-, SGLT1-and SGLT2-mediated Intestinal Glucose Transport in Goldfish (Carassius auratus). *Sci. Rep.* **2017**, *7*, 1–16, doi:10.1038/srep45024.

25. Polakof, S.; Álvarez, R.; Soengas, J.L. Gut glucose metabolism in rainbow trout: implications in glucose homeostasis and glucosensing capacity. *Am J Physiol Regul Integr Comp Physiol* **2010**, *299*, 19–32, doi:10.1152/ajpregu.00005.2010.-The.

26. Senol Development of the liver and pancreas in the rainbow trout (Oncorhynchus mykiss). *Süleyman Demirel Üniversitesi Eğirdir Su Ürünleri Fakültesi Derg.* **2005**, *1*.

27. Burnstock, G. *The Morphology of the Gut of the Brown Trout (Salmo trutta)*;

28. Lkka, G.; Austb, L.; Falk, K.; Bjerkås, I.; Koppang, E.O. Intestinal morphology of the wild atlantic salmon (Salmo salar). *J. Morphol.* **2013**, *274*, 859–876, doi:10.1002/jmor.20142.

29. Banan Khojasteh, S.M.; Sheikhzadeh, F.; Mohammadnejad, D.; Azami, A. Histological, Histochemical and Ultrastructural Study of the Intestine of Rainbow Trout (Oncorhynchus

mykiss). *World Appl. Sci. J.* **2009**, *6*, 1525–1531.

30. Bjørgen, H.; Li, Y.; Kortner, T.M.; Krogdahl, Å.; Koppang, E.O. Anatomy, immunology, digestive physiology and microbiota of the salmonid intestine: Knowns and unknowns under the impact of an expanding industrialized production. *Fish Shellfish Immunol.* **2020**, *107*, 172–186, doi:10.1016/j.fsi.2020.09.032.

31. Clevers, H.C.; Bevins, C.L. Paneth Cells: Maestros of the Small Intestinal Crypts. *Annu. Rev. Physiol.* **2013**, *75*, 289–311, doi:10.1146/annurev-physiol-030212-183744.

32. Aghaallaei, N.; Gruhl, F.; Schaefer, C.Q.; Wernet, T.; Weinhardt, V.; Centanin, L.; Loosli, F.; Baumbach, T.; Wittbrodt, J. Identification, visualization and clonal analysis of intestinal stem cells in fish. *Development* **2016**, dev.134098, doi:10.1242/dev.134098.

33. Snoeck, V.; Goddeeris, B.; Cox, E. The role of enterocytes in the intestinal barrier function and antigen uptake. *Microbes Infect.* **2005**, *7*, 997–1004, doi:10.1016/j.micinf.2005.04.003.

34. Bilski, J.; Mazur-Bialy, A.; Wojcik, D.; Zahradnik-Bilska, J.; Brzozowski, B.; Magierowski, M.; Mach, T.; Magierowska, K.; Brzozowski, T. The Role of Intestinal Alkaline Phosphatase in Inflammatory Disorders of Gastrointestinal Tract. *Mediators Inflamm.* **2017**, *2017*, doi:10.1155/2017/9074601.

35. Lallès, J.P. Intestinal alkaline phosphatase: Novel functions and protective effects. *Nutr. Rev.* **2014**, *72*, 82–94, doi:10.1111/nure.12082.

36. Specian, R.D.; Oliver, M.G. Functional biology of intestinal goblet cells. *Am. J. Physiol. - Cell Physiol.* **1991**, *260*, 83–93, doi:10.1152/ajpcell.1991.260.2.c183.

37. Kim, J.J.; Khan, W.I. Goblet cells and mucins: Role in innate defense in enteric infections. *Pathogens* 2013, *2*, 55–70.

38. Dall'aglio, C.; Mercati, F.; Faeti, V.; Acuti, G.; Trabalza-Marinucci, M.; De Felice, E.; Tardella, F.M.; Franciosini, M.P.; Proietti, P.C.; Catorci, D.; et al. *Immuno-and glyco-histochemistry as a tool to evaluate the oregano supplemented feed effects in pig gut*; 2020; Vol. 64;.

39. Mercati, F.; Dall'Aglio, C.; Acuti, G.; Faeti, V.; Tardella, F.M.; Pirino, C.; Felice, E. De; Scocco, P. Oregano feed supplementation affects glycoconjugates production in swine gut. *Animals* **2020**, *10*, doi:10.3390/ani10010149.

40. Arman, S.; Üçüncü, S.I. Histochemical characterization of convict cichlid (Amatitlania nigrofasciata) intestinal goblet cells. *Pak. J. Zool.* **2017**, *49*, 445–453, doi:10.17582/journal.pjz/2017.49.2.445.453.

41. Latorre, R.; Sternini, C.; De Giorgio, R.; Greenwood-Van Meerveld, B. Enteroendocrine cells: A review of their role in brain-gut communication. *Neurogastroenterol. Motil.* **2016**, *28*, 620–630, doi:10.1111/nmo.12754.

42. Clevers, H.C.; Bevins, C.L. Paneth Cells: Maestros of the Small Intestinal Crypts. *Annu. Rev. Physiol.* **2013**, *75*, 289–311, doi:10.1146/annurev-physiol-030212-183744.

43. Dominguez-Brauer, C.; Hao, Z.; Elia, A.J.; Fortin, J.M.; Nechanitzky, R.; Brauer, P.M.; Sheng, Y.; Mana, M.D.; Chio, I.I.C.; Haight, J.; et al. Mule Regulates the Intestinal Stem Cell Niche via the Wnt Pathway and Targets EphB3 for Proteasomal and Lysosomal Degradation. *Cell*

Stem Cell **2016**, *19*, 205–216, doi:10.1016/j.stem.2016.04.002.

44. Lueschow, S.R.; McElroy, S.J. The Paneth Cell: The Curator and Defender of the Immature Small Intestine. *Front. Immunol.* 2020, *11*.

45. Hou, Q.; Huang, J.; Ayansola, H.; Masatoshi, H.; Zhang, B. Intestinal Stem Cells and Immune Cell Relationships: Potential Therapeutic Targets for Inflammatory Bowel Diseases. *Front. Immunol.* **2021**, *11*, 1–14, doi:10.3389/fimmu.2020.623691.

46. Verdile, N.; Mirmahmoudi, R.; Brevini, T.A.L.; Gandolfi, F. Evolution of pig intestinal stem cells from birth to weaning. *Animal* **2019**, *3*, 1–10, doi:10.1017/S1751731119001319.

47. Sveinbjornsson, B.; Olsen, R.; Paulsen, S. Immunocytochemical localization of lysozyme in intestinal eosinophilic granule cells (EGCs) of Atlantic salmon, Salmo salar L. *J. Fish Dis.* **1996**, *19*, 349–355, doi:10.1046/j.1365-2761.1996.d01-87.x.

48. Wang, Y.; George, S.P.; Roy, S.; Pham, E.; Esmaeilniakooshkghazi, A.; Khurana, S. Both the anti-and pro-apoptotic functions of villin regulate cell turnover and intestinal homeostasis. *Sci. Rep.* **2016**, *6*, doi:10.1038/srep35491.

49. Potten, C.S.; Wilson, J.W.; Booth, C. Regulation and significance of apoptosis in the stem cells of the gastrointestinal epithelium. *Stem Cells* **1997**, *15*, 82–93, doi:10.1002/stem.150082.

50. Ferraro, F.; Lo Celso, C.; Scadden, D.; Meshorer, E.; Plath, K. ADULT STEM CELLS AND THEIR NICHES The Cell Biology of Stem Cells, edited by. *Cell Biol. Stem Cells* **2010**, 155–168.

51. Cheng, H. Origin, differentiation and renewal of the four main epithelial cell types in the mouse small intestine II. Mucous cells. *Am. J. Anat.* **1974**, *141*, 481–501, doi:10.1002/aja.1001410404.

52. Barker, N. Adult intestinal stem cells : critical drivers of epithelial homeostasis and regeneration. *Nat. Publ. Gr.* **2013**, *15*, 19–33, doi:10.1038/nrm3721.

53. Freeman, H.J. Crypt region localization of intestinal stem cells in adults. *World J. Gastroenterol.* **2008**, *14*, 7160–7162, doi:10.3748/wjg.14.7160.

54. CHRISTOPHER s. POTTEN, L.K.A.E.H. CCONTINUOUS LABELLING STUDIES ON MOUSE SKIN AND INTESTINE. **1974**.

55. Li, N.; Clevers, H. Coexistence of quiescent and active adult stem cells in mammals. *Science (80-.).* **2010**, *327*, 542–545, doi:10.1126/science.1180794.

56. Yan, K.; Chia, L.; Li, X. The intestinal stem cell markers Bmi1 and Lgr5 identify two functionally distinct populations. *Pnas* **2012**, *109*, 466–471, doi:10.1073/pnas.1118857109/-/DCSupplemental.www.pnas.org/cgi/doi/10.1073/pnas.1118857109.

57. He, S.; Zhou, H.; Zhu, X.; Hu, S.; Fei, M.; Wan, D.; Gu, W.; Yang, X.; Shi, D.; Zhou, J.; et al. Expression of Lgr5, a marker of intestinal stem cells, in colorectal cancer and its clinicopathological significance. *Biomed. Pharmacother.* **2014**, *68*, 507–513, doi:10.1016/j.biopha.2014.03.016.

58. Gonzalez, L.M.; Williamson, I.; Piedrahita, J.A.; Blikslager, A.T.; Magness, S.T. Cell Lineage Identification and Stem Cell Culture in a Porcine Model for the Study of Intestinal Epithelial

Regeneration. *PLoS One* **2013**, *8*, doi:10.1371/journal.pone.0066465.

59.   Bankaitis, E.D.; Ha, A.; Kuo, C.J.; Magness, S.T. Reserve Stem Cells in Intestinal Homeostasis and Injury. *Gastroenterology* **2018**, *155*, 1348–1361, doi:10.1053/j.gastro.2018.08.016.

60.   Shoshkes-Carmel, M.; Wang, Y.J.; Wangensteen, K.J.; Tóth, B.; Kondo, A.; Massassa, E.E.; Itzkovitz, S.; Kaestner, K.H. Subepithelial telocytes are an important source of Wnts that supports intestinal crypts. *Nature* **2018**, *557*, 242–246, doi:10.1038/s41586-018-0084-4.

61.   Vannucchi, M.G.; Traini, C. Interstitial cells of Cajal and telocytes in the gut: Twins, related or simply neighbor cells? *Biomol. Concepts* **2016**, *7*, 93–102, doi:10.1515/bmc-2015-0034.

62.   Flanagan, D.J.; Austin, C.R.; Vincan, E.; Phesse, T.J. Wnt signalling in gastrointestinal epithelial stem cells. *Genes (Basel).* 2018, *9*.

63.   Gregorieff, A.; Clevers, H. Wnt signaling in the intestinal epithelium: From endoderm to cancer. *Genes Dev.* **2005**, *19*, 877–890, doi:10.1101/gad.1295405.

64.   Schuijers, J.; Clevers, H. Adult mammalian stem cells: The role of Wnt, Lgr5 and R-spondins. *EMBO J.* **2012**, *31*, 2685–2696, doi:10.1038/emboj.2012.149.

65.   Verdile, N.; Pasquariello, R.; Scolari, M.; Scirè, G.; Brevini, T.A.L.; Gandolfi, F. A Detailed Study of Rainbow Trout (Onchorhynchus mykiss) Intestine Revealed That Digestive and Absorptive Functions Are Not Linearly Distributed along Its Length. *Animals* **2020**, *10*, 745, doi:10.3390/ani10040745.

66.   Urdaci, M.C.; Regnault, B.; Grimont, P.A.D. *Identification by in situ hybridization of segmented filamentous bacteria in the intestine of diarrheic rainbow trout (Oncorhynchus mykiss)*; 2001; Vol. 152;.

67.   Keat-Chuan Ng, C.; Aun-Chuan Ooi, P.; Wong, W..; Khoo, G. A Review of Fish Taxonomy Conventions and Species Identification Techniques. *J. Surv. Fish. Sci.* **2017**, *4*, 54–93, doi:10.18331/sfs2017.4.1.6.

68.   Albl, B.; Haesner, S.; Braun-Reichhart, C.; Streckel, E.; Renner, S.; Seeliger, F.; Wolf, E.; Wanke, R.; Blutke, A. Tissue Sampling Guides for Porcine Biomedical Models. *Toxicol. Pathol.* **2016**, *44*, 414–420, doi:10.1177/0192623316631023.

69.   Hassanpour, M.; Joss, J. Anatomy and Histology of the Spiral Valve Intestine in Juvenile Australian Lungfish, Neoceratodus forsteri~!2009-02-25~!2009-04-08~!2009-06-02~! *Open Zool. J.* **2009**, *2*, 62–85, doi:10.2174/1874336600902000062.

70.   Burnstock, G. The Morphology of the Gut of the Brown Trout (Salmo trutta). *J. Cell Sci. 1959 s3-100 183-198* **1959**, *s3-100*, 183–198.

71.   Li, Y.; Kortner, T.M.; Chikwati, E.M.; Munang'andu, H.M.; Lock, E.J.; Krogdahl, Å. Gut health and vaccination response in pre-smolt Atlantic salmon (Salmo salar) fed black soldier fly (Hermetia illucens) larvae meal. *Fish Shellfish Immunol.* **2019**, *86*, 1106–1113, doi:10.1016/j.fsi.2018.12.057.

72.   Henningsen, A.D.; Whitaker, B.R.; Walker, I.D. Protrusion of the valvular intestine in captive smalltooth sawfish and comments on pristid gastrointestinal anatomy and intestinal valve types. *J. Aquat. Anim. Health* **2005**, *17*, 289–295, doi:10.1577/H04-063.1.

73.   Argyriou, T.; Clauss, M.; Maxwell, E.E.; Furrer, H.; Sánchez-Villagra, M.R. Exceptional preservation reveals gastrointestinal anatomy and evolution in early actinopterygian fishes. *Sci. Rep.* **2016**, *6*, doi:10.1038/srep18758.

74.   Glover, C.N.; Petri, D.; Tollefsen, K.E.; Jørum, N.; Handy, R.D.; Berntssen, M.H.G. Assessing the sensitivity of Atlantic salmon (Salmo salar) to dietary endosulfan exposure using tissue biochemistry   and   histology.   *Aquat.   Toxicol.*   **2007**,   *84*,   346–355, doi:10.1016/j.aquatox.2007.06.013.

75.   Gauthier, G.F.; Landis', S.C. *The Relationship of Ultrastructural and Cytochemical Features to Absorptive Activity in the Goldfish Intestine*;

76.   Bosi, G.; DePasquale, J.A.; Manera, M.; Castaldelli, G.; Giari, L.; Sayyaf Dezfuli, B. Histochemical and immunohistochemical characterization of rodlet cells in the intestine of two teleosts, Anguilla anguilla and Cyprinus carpio. *J. Fish Dis.* **2018**, *41*, 475–485, doi:10.1111/jfd.12751.

77.   Elia, A.C.; Capucchio, M.T.; Caldaroni, B.; Magara, G.; Dörr, A.J.M.; Biasato, I.; Biasibetti, E.; Righetti, M.; Pastorino, P.; Prearo, M.; et al. Influence of Hermetia illucens meal dietary inclusion on the histological traits, gut mucin composition and the oxidative stress biomarkers in rainbow trout (Oncorhynchus mykiss). *Aquaculture* **2018**, *496*, 50–57, doi:10.1016/j.aquaculture.2018.07.009.

78.   Khojasteh, S.M.B.; Sheikhzadeh, F.; Mohammadnejad, D.; Azami, A. Histological, Histochemical and Ultrastructural Study of the Intestine of Rainbow Trout (Oncorhynchus mykiss). *World Appl. Sci. J.* **2009**, *6*, 1525–1531.

79.   Hamidian, G.; Zirak, K.; Sheikhzadeh, N.; Khani Oushani, A.; Shabanzadeh, S.; Divband, B. Intestinal histology and stereology in rainbow trout (Oncorhynchus mykiss) administrated with nanochitosan/zeolite and chitosan/zeolite composites. *Aquac. Res.* **2018**, *49*, 1803–1815, doi:10.1111/are.13634.

80.   Bosi, G.; Arrighi, S.; Di Giancamillo, A.; Domeneghini, C. Histochemistry of glycoconjugates in mucous cells of Salmo trutta uninfected and naturally parasitized with intestinal helminths. *Dis. Aquat. Organ.* **2005**, *64*, 45–51, doi:10.3354/dao064045.

81.   Krystel-Whittemore, M.; Dileepan, K.N.; Wood, J.G. Mast cell: A multi-functional master cell. *Front. Immunol.* 2016, *6*.

82.   Reite, O.B.; Evensen, Ø. Inflammatory cells of teleostean fish: A review focusing on mast cells/eosinophilic granule cells and rodlet cells. In Proceedings of the Fish and Shellfish Immunology; Academic Press, 2006; Vol. 20, pp. 192–208.

83.   Dezfuli, B.S.; Giari, L.; Lui, A.; Squerzanti, S.; Castaldelli, G.; Shinn, A.P.; Manera, M.; Lorenzoni, M. Proliferative cell nuclear antigen (PCNA) expression in the intestine of Salmo trutta trutta naturally infected with an acanthocephalan. *Parasites and Vectors* **2012**, *5*, doi:10.1186/1756-3305-5-198.

84.   Shin, J.; Carr, A.; Corner, G.A.; Tögel, L.; Dávaos-Salas, M.; Tran, H.; Chueh, A.C.; Al-Obaidi, S.; Chionh, F.; Ahmed, N.; et al. The intestinal epithelial cell differentiation marker intestinal alkaline phosphatase (ALPi) is selectively induced by histone deacetylase inhibitors (HDACi) in colon cancer cells in a Kruppel-like Factor 5 (KLF5)-defendent manner. *J. Biol. Chem.* **2014**, *289*, 25306–25316, doi:10.1074/jbc.M114.557546.

85.   Moss, S.F.; Attia, L.; Scholes, J. V.; Walters, J.R.F.; Holt, P.R. Increased small intestinal apoptosis in coeliac disease. *Gut* **1996**, *39*, 811–817, doi:10.1136/gut.39.6.811.

86.   Liang, R.; Fei, Y.J.; Prasad, P.D.; Ramamoorthy, S.; Han, H.; Yang-Feng, T.L.; Hediger, M.A.; Ganapathy, V.; Leibach, F.H. Human intestinal H+/peptide cotransporter. Cloning, functional expression, and chromosomal localization. *J. Biol. Chem.* **1995**, *270*, 6456–6463, doi:10.1074/jbc.270.12.6456.

87.   Ostaszewska, T.; Kamaszewski, M.; Grochowski, P.; Dabrowski, K.; Verri, T.; Aksakal, E.; Szatkowska, I.; Nowak, Z.; Dobosz, S. The effect of peptide absorption on PepT1 gene expression and digestive system hormones in rainbow trout (Oncorhynchus mykiss). *Comp. Biochem. Physiol. - A Mol. Integr. Physiol.* **2010**, *155*, 107–114, doi:10.1016/j.cbpa.2009.10.017.

88.   Romano, A.; Barca, A.; Storelli, C.; Verri, T. Teleost fish models in membrane transport research: The PEPT1(SLC15A1) H+-oligopeptide transporter as a case study. *J. Physiol.* **2014**, *592*, 881–897, doi:10.1113/jphysiol.2013.259622.

89.   Kamalam, B.S.; Panserat, S.; Aguirre, P.; Geurden, I.; Fontagné-Dicharry, S.; Médale, F. Selection for high muscle fat in rainbow trout induces potentially higher chylomicron synthesis and PUFA biosynthesis in the intestine. *Comp. Biochem. Physiol. - A Mol. Integr. Physiol.* **2013**, *164*, 417–427, doi:10.1016/j.cbpa.2012.11.020.

90.   Terova, G.; Robaina, L.; Izquierdo, M.; Cattaneo, A.G.; Molinari, S.; Bernardini, G.; Saroglia, M. PepT1 mRNA expression levels in sea bream (Sparus aurata) fed different plant protein sources. *Springerplus* **2013**, *2*, 1–14, doi:10.1186/2193-1801-2-17.

91.   Subramaniam, M.; Weber, L.P.; Loewen, M.E. Intestinal electrogenic sodium-dependent glucose absorption in tilapia and trout reveal species differences in SLC5A-associated kinetic segmental segregation. *Am J Physiol Regul Integr Comp Physiol* **2019**, *316*, 222–234, doi:10.1152/ajpregu.00304.2018.-Electro.

92.   Venold, F.F.; Penn, M.H.; Thorsen, J.; Gu, J.; Kortner, T.M.; Krogdahl, Å.; Bakke, A.M. Intestinal fatty acid binding protein (fabp2) in Atlantic salmon (Salmo salar): Localization and alteration of expression during development of diet induced enteritis. *Comp. Biochem. Physiol. - A Mol. Integr. Physiol.* **2013**, *164*, 229–240, doi:10.1016/j.cbpa.2012.09.009.

93.   Verdile, N.; Pasquariello, R.; Brevini, T.A.L.; Gandolfi, F. The 3d pattern of the rainbow trout (Oncorhynchus mykiss) enterocytes and intestinal stem cells. *Int. J. Mol. Sci.* **2020**, *21*, 1–30, doi:10.3390/ijms21239192.

94.   Li, J.; Prochaska, M.; Maney, L.; Wallace, K.N. Development and Organization of the Zebrafish Intestinal Epithelial Stem Cell Niche. *Dev. Dyn.* **2020**, *249*, 76–87, doi:10.1002/dvdy.

95.   Crosnier, C.; Vargesson, N.; Gschmeissner, S.; Ariza-McNaughton, L.; Morrison, A.; Lewis, J. Delta-Notch signalling controls commitment to a secretory fate in the zebrafish intestine. *Development* **2005**, *132*, 1093–1104, doi:10.1242/dev.01644.

96.   Cheesman, S.E.; Neal, J.T.; Mittge, E.; Seredick, B.M.; Guillemin, K. Epithelial cell proliferation in the developing zebrafish intestine is regulated by the Wnt pathway and microbial signaling via Myd88. *Proc. Natl. Acad. Sci. U. S. A.* **2011**, *108*, 4570–4577, doi:10.1073/pnas.1000072107.

97.   Aghaallaei, N.; Gruhl, F.; Schaefer, C.Q.; Wernet, T.; Weinhardt, V.; Centanin, L.; Loosli, F.;

Baumbach, T.; Wittbrodt, J. Identification, visualization and clonal analysis of intestinal stem cells in fish. *Dev.* **2016**, *143*, 3470–3480, doi:10.1242/dev.134098.

98. Bahar Halpern, K.; Massalha, H.; Zwick, R.K.; Moor, A.E.; Castillo-Azofeifa, D.; Rozenberg, M.; Farack, L.; Egozi, A.; Miller, D.R.; Averbukh, I.; et al. Lgr5+ telocytes are a signaling source at the intestinal villus tip. *Nat. Commun.* **2020**, *11*, doi:10.1038/s41467-020-15714-x.

99. Neal, M.D.; Richardson, W.M.; Sodhi, C.P.; Russo, A.; Hackam, D.J. Intestinal stem cells and their roles during mucosal injury and repair. *J. Surg. Res.* **2011**, *167*, 1–8, doi:10.1016/j.jss.2010.04.037.

100. Formeister, E.J.; Sionas, A.L.; Lorance, D.K.; Barkley, C.L.; Lee, G.H.; Magness, S.T. Distinct SOX9 levels differentially mark stem/progenitor populations and enteroendocrine cells of the small intestine epithelium. *AJP Gastrointest. Liver Physiol.* **2009**, *296*, G1108–G1118, doi:10.1152/ajpgi.00004.2009.

101. Bohin, N.; Keeley, T.M.; Carulli, A.J.; Walker, E.M.; Carlson, E.A.; Gao, J.; Aifantis, I.; Siebel, C.W.; Rajala, M.W.; Myers, M.G.; et al. Rapid Crypt Cell Remodeling Regenerates the Intestinal Stem Cell Niche after Notch Inhibition. *Stem Cell Reports* **2020**, doi:10.1016/j.stemcr.2020.05.010.

102. Farin, H.F.; Van Es, J.H.; Clevers, H. Redundant sources of Wnt regulate intestinal stem cells and promote formation of paneth cells. *Gastroenterology* **2012**, *143*, doi:10.1053/j.gastro.2012.08.031.

103. Verdile, N.; Pasquariello, R.; Cardinaletti, G.; Tibaldi Emilio, Brevini Tiziana A.L., G.F. Telocytes: Active Players in the Rainbow Trout (Oncorhynchus mykiss) Intestinal Stem-Cell Niche. *Animals* **2022**.

104. McCarthy, N.; Manieri, E.; Storm, E.E.; Saadatpour, A.; Luoma, A.M.; Kapoor, V.N.; Madha, S.; Gaynor, L.T.; Cox, C.; Keerthivasan, S.; et al. Distinct Mesenchymal Cell Populations Generate the Essential Intestinal BMP Signaling Gradient. *Cell Stem Cell* **2020**, *26*, 391-402.e5, doi:10.1016/j.stem.2020.01.008.

105. Fuchs, E.; Blau, H.M. Tissue Stem Cells: Architects of Their Niches. *Cell Stem Cell* **2020**, *27*, 532–556, doi:10.1016/j.stem.2020.09.011.

106. Vannucchi, M.G. The telocytes: Ten years after their introduction in the scientific literature. an update on their morphology, distribution, and potential roles in the gut. *Int. J. Mol. Sci.* **2020**, *21*, 1–15, doi:10.3390/ijms21124478.

107. Condrat, C.E.; Barbu, M.G.; Thompson, D.C.; Dănilă, C.A.; Boboc, A.E.; Suciu, N.; Crețoiu, D.; Voinea, S.C. *Roles and distribution of telocytes in tissue organization in health and disease*; 2021; ISBN 9780128185612.

108. Rosa, I.; Marini, M.; Manetti, M. Telocytes: An Emerging Component of Stem Cell Niche Microenvironment. *J. Histochem. Cytochem.* **2021**, 002215542110254, doi:10.1369/00221554211025489.

109. Bojin, F.M.; Gavriliuc, O.I.; Cristea, M.I.; Tanasie, G.; Tatu, C.S.; Panaitescu, C.; Paunescu, V. Telocytes within human skeletal muscle stem cell niche. *J. Cell. Mol. Med.* **2011**, *15*, 2269–2272, doi:10.1111/j.1582-4934.2011.01386.x.

110. Kostin, S. Cardiac telocytes in normal and diseased hearts. *Semin. Cell Dev. Biol.* **2016**, *55*, 22–30, doi:10.1016/j.semcdb.2016.02.023.

111. Kim, J.E.; Fei, L.; Yin, W.C.; Coquenlorge, S.; Rao-Bhatia, A.; Zhang, X.; Shi, S.S.W.; Lee, J.H.; Hahn, N.A.; Rizvi, W.; et al. Single cell and genetic analyses reveal conserved populations and signaling mechanisms of gastrointestinal stromal niches. *Nat. Commun.* **2020**, *11*, 1–15, doi:10.1038/s41467-019-14058-5.

112. Vannucchi, M.G.; Traini, C.; Manetti, M.; Ibba-Manneschi, L.; Faussone-Pellegrini, M.S. Telocytes express PDGFRα in the human gastrointestinal tract. *J. Cell. Mol. Med.* **2013**, *17*, 1099–1108, doi:10.1111/jcmm.12134.

113. Othman, E.R.; Elgamal, D.A.; Refaiy, A.M.; Abdelaal, I.I.; Abdel-Mola, A.F.; Al-Hendy, A. Identification and potential role of telocytes in human uterine leiomyoma. *Contracept. Reprod. Med.* **2016**, *1*, 1–7, doi:10.1186/s40834-016-0022-5.

114. David, M.B.; Valenta, T.; Fazilaty, H.; Hausmann, G.; Basler, K. Distinct populations of crypt-associated fibroblasts act as signaling hubs to control colon homeostasis. *PLoS Biol.* **2020**, *18*, 1–20, doi:10.1371/journal.pbio.3001032.

115. Zheng, Y.; Bai, C.; Wang, X. Telocyte morphologies and potential roles in diseases. *J. Cell. Physiol.* **2012**, *227*, 2311–2317, doi:10.1002/jcp.23022.

116. Gherghiceanu, M.; Manole, C.G.; Popescu, L.M. Telocytes in endocardium: Electron microscope evidence. *J. Cell. Mol. Med.* **2010**, *14*, 2330–2334, doi:10.1111/j.1582-4934.2010.01133.x.

117. Niculite, C.M.; Regalia, T.M.; Gherghiceanu, M.; Huica, R.; Surcel, M.; Ursaciuc, C.; Leabu, M.; Popescu, L.M. Dynamics of telopodes (telocyte prolongations) in cell culture depends on extracellular matrix protein. *Mol. Cell. Biochem.* **2015**, *398*, 157–164, doi:10.1007/s11010-014-2215-z.

118. Cretoiu, S.M.; Popescu, L.M. Telocytes revisited. *Biomol. Concepts* **2014**, *5*, 353–369, doi:10.1515/bmc-2014-0029.

119. Gandahi, N.S.; Ding, B.; Shi, Y.; Bai, X.; Gandahi, J.A.; Vistro, W.A.; Chen, Q.; Yang, P. Identification of telocytes in the pancreas of Turtles—A role in cellular communication. *Int. J. Mol. Sci.* **2020**, *21*, doi:10.3390/ijms21062057.

120. Abd-Elhafeez, H.H.; Abou-Elhamd, A.S.; Soliman, S.A. Morphological and immunohistochemical phenotype of TCs in the intestinal bulb of Grass carp and their potential role in intestinal immunity. *Sci. Rep.* **2020**, *10*, 1–17, doi:10.1038/s41598-020-70032-y.

121. Abd-Elhafeez, H.H.; Abdo, W.; Kamal, B.M.; Soliman, S.A. Fish telocytes and their relation to rodlet cells in ruby-red-fin shark (rainbow shark) Epalzeorhynchos frenatum (Teleostei: Cyprinidae). *Sci. Rep.* **2020**, *10*, 1–18, doi:10.1038/s41598-020-75677-3.

122. Carmona, I.C.; Bartolomé, M.J.L.; Escribano, C.J. Identification of telocytes in the lamina propria of rat duodenum: Transmission electron microscopy. *J. Cell. Mol. Med.* **2011**, *15*, 26–30, doi:10.1111/j.1582-4934.2010.01207.x.

123. Ratajczak, M.Z.; Ratajczak, J. Extracellular microvesicles/exosomes: discovery, disbelief, acceptance, and the future? *Leukemia* **2020**, *34*, 3126–3135, doi:10.1038/s41375-020-01041-z.

124. Chen, J.; Li, C.; Chen, L. The role of microvesicles derived from mesenchymal stem cells in lung diseases. *Biomed Res. Int.* **2015**, *2015*, doi:10.1155/2015/985814.

125. Hoch, R. V.; Soriano, P. Roles of PDGF in animal development. *Development* **2003**, *130*, 4769–4784, doi:10.1242/dev.00721.

126. Kaestner, K.H. The Intestinal Stem Cell Niche: A Central Role for Foxl1-Expressing Subepithelial Telocytes. *Cmgh* **2019**, *8*, 111–117, doi:10.1016/j.jcmgh.2019.04.001.

127. Greicius, G.; Kabiri, Z.; Sigmundsson, K.; Liang, C.; Bunte, R.; Singh, M.K.; Virshup, D.M. PDGFRα+ pericryptal stromal cells are the critical source of Wnts and RSPO3 for murine intestinal stem cells in vivo. *Proc. Natl. Acad. Sci. U. S. A.* **2018**, doi:10.1073/pnas.1713510115.

128. Horikawa, S.; Ishii, Y.; Hamashima, T.; Yamamoto, S.; Mori, H.; Fujimori, T.; Shen, J.; Inoue, R.; Nishizono, H.; Itoh, H.; et al. PDGFRα plays a crucial role in connective tissue remodeling. *Sci. Rep.* **2015**, *5*, 1–14, doi:10.1038/srep17948.

129. Aoki, R.; Shoshkes-Carmel, M.; Gao, N.; Shin, S.; May, C.L.; Golson, M.L.; Zahm, A.M.; Ray, M.; Wiser, C.L.; Wright, C.V.E.; et al. Foxl1-Expressing Mesenchymal Cells Constitute the Intestinal Stem Cell Niche. *Cmgh* **2016**, *2*, 175–188, doi:10.1016/j.jcmgh.2015.12.004.

130. Manzoni, E.F.M.; Pennarossa, G.; Deeguileor, M.; Tettamanti, G.; Gandolfi, F.; Brevini, T.A.L. 5-azacytidine affects TET2 and histone transcription and reshapes morphology of human skin fibroblasts. *Sci. Rep.* **2016**, *6*, 1–13, doi:10.1038/srep37017.

131. Ayadi, F.Y.; Rosentrate, K.A.; Muthukumar, K. Alternative Protein Sources for Aquaculture Feeds. *J. Aquac. Feed Sci. Nutr.* 2012, *4*, 1–26.

132. Desai, A.R.; Links, M.G.; Collins, S.A.; Mansfield, G.S.; Drew, M.D.; Van Kessel, A.G.; Hill, J.E. Effects of plant-based diets on the distal gut microbiome of rainbow trout (Oncorhynchus mykiss). *Aquaculture* **2012**, *350–353*, 134–142, doi:10.1016/j.aquaculture.2012.04.005.

133. Khalil, H.A.; Lei, N.Y.; Brinkley, G.; Scott, A.; Wang, J.; Kar, U.K.; Jabaji, Z.B.; Lewis, M.; Martín, M.G.; Dunn, J.C.Y.; et al. A novel culture system for adult porcine intestinal crypts. *Cell Tissue Res.* **2016**, *365*, 123–134, doi:10.1007/s00441-016-2367-0.

134. Zachos, N.C.; Kovbasnjuk, O.; Foulke-Abel, J.; In, J.; Blutt, S.E.; de Jonge, H.R.; Estes, M.K.; Donowitz, M. Human Enteroids/Colonoids and Intestinal Organoids Functionally Recapitulate Normal Intestinal Physiology and Pathophysiology. *J. Biol. Chem.* **2016**, *291*, 3759–3766, doi:10.1074/jbc.R114.635995.

135. Nicole Verdile, Anna Szabo′, Rolando Pasquariello, Tiziana A.L. Brevini, Sandra Van Vlierberghe, and F.G. Preparation of Biological Scaffolds and Primary Intestinal Epithelial Cells to Efficiently 3D Model the Fish Intestinal Mucosa. *Next Gener. Cult. Platforms Reliab. Vitr. Model.* **2013**, *2273*, 1–32, doi:10.1016/B978-1-4160-3106-2.00019-2.

136. Pasquariello, R.; Verdile, N.; Pavlovic, R.; Panseri, S.; Schirmer, K.; Brevini, T.A.L.; Gandolfi, F. New Stable Cell Lines Derived from the Proximal and Distal Intestine of Rainbow Trout (Oncorhynchus mykiss) Retain Several Properties Observed In Vivo. **2021**.

137. Olson, A.; Le, V.; Aldahl, J.; Yu, E.J.; Hooker, E.; He, Y.; Lee, D.H.; Kim, W.K.; Cardiff, R.D.; Geradts, J.; et al. The comprehensive role of E-cadherin in maintaining prostatic epithelial integrity during oncogenic transformation and tumor progression. *PLoS Genet.* **2019**, *15*, 1–

26, doi:10.1371/journal.pgen.1008451.

138. Bauer, H.; Zweimueller-Mayer, J.; Steinbacher, P.; Lametschwandtner, A.; Bauer, H.C. The dual role of zonula occludens (ZO) proteins. *J. Biomed. Biotechnol.* **2010**, *2010*, doi:10.1155/2010/402593.

139. Verhulsel, M.; Simon, A.; Bernheim-Dennery, M.; Gannavarapu, V.R.; Gérémie, L.; Ferraro, D.; Krndija, D.; Talini, L.; Viovy, J.L.; Vignjevic, D.M.; et al. Developing an advanced gut on chip model enabling the study of epithelial cell/fibroblast interactions. *Lab Chip* **2021**, *21*, 365–377, doi:10.1039/d0lc00672f.

140. Costa, J.; Ahluwalia, A. Advances and Current Challenges in Intestinal in vitro Model Engineering: A Digest. *Front. Bioeng. Biotechnol.* **2019**, *7*, 1–14, doi:10.3389/fbioe.2019.00144.

141. Sirakov, M.; Borra, M.; Cambuli, F.M.; Plateroti, M. Defining suitable reference genes for RT-qPCR analysis on intestinal epithelial cells. *Mol. Biotechnol.* **2013**, *54*, 930–938, doi:10.1007/s12033-012-9643-3.

142. Turner, J.R.; Lencer, W.I.; Carlson, S.; Madara, J.L. Carboxyl-terminal vesicular stomatitis virus G protein-tagged intestinal Na+-dependent glucose cotransporter (SGLT1): Maintenance of surface expression and global transport function with selective perturbation of transport kinetics and polarized expressio. *J. Biol. Chem.* **1996**, *271*, 7738–7744, doi:10.1074/jbc.271.13.7738.

143. Steffansen, B.; Pedersen, M.D.L.; Laghmoch, A.M.; Nielsen, C.U. SGLT1-Mediated Transport in Caco-2 Cells Is Highly Dependent on Cell Bank Origin. *J. Pharm. Sci.* **2017**, *106*, 2664–2670, doi:10.1016/j.xphs.2017.04.033.

144. Grefner, N.M.; Gromova, L. V.; Gruzdkov, A.A.; Komissarchik, Y.Y. Caco2 cell culture as an intestinal epithelium model to study hexose transport. *Cell tissue biol.* **2012**, *6*, 335–340, doi:10.1134/S1990519X12040062.

145. Hayeshi, R.; Hilgendorf, C.; Artursson, P.; Augustijns, P.; Brodin, B.; Dehertogh, P.; Fisher, K.; Fossati, L.; Hovenkamp, E.; Korjamo, T.; et al. Comparison of drug transporter gene expression and functionality in Caco-2 cells from 10 different laboratories. *Eur. J. Pharm. Sci.* **2008**, *35*, 383–396, doi:10.1016/j.ejps.2008.08.004.

146. Wenzel, U.; Meissner, B.; Döring, F.; Daniel, H. PEPT1-mediated uptake of dipeptides enhances the intestinal absorption of amino acids via transport system b 0,+. *J. Cell. Physiol.* **2001**, *186*, 251–259, doi:10.1002/1097-4652(200102)186:2<251::AID-JCP1027>3.0.CO;2-F.

Annexes

animals

MDPI

Article

A Detailed Study of Rainbow Trout (Oncorhynchus mykiss) Intestine Revealed That Digestive and Absorptive Functions Are Not Linearly Distributed along Its Length

Nicole Verdile [1,*], Rolando Pasquariello [1] , Marco Scolari [2], Giulia Scirè [2], Tiziana A. L. Brevini [3] and Fulvio Gandolfi [1,*]

Department of Agricultural and Environmental Sciences, University of Milan, 20133 Milano, Italy; Rolando.pasquariello@unimi.it
Skretting Aquaculture Research Centre, 37100 Verona, Italy; Marco.Scolari@nutreco.com (M.S.); giulia.scire@skretting.com (G.S.)
Department of Health, Animal Science and Food Safety, University of Milan, 20133 Milano, Italy; *tiziana.brevini@unimi.it*
Correspondence: nicole.verdile@unimi.it (N.V.); fulvio.gandolfi@unimi.it (F.G.);

Tel.: +39-02-5031-6449 (N.V.); +39-02-5031-7990 (F.G.)

Simple Summary: Aquaculture is the fastest growing food-producing sector due to the increase of fish intended for human consumption. However, aquaculture growth generates concerns, since carnivorous fish are extensively fed using fish-meal and fish-oil. This constitutes a severe limit to the aquaculture industry, questioning its sustainability. Consequently, alternative feeds are continuously searched through extensive in vivo feeding trials. Undoubtedly, to evaluate their impact on the gastrointestinal tract health, detailed knowledge of the intestine morphology and physiology is required. To date, extensive studies have been performed in several livestock species; however, available information on fish is limited nowadays, most importantly because their alimentary canal is able to easily adapt to external stimuli, and their intestinal morphology is affected by external factors. Therefore, it is essential to establish accurate reference values, especially along the productive cycle of animals raised in standardized conditions. Here, we performed a detailed characterization of the epithelial cells lining the intestinal mucosa in rainbow trout along the first year of development. We studied the absorptive and secretory activity as well as its ability to self-renewal. Our results indicate that, in this species, both digestive and absorptive functions are not linearly distributed along the intestinal length.

Abstract: To increase the sustainability of trout farming, the industry requires alternatives to fish-based meals that do not compromise animal health and growth performances. To develop new feeds, detailed knowledge of intestinal morphology and physiology is required. We performed histological, histochemical, immunohistochemical and morphometric analysis at typical time points of in vivo feeding trials (50, 150 and 500 g). Only minor changes occurred during growth whereas differences characterized two compartments, not linearly distributed along the intestine. The first included the pyloric caeca, the basal part of the complex folds and the villi of the distal intestine. This was characterized by a significantly smaller number of goblet cells with smaller mucus vacuoles, higher proliferation and higher apoptotic rate but a smaller extension of fully differentiated epithelial cells and by the presence of numerous pinocytotic vacuolization. The second compartment was formed by the proximal intestine and the apical part of the posterior intestine complex folds. Here we observed more abundant goblet cells with bigger vacuoles, low proliferation rate, few round apoptotic cells, a more extended area of fully differentiated cells and no pinocytotic vacuoles. Our results suggest that rainbow trout intestine is physiologically arranged to mingle digestive and absorptive functions along its length.

Article

The 3D Pattern of the Rainbow Trout (*Oncorhynchus mykiss*) Enterocytes and Intestinal Stem Cells

Nicole Verdile [1], Rolando Pasquariello [1] , Tiziana A. L. Brevini [2] and Fulvio Gandolfi [1,*]

[1]   Department of Agricultural and Environmental Sciences, University of Milan, 20133 Milano, Italy;
      Nicole.verdile@unimi.it (N.V.); Rolando.pasquariello@unimi.it (R.P.)
[2]   Department of Health, Animal Science and Food Safety, University of Milan, 20133 Milano, Italy;
      tiziana.brevini@unimi.it

*Correspondence: fulvio.gandolfi@unimi.it; Tel.: + 39-02-5031-7990

Abstract: We previously showed that, according to the frequency and distribution of specific cell types, the rainbow trout (RT) intestinal mucosa can be divided in two regions that form a complex nonlinear three-dimensional (3D) pattern and have a different renewal rate. This work had two aims. First, we investigated whether the unusual distribution of cell populations reflects a similar distribution of functional activities. To this end, we determined the protein expression pattern of three well-defined enterocytes functional markers: peptide transporter 1 (PepT1), sodium–glucose/galactose transporter 1 (SGLT-1), and fatty-acid-binding protein 2 (Fabp2). Second, we characterized the structure of RT intestinal stem-cell (ISC) niche and determined whether the different proliferative is accompanied by a different organization and/or extension of the stem-cell population. We studied the expression and localization of well-characterized mammal ISC markers: LGR5, HOPX, SOX9, NOTCH1, DLL1, and WNT3A. Our results indicate that morphological similarity is associated with similar function only between the first portion of the mid-intestine and the apical part of the complex folds in the second portion. Mammal ISC markers are all expressed in RT, but their localization is completely different, suggesting also substantial functional differences. Lastly, higher renewal rates are supported by a more abundant ISC population.

animals

Article

Telocytes: Active Players in the Rainbow Trout (*Oncorhynchus mykiss*) Intestinal Stem-Cell Niche

Nicole Verdile [1], Rolando Pasquariello [1], Gloriana Cardinaletti [2], Emilio Tibaldi [2], Tiziana A. L. Brevini [3] and Fulvio Gandolfi

[1] Department of Agricultural and Environmental Sciences, University of Milan, 20133 Milan, Italy; nicole.verdile@unimi.it (N.V.); rolando.pasquariello@unimi.it (R.P.)

[2] Department of Agricultural, Food, Environmental and Animal Sciences, University of Udine, 33100 Udine, Italy; gloriana.cardinaletti@uniud.it (G.C.); emilio.tibaldi@uniud.it (E.T.)

[3] Department of Health, Animal Science and Food Safety, University of Milan, 20133 Milan, Italy; tiziana.brevini@unimi.it

*Correspondence: fulvio.gandolfi@unimi.it

Simple Summary: Aquaculture is expanding due to the high demand of fish for human consumption. However, since carnivorous fish are fed using fish-derived proteins and lipids, the sustainability of this food-producing sector is debated. Therefore, feed industries and academia are dedicating their efforts to the search for suitable raw materials and more sustainable alternative feeds that are able to ensure the health of the fish. To properly evaluate the effect of these feed formulations, extensive knowledge of the intestinal morphology and physiology is required. Moreover, the intestine is a dynamic environment in which homeostasis is controlled by highly specialized intestinal stem-cell niches. These defined functional units consist of epithelial stem cells, the supportive mesenchymal cell population, and acellular components. While they have been widely studied in the mouse intestine, this understanding is almost absent in fish species. We have previously characterized the organization of the stem-cell niche in the rainbow trout intestine; here, we expand that knowledge by examining telocytes as active stromal components of the niche. Our results indicate that this cell type is also present in rainbow trout and that it represents a key mediator of intestinal homeostasis by virtue of its active interaction with the stem cells.

Abstract: In order to improve the sustainability of trout farming, it is essential to develop alternatives to fish-based meals that prevent intestinal disorders and support growth performances. Therefore, an accurate knowledge of intestinal morphology and physiology is desirable. We previously described the epithelial component of the intestinal stem-cell (ISC) niche in rainbow trout *(Oncorhynchus mykiss)*, which is one of the most successfully farmed species and a representative model of the salmonids family. This work aims to expand that knowledge by investigating the niche stromal components that contribute to intestinal homeostasis. We analyzed samples belonging to five individuals collected from a local commercial farm. Histological and ultrastructural studies revealed peculiar mesenchymal cells adjacent to the epithelium that generated an intricate mesh spanning from the folds' base to their apex. Their voluminous nuclei, limited cytoplasm and long cytoplasmic projections characterized them as telocytes (TCs). TEM analysis showed the secretion of extracellular vesicles, suggesting their functional implication in cell-to-cell communication. Furthermore, we evaluated the localization of well-defined mouse TC markers (*pdgfrα* and *foxl1*) and their relationship with the epithelial component of the niche. TCs establish a direct connection with ISCs and provide short-range signaling, which also indicates their key role as the mesenchymal component of the stem-cell niche in this species. Interestingly, the TC distribution and gene-expression pattern in rainbow trout closely overlapped with those observed in mice, indicating that they have the same functions in both species. These results substantially improve our understanding of the mechanisms regulating intestinal homeostasis and will enable a more detailed evaluation of innovative feed effects.

Chapter 19

Preparation of Biological Scaffolds and Primary Intestinal Epithelial Cells to Efficiently 3D Model the Fish Intestinal Mucosa

Nicole Verdile, Anna Szabo´, Rolando Pasquariello, Tiziana A.L. Brevini, Sandra Van Vlierberghe, and Fulvio Gandolfi

Abstract

Tissue engineering is an elegant tool to create organs in vitro, that can help obviate the lack of organ donors in transplantation medicine and provide the opportunity of studying complex biological systems in vitro, thereby reducing the need for animal experiments. Artificial intestine models are at the core of Fish-AI, an EU FET-Open research project dedicated to the development of a 3D in vitro platform that is intended to enable the aquaculture feed industry to predict the nutritional and health value of alternative feed sources accurately and efficiently.

At present, it is impossible to infer the health and nutrition value through the chemical characterization of any given feed. Therefore, each new feed must be tested through in vivo growth trials. The procedure is lengthy, expensive and requires the use of many animals. Furthermore, although this process allows for a precise evaluation of the final effect of each feed, it does not improve our basic knowledge of the cellular and molecular mechanisms determining such end-results. In turn, this lack of mechanistic knowledge severely limits the capacity to understand and predict the biological value of a single raw material and of their different combinations. The protocol described herein allows to develop the two main components essential to produce a functional platform for the efficient and reliable screening of feeds that the feed industry is currently developing for improving their health and nutritional value. It is here applied to the Rainbow Trout, but it can be fruitfully used to many other fish species.

Key words: Artificial intestine, In vitro model, Fish intestine, Polymer scaffold, Gelatin derivatives, Polymer synthesis, Primary cell line, Rainbow trout

---

Nicole Verdile and Anna Szabo contributed equally to this work.

Article

New Stable Cell Lines Derived from the Proximal and Distal Intestine of Rainbow Trout (*Oncorhynchus mykiss*) Retain Several Properties Observed In Vivo

Rolando Pasquariello, Nicole Verdile [1], Radmila Pavlovic [2], Sara Panseri [2], Kristin Schirmer [3,4,5], Tiziana A. L. Brevini [2] and Fulvio Gandolfi [1,*

[1]Department of Agricultural and Environmental Sciences, University of Milan, 20133 Milano, Italy; rolando.pasquariello@unimi.it (R.P.); nicole.verdile@unimi.it (N.V.)

[2]Department of Health, Animal Science and Food Safety, University of Milan, 20133 Milano, Italy; radmila.pavlovic1@unimi.it (R.P.); sara.panseri@unimi.it (S.P.); tiziana.brevini@unimi.it (T.A.L.B.)

[3]Department of Environmental Toxicology, Eawag, Swiss Federal Institute of Aquatic Science and Technology, 8600 Dübendorf, Switzerland; kristin.schirmer@eawag.ch

[4]Department of Environmental Systems Science, ETH Zürich, 8092 Zürich, Switzerland

[5]School of Architecture, Civil and Environmental Engineering, EPFL Lausanne, 1015 Lausanne, Switzerland

**Correspondence: fulvio.gandolfi@unimi.it

Abstract: We derived two novel cell lines from rainbow trout (RT) proximal (RTpi-MI) and distal intestine (RTdi-MI) and compared them with the previously established continuous cell line RTgutGC. Intestinal stem cells, differentiating and differentiated epithelial cells, and connective cells were found in all cell lines. The cell lines formed a polarized barrier, which was not permeable to large molecules and absorbed proline and glucose. High seeding density induced their differentiation into more mature phenotypes, as indicated by the downregulation of intestinal stem cell-related genes (i.e., *sox9*, *hopx* and *lgr5*), whereas alkaline phosphatase activity was upregulated. Other enterocyte markers (i.e., sglt1 and pept1), however, were not regulated as expected. In all cell lines, the presence of a mixed population of epithelial and stromal cells was characterized for the first time. The expression by the stromal component of *lgr5*, a stem cell niche regulatory molecule, may explain why these lines proliferate stably in vitro. Although most parameters were conserved among the three cell lines, some significant differences were observed, suggesting that characteristics typical of each tract are partly conserved in vitro as well.

Keywords: fish; intestinal cell lines; intestinal stem cells; enterocyte differentiation markers; intestinal barrier in vitro; cell differentiation; nutrition